THE DENSITY DEPENDENCE OF THE REFRACTIVITY OF GASES

by

ROBERT CHARLES BURNS, M.Sc. (NATAL)

A thesis submitted in partial fulfilment of the requirements for the degree of Doctor of Philosophy in the Department of Physics, University of Natal.

1978

Pietermaritzburg

I hereby certify that this research is the result of my own investigation, which has not already been accepted in substance for any degree, and is not being concurrently submitted in candidature for any other degree.

Signed . . . . . R.C. Burns . . . .

I hereby certify that the above statement is correct.

Signed . . . . . C. Graham . . . . .

Dr. C. Graham, M.Sc., Ph.D. (Natal), Ph.D. (Cantab.)

Department of Physics,
University of Natal,
Pietermaritzburg.

ACKNOWLEDGEMENTS

I wish to express my sincere appreciation to my supervisor, Dr. C. Graham, for his inspiring guidance and encouragement throughout this work.

I would like to thank Professor R.E. Raab for the departmental facilities he made available, and express appreciation of his tenacious efforts in organizing finance for the purchase of equipment and for personal grants.

I am indebted to Messrs. R.H. Barker and D.R. Leibbrandt of the Physics Department Workshop and Messrs. L.J. van Schaik and A.R. Davis of the Electronics Workshop for their practical assistance whenever needed.

The help of Dr. E. Kyle and Dr. N.W. Reid of the Department of Chemistry with the mass spectrometric analyses of gas samples is acknowledged.

I am indebted to the Industrial Development Corporation of South Africa for the award of a scholarship for part of this project and the South African Council for Scientific and Industrial Research, and the University Research Fund for their personal grants and the award of grants for the purchase of equipment. The generous gift of research grade samples of krypton and xenon from AFROX Limited is gratefully acknowledged.

Finally. I would like to thank my mother, Natalie, for her encouragement and financial help and, not least, my thanks to Mrs. Cockburn for kindly typing this manuscript.

A B S T R A C T

An apparatus which was developed by Buckingham & Graham (1974)* has been assembled; and direct measurements of the density dependence of the refractive index and molar refractivity have been carried out using a sensitive differential - interferometric technique. Measurements of the second refractivity virial coefficient, B_R, are presented at four wavelengths (457.9 nm, 488.0 nm, 514.5 nm and 632.8 nm) in the visible, for the inert gases, neon, argon, krypton and xenon; methane and its fluorinated derivatives, fluoromethane, difluoromethane, trifluoromethane and tetrafluoromethane; and three common gases, carbon dioxide, nitrogen and sulphur hexafluoride. The design and construction details of the system are discussed. A feature of the B_R values for the molecular series methane to tetrafluoromethane is the absence of systematic trends; and dispersion plots of B_R for the above range of gases showed irregular variations over the wavelength range 457.9 nm to 514.5 nm. A statistical mechanical theory of B_R has been reviewed and molecular expressions for B_R, in terms of isolated-molecule electric properties, are derived. In these expressions the intermolecular potential energy consists of a Lennard-Jones 6:12 potential modified by dipole and quadrupole forces and the anisotropy of repulsive forces. The integrals in the expressions for B_R have been evaluated numerically by computer using Simpson's rule, and the calculated and observed values of B_R are compared.

* Buckingham, A.D. & Graham, C. 1974 *Proc. R. Soc. Lond. A* 336, 275.

CONTENTS

CHAPTER 1

INTRODUCTION TO REFRACTIVITY VIRIAL COEFFICIENTS

§1. Phenomenology

In 1880 L. Lorenz and H.A. Lorentz independently derived an equation which related the mean polarizability α of a molecule to the refractive index n of a bulk sample at equilibrium. This equation was later known as the Lorentz-Lorenz equation and has the form

$$\frac{n^2 - 1}{n^2 + 2} V = \frac{N\alpha}{3\varepsilon_o} , \qquad (1.1)$$

where ε_o is the permittivity of free space. If V is the molar volume V_m the left-hand side of (1.1) is the molar refraction R_m, and N is Avogadro's number N_A.

An important assumption in the derivation of (1.1), which has been the subject of theoretical and experimental investigation, is that α is a constant independent of density. Magri (1905) and Bennett (1934; 1940) found that R_m was constant within experimental error over a wide range of density conditions. However, more accurate experimental techniques (Everett & Munn 1963; Beaume & Coulon 1967; Orcutt & Cole 1967; Sliwinski 1969; Buckingham & Graham 1974; Olson 1975; St-Arnaud & Bose 1976) revealed significant deviations from the simple Lorentz-Lorenz equation. Measurements of these deviations coupled with reliable interpretations of the effects give information about the details of molecular interactions (Buckingham & Pople 1956a).

For a gas these effects may be examined systematically by means of a virial-type expansion of the molar refraction (Buckingham 1956a),

$$R_m \equiv \frac{n^2 - 1}{n^2 + 2} V_m = A_R + \frac{B_R}{V_m} + \frac{C_R}{V_m^2} + \cdots , \qquad (1.2)$$

where A_R, B_R, C_R .... are called the first, second, third ..... refractivity virial coefficients. These coefficients are functions of frequency and temperature but not of density. A_R is the ideal gas value corresponding to an independent-molecule treatment; that is, it may be evaluated by taking N_A times the contribution of an isolated molecule. In this limit the Lorentz-Lorenz equation is rigorously correct and from (1.1) and (1.2) we find,

$$A_R = \lim_{V_m \to \infty} [R_m] = \frac{N_A \alpha_o}{3\varepsilon_o} \quad , \tag{1.3}$$

where α_o is the polarizability of an isolated molecule. In (1.2) B_R/V_m describes the initial deviations from ideal gas behaviour due to pair interactions which the Lorentz-Lorenz equation fails to take into account. Kirkwood (1936) and Brown (1950) have shown that the Lorentz-Lorenz equation is a direct consequence of the Lorentz local field approximation which takes into account bulk polarization effects, but which neglects fluctuations in molecular interactions. In a real gas at higher densities collisions will inevitably occur and B_R/V_m may be related to the mean contribution of interacting pairs of molecules. From (1.2) we find,

$$B_R = \lim_{V_m \to \infty} [(R_m - A_R) V_m] \quad , \tag{1.4}$$

which may be shown to have the classical statistical mechanical form of Buckingham (1956a),

$$B_R = \frac{N_A^2}{3\varepsilon_o \Omega} \int (\tfrac{1}{2} \alpha_{12}(\tau) - \alpha_o) \exp(-U_{12}(\tau)/kT) \, d\tau \quad , \tag{1.5}$$

where $\alpha_{12}(\tau)$ is the mean polarizability of a pair of molecules, $U_{12}(\tau)$ the intermolecular potential energy for the molecules 1 and 2 in a relative configuration τ and Ω is defined by the equation,

$$\int d\tau = \Omega V_m \quad . \tag{1.6}$$

Since most experimental work, including our own, has been concerned with the initial deviations from ideal gas behaviour, no higher coefficients will be considered.

It is interesting to note that not only the refractivity is affected by collision induced fluctuations in the polarizability α but it also contributes to deviations from the Clausius-Mossotti formula for the dielectric constant (Buckingham & Pople 1955a and 1956b; Jansen & Mazur 1955; Orcutt & Cole 1967; Ely & McQuarrie 1971; Buckingham & Watts 1973; O'Brien, Gutschick, McKoy & McTague 1973), and the Kerr effect (Buckingham & Dunmur 1968). Fluctuations in α also lead to light scattering from fluids (Thibeau, Oksengorn & Vodar 1968; Gray & Ralph 1970; Levine & Birnbaum 1971; McTague, Ellenson & Hall 1972).

Phenomenological explanations of four possible contributions to $(\tfrac{1}{2} \alpha_{12}(\tau) - \alpha_o)$ have been suggested by Buckingham & Graham (1974) namely :

(i) The 'fluctuation' contribution of Kirkwood (1936) and Yvon (1936). The effective polarizability of each member of an interacting pair is modified by the extra field at one due to the induced dipole moment in the other. This is a classical effect which was first investigated by Silberstein (1917) who showed that if two molecules each have an intrinsic isotropic polarizability α_o and are separated by r ,

$$\frac{1}{2}\alpha_{12}(r) - \alpha_o = \frac{1}{3}\alpha_o\left[\left(1 - \frac{2\alpha_o r^{-3}}{4\pi\varepsilon_o}\right)^{-1} + 2\left(1 + \frac{\alpha_o r^{-3}}{4\pi\varepsilon_o}\right)^{-1} - 3\right] . \quad (1.7)$$

The expression diverges at the separation $r = \left(\frac{2\alpha_o}{4\pi\varepsilon_o}\right)^{\frac{1}{3}}$, and for large r

$$\frac{1}{2}\alpha_{12}(r) - \alpha_o = \frac{2\alpha_o^3 r^{-6}}{(4\pi\varepsilon_o)^2} .$$

The divergence cannot be investigated with the point dipole model since it occurs at a separation for which there is extensive overlap of the electron clouds. This effect makes a positive contribution to B_R and is readily evaluated for most intermolecular potential energies $U_{12}(r)$.

(ii) The intrinsic molecular polarizability changes as a result of dispersion-type interactions at large r. These effects were initially investigated by Jansen & Mazur (1955) using a perturbation formalism. They showed that these effects make a positive contribution to α_{12} that varies as r^{-6} at large r. This effect has also been studied by Buckingham (1956b), Heinricks (1969), Certain & Fortune (1971) and Buckingham, Martin & Watts (1973) and may be attributed to distortion of the electronic structure of the molecular pair by the dispersion interactions.

(iii) Electron cloud overlap at short range modifies α_{12} . This effect has been investigated by de Boer, van der Maesen & ten Seldam (1953), Du Pré & McTague (1969), Lim, Linder & Kromhout (1970), O'Brien *et al.* (1973) and Buckingham & Watts (1973). Their results together with the experimental value of the second dielectric virial coefficient B_ε of Orcutt & Cole (1967) for helium suggest that the effect probably contributes negatively to B_R .

(iv) The strong intermolecular field due to permanent multipole moments can grossly distort the electronic structure of the molecular pair and may lead to non-linear polarization effects. These are described by molecular hyperpolarizabilities (Buckingham & Pople 1955b; Buckingham & Orr 1967).

Although many theoretical explanations for the density dependence of the polarizability have been given, relatively sparse, however, are reliable values of B_R. The paucity of experimental values is due in part to the smallness of the effect (B_R is typically 1 part in 10^4 of R_m at 500 kPa). In this work we present new measurements of B_R which have been obtained using a differential interferometric technique initially due to Buckingham & Graham (1974). Measurements have been made on a wide range of polar and non-polar gases at four wavelengths in the visible spectrum (457.9 nm, 488.0 nm, 514.5 nm and 632.8 nm). The gases may be divided into three separate groups, namely methane and its fluorinated derivatives (CH_4, CH_3F, CH_2F_2, CHF_3 and CF_4); the inert gases (Ne, Ar, Kr, and Xe) and three common gases (CO_2, N_2 and SF_6) for which many molecular parameters are known.

Later in this study the different approaches used to evaluate $(\frac{1}{2}\alpha_{12}(\tau) - \alpha_o)$ are reviewed and the statistical mechanical derivation of (1.5) is given. A classical model is used to describe molecular pair interactions and $(\frac{1}{2}\alpha_{12}(\tau) - \alpha_o)$ is expressed in terms of molecular polarizability parameters. Finally, we assume an interaction potential energy which takes into account central forces, dipole and quadrupole forces and the anisotropy of repulsive forces, and undertake computer evaluations of B_R by numerical integration of the expressions presented.

REFERENCES

Beaume, R. & Coulon, R. 1967 *C.r. hebd. Séanc. Acad. Sci.*, Paris B 265, 309.

Bennett, C.E. 1934 *Phys. Rev.* 45, 200.

Bennett, C.E. 1940 *Phys. Rev.* 58, 263.

Brown, W.F. 1950 *J. Chem. Phys.* 18, 1193.

Buckingham, A.D. 1956a *Trans. Faraday Soc.* 52, 747.

Buckingham, A.D. 1956b *Trans. Faraday Soc.* 52, 1035.

Buckingham, A.D. & Dunmur, D.A. 1968 *Trans. Faraday Soc.* 64, 1776.

Buckingham, A.D. & Graham, C. 1974 *Proc. R. Soc. Lond. A* 336, 275.

Buckingham, A.D., Martin, P.H. & Watts, R.S. 1973 *Chem. Phys. Lett.* 21, 186.

Buckingham, A.D. & Orr, B.J. 1967 *Q. Rev. Chem. Soc. Lond.* 21, 195.

Buckingham, A.D. & Pople, J.A. 1955a *Trans. Faraday Soc.* 51, 1029.

Buckingham, A.D. & Pople, J.A. 1955b *Proc. Phys. Soc. A* 68, 905.

Buckingham, A.D. & Pople, J.A. 1956a *Disc. Faraday Soc.* 22, 17.

Buckingham, A.D. & Pople, J.A. 1956b *Trans. Faraday Soc.* 52, 1035.

Buckingham, A.D. & Watts, R.S. 1973 *Molec. Phys.* 26, 7.

Certain, P.R. & Fortune, P.J. 1971 *J. Chem. Phys.* 55, 5818.

De Boer, J., van der Maesen, F. & ten Seldam, C.A. 1953 *Physica* 19, 265.

Du Pré, D.B. & McTague, J.P. 1969 *J. Chem. Phys.* 50, 2024.

Ely, J.F. & McQuarrie, D.A. 1971 *J. Chem. Phys.* 54, 2885.

Everett, D.H. & Munn, R.J. 1963 *Trans. Faraday Soc.* 59, 2486.

Gray, C.G. & Ralph, H.I. 1970 *Phys. Lett. A* 33, 165.

Heinricks, J. 1969 *Chem. Phys. Lett.* 4, 151.

Jansen, L. & Mazur, P. 1955 *Physica* 21, 193, 208.

Kirkwood, J.G. 1936 *J. Chem. Phys.* 4, 592.

Levine, H.B. & Birnbaum, G. 1971 *J. Chem. Phys.* 55, 2914.

Lim, T.K., Linder, B. & Kromhout, R.A. 1970 *J. Chem. Phys.* 49, 4181.

Lorentz, H.A. 1880 *Wiedem Ann.* 9, 641.

Lorenz, L. 1880 *Wiedem Ann.* 11, 70.

Magri, L. 1905 *Phys. Zeits.* 6, 629.

McTague, J.P., Ellenson, W.D. & Hall, L.H., 1972 *J. Phys.* 33, C1-241.

O'Brien, E.F., Gutschick, V.P., McKoy, C. & McTague, J.P. 1973 *Phys. Rev. A* 8, 690.

Olson, J.D. 1975 *J. Chem. Phys.* 63, 474.

Orcutt, R.H. & Cole, R.H. 1967 *J. Chem. Phys.* 46, 697.

Silberstein, L. 1917 *Phil. Mag.* 33, 521.

Sliwinski, P. 1969 *Z Phys. Chem.* 63, 263.

St-Arnaud, J.M. & Bose, T.K. 1976 *J. Chem. Phys.* 65, 4854.

Thibeau, M., Oksengorn, B. & Vodar, B. 1968 *J. Phys.* 29, 287.

Yvon, J. 1936 *C.r. hebd. Séanc. Acad. Sci.*, Paris B 202, 35.

gas or vapour	temperature / K	wavelength / nm	$10^6 A_R$ / $m^3\,mol^{-1}$	$10^{12} B_R$ / $m^6\,mol^{-2}$	references
Ne	300	632.8	1.003 ± 0.002	−0.06 ± 0.14	Buckingham & Graham 1974
Ar	298.2	447.1 to 667.8	4.257 ± 0.010	−1.0 ± 1.0	Michels & Botzen 1949; see Orcutt & Cole 1967
	299	632.8	4.196 ± 0.002	2.16 ± 0.34	Buckingham & Graham 1974
N_2	298.2	447.1 to 667.8	4.470 ± 0.005	0.8 ± 0.8	Michels *et al.* 1947; see Orcutt & Cole 1967
	299	632.8	4.458 ± 0.002	1.0 ± 0.31	Buckingham & Graham 1974
CO_2	307.2	546.1	6.686 ± 0.0015	0.4 ± 0.36	Phillips 1920; see Orcutt & Cole 1967
	323.2	447.1 to 667.8	6.679 ± 0.006	5.3 ± 0.9	Michels & Hamers 1937; see Orcutt & Cole 1967
	373.2	447.1 to 587.6	6.724 ± 0.010	2.7 ± 1.4	Michels & Hamers 1937; see Orcutt & Cole 1967
	299	632.8	6.647 ± 0.002	3.2 ± 1.6	Buckingham & Graham 1974
CH_4	299	632.8	6.600 ± 0.002	7.15 ± 0.35	Buckingham & Graham 1974
	300	546.2	6.614 ± 0.002	5.5 ± 1.0 †	Olson 1975
	302	632.8	6.553 ± 0.002	6.60 ± 0.38	St-Arnaud & Bose 1976
SO_2	298.2	546.0	9.888 ± 0.006	−89 ± 158 *	Blythe, Lambert, Petter & Spoel 1960
CF_4	298.2	546.0	7.225 ± 0.007	−14 ± 144 *	Blythe *et al.* 1960
CH_3F	298.2	546.0	6.640 ± 0.007	7 ± 100 *	Blythe *et al.* 1960
CH_3Cl	298.2	546.0	11.510 ± 0.006	−23 ± 138 *	Blythe *et al.* 1960
NH_3	298.2	546.0	5.561 ± 0.006	−122 ± 122 *	Blythe *et al.* 1960
	298.2	447.1	5.557 ± 0.002	950 ± 100 *	Beaume & Coulon 1967
	298.2	501.5	5.508 ± 0.002	674 ± 100 *	Beaume & Coulon 1967
	298.2	587.6	5.482 ± 0.004	566 ± 100 *	Beaume & Coulon 1967
	298.2	667.8	5.462 ± 0.004	373 ± 100 *	Beaume & Coulon 1967
SF_6	299	632.8	11.34 ± 0.02	29 ± 5.4	Buckingham & Graham 1974
CHF_3	299	632.8	7.052 ± 0.002	3.4 ± 1.1	Buckingham & Graham 1974
CH_3OH	303.4	546.2	8.18	25358 ± 1227	Everett & Munn 1963
$(CH_3CH_2)_2NH$	303.7	546.2	23.37	82963 ± 3505	Everett & Munn 1963
$(CH_3CH_2)_3N$	313.6	546.2	34.13	49488 ± 5119	Everett & Munn 1963
CH_3CH_3	various	589.3	11.26 ± 0.02	23.2 ± 0.6 †	Sliwinski 1969
$CH_3CH_2CH_3$	various	589.3	15.92 ± 0.02	83.5 ± 2.5 †	Sliwinski 1969
$CH_3(CH_2)_2CH_3$	various	589.3	20.62 ± 0.04	141.0 ± 4.0 †	Sliwinski 1969
$(CH_3)_3CH$	various	589.3	20.68 ± 0.04	143.0 ± 4.0 †	Sliwinski 1969

* Uncertainties not stated in the original paper. Those which are given above were derived from the uncertainties in the pressure measurements and B_p

† These uncertainties are probably deviations from a fitted curve.

Table 1. Summary of published first and second refractivity virial coefficients A_R and B_R.

CHAPTER 2

EXPERIMENTAL REVIEW

§1. Introduction

In almost all work carried out prior to 1974, the second refractivity virial coefficient B_R was determined from refractive index measurements made at varying gas densities. Since $\frac{B_R}{V_m}$ contributes a small fraction (typically 1 part in 10^4 at 500 kPa) to the molar refraction R_m,

$$\frac{B_R}{V_m} = \frac{n_2 - 1}{n_2 + 2} V_m - A_R \qquad (2.1)$$

is a small difference between two much larger quantities and small errors in the density and hence V_m may seriously limit the accuracy of the procedure; errors in reported work using this technique are typically 100% and more (Blythe, Lambert, Petter & Spoel 1960; Everett & Munn 1963; Beaume & Coulon 1967; Orcutt & Cole 1967; Hadrich 1975). The order of accuracy required in measurements of the refractive index n and molar volume V_m for refractivity virial coefficient determinations may be illustrated by using the following approximate data for sulphur hexafluoride at 500 kPa and 298K :
$A_R = 10 \times 10^{-6}\ m^3\ mol^{-1}$; $B_R = 30 \times 10^{-12}\ m^6\ mol^{-2}$; $V_m = 5 \times 10^{-3}\ m^3\ mol^{-1}$
We note that $\frac{B_R}{V_m} = 6 \times 10^{-9}\ m^3\ mol^{-1}$, namely about 1 part in 10^3 of A_R. Hence to determine B_R to an accuracy of 10%, R_m must be known to be about 1 part in 10^4 or better. In practice the refractive index can be measured interferometrically to better than this accuracy, but accurate measurement of V_m is more difficult. In this review we outline the techniques used to determine B_R and show how the accuracy of V_m effectively determines the uncertainty in B_R. In table 1 we list all known published values of B_R.

§2. Determination of B_R from refractive index measurements made at varying density

§§2.1 Measurements in which the density is determined from an equation of state

Blythe *et al.* (1960) have reported B_R values for carbon tetrafluoride, fluoromethane, chloromethane, ammonia and sulphur dioxide, whilst Everett & Munn (1963) have determined B_R for the vapours methanol, diethylamine and triethylamine. In these experiments a Rayleigh refractometer was used to measure the refractive index at pressures up to 250 mm Hg. Gas was slowly bled into a cell in one arm of the refractometer while the reference cell

was under vacuum and the displacement of the fringe system was monitored (to ±0.02 of a fringe) as a function of pressure. In their calculations V_m was determined indirectly from pressure measurements using an equation of state, namely

$$\frac{PV_m}{RT} = 1 + \frac{B_p}{V_m} + \frac{C_p}{V_m^2} + \cdots , \qquad (2.2)$$

where B_p, C_p .... are the pressure virial coefficients. The molar refraction R_m may be written as

$$R_m \equiv \frac{n^2 - 1}{n^2 + 2} V_m = A_R + \frac{B_R}{V_m} + \frac{C_R}{V_m^2} + \cdots \qquad (2.3)$$

and may be combined with (2.2) to eliminate V_m.

Neglecting C_p and C_R we get

$$\frac{n^2 - 1}{n^2 + 2} \frac{RT}{P} = A_R + (B_R - A_R B_p) \frac{P}{RT} . \qquad (2.4)$$

A plot of $\frac{n^2 - 1}{n^2 + 2} \frac{RT}{P}$ as ordinate and $\frac{P}{RT}$ as abscissa yields a straight line with intercept A_R and slope $(B_R - A_R B_p)$. The first refractivity virial coefficients determined in this way are potentially reliable to about 1 part in 10^4 depending on the accuracy of the measured quantities P, T and n. However, B_R appears in combination with $A_R B_p$ and errors in this quantity may seriously affect the accuracy of B_R if $A_R B_p > B_R$. We note from the data of Blythe *et al.* (1960) for fluoromethane at 546.0 nm that $B_p = -209 \pm 5 \times 10^{-6}\ m^3\ mol^{-1}$, $A_R = 6.640 \pm 0.007 \times 10^{-6}\ m^3\ mol^{-1}$ and $B_R = 7 \times 10^{-12}\ m^6\ mol^{-2}$. Hence $A_R B_p = 1388 \times 10^{-12}\ m^6\ mol^{-2}$. The uncertainty of $\pm 5 \times 10^{-6}\ m^3\ mol^{-1}$ in B_p leads to an uncertainty of $\pm 35 \times 10^{-12}\ m^6\ mol^{-2}$ in B_R, namely about five times the observed value. An additional uncertainty of about $\pm 66 \times 10^{-12}\ m^6\ mol^{-2}$ is also evident due to scatter in the pressure measurements.

Measurements on the vapours methanol, diethylamine, and triethylamine are less affected by errors in B_p since $B_R >> A_R B_p$. Uncertainties in B_R for these samples arise mainly from scatter in the pressure measurements. The high B_R values for the first two vapours may possibly be due to hydrogen bonding but such effects should not be present in triethylamine. In general, the procedure of deriving B_R from a linear plot of (2.4) is of little use except in the case where B_R is of the same order of magnitude or larger than

$A_R B_p$. For real gases this condition is rarely satisfied and the difficulties encountered by Blythe *et al.* (1960) are likely to be more representative of the difficulties which may be anticipated in measurements of B_R.

Beaume & Coulon (1967) determined R_m for ammonia as a function of pressure and frequency. Plots of their data show that R_m increases as the wavelength of the applied light beam changes from 667.8 to 447.1 nm. Although no values of B_R are given in their paper, values of B_R were deduced from a least squares fit of their data to (2.3). The uncertainties for their measurements are due to uncertainties in B_p. We noted significant disagreement between the values of B_R for ammonia observed by Blythe *et al.* (1960) at λ = 546.0 nm and Beaume & Coulon (1967). Since in both cases B_R was deduced from refractive index measurements made at varying gas pressures, a probable source of the discrepancy is the use of different equations of state. The frequency dependence of B_R is, however, independent of the equation of state and unexpected since the first electronic transition for ammonia occurs in the ultraviolet.

Orcutt & Cole (1967) have reported B_R values for argon, nitrogen and carbon dioxide by fitting the refractive index data of Phillips (1920) and Michels and co-workers (1937; 1947; 1949) to (2.3) using a least squares technique. The results are listed in table 1 and are for the wavelength stated or are averages of data for several wavelengths.

Olson (1975) measured the refractive index of gaseous and liquid methane between 95 and 300K at pressures up to 22500 kPa. The measurements were performed at λ = 546.2 nm using a Fabry-Perot interferometer referred to vacuum. The refractive index measurements (made to an accuracy of ± 0.1%) were combined with density values (accurate to ± 0.1%) derived from data reported by Goodwin & Prydz (1972) to calculate R_m. A B_R value of $5.5 \pm 1.0 \times 10^{-12}\ m^6\ mol^{-2}$ was determined from a least squares fit of this data to (2.3); A_R was determined from a linear plot of $\frac{n^2 - 1}{n^2 + 2}\ \frac{RT}{P}$ versus $\frac{P}{RT}$ as described earlier using low pressure data (300 - 700 kPa) at 300 K.

Hadrich (1975) presents values of B_R for gaseous ethane, propane and n-butane in graphical form as a function of $\frac{1}{T}$. His graphs depict B_R, for these samples, as varying inversely with the temperature. However, no discussion is given of the errors, and uncertainties in these measurements may be large due to uncertainties in the density. These B_R values are not reported in table 1 due to the difficulty of deducing reliable values from the small graphs.

§§2.2 Measurements in which the density is determined directly

Sliwinski (1969) studied the density dependence of R_m in saturated vapours of ethane, propane, n-butane and 2-methylpropane at λ = 589.3 nm using a Mach-Zehnder interferometer. The densities of the vapours were determined pyknometrically and thus avoided the errors introduced in R_m from deducing the density indirectly from pressure measurements and an equation of state. Depending on the pressure range either a glass pyknometer (< 15 atm) or a metal pyknometer (15 atm upwards) was used. The volumes of the pyknometers were measured using the accurately known density of mercury and corrections to the volume as a result of pressure and temperature expansion were determined for each sample. The pyknometer was filled with a sample at a temperature below its boiling point and density variations at constant mass were achieved by varying the temperature of the pyknometer. Changes in the height of the liquid-vapour boundary were measured with the aid of a cathotometer relative to a fixed mark on the pyknometer stem. On the basis of the errors in the weight and volume determinations, an error of about ± 0.01% was obtained in the density measurements. The first refractivity virial coefficient A_R was deduced by extrapolating R_m to zero density and B_R was determined from a least squares fit of the experimental data to (2.3).

In the next chapter we give a detailed description of a precise interferometric technique which allows direct measurement of imperfect gas contributions to R_m (Buckingham & Graham 1974). The technique involves changing the density but not the amount of gas in the optical path. They carried out measurements of B_R at 500 kPa on neon, argon, nitrogen, carbon dioxide, methane, sulphur hexafluoride and trifluoromethane. We note from table 1 that the relative error (typically 20%) for these measurements is significantly reduced compared to those of other workers. This technique has also been exploited by St-Arnaud and Bose (1976) who measured B_R for methane at pressures between 120 to 180 atm†.

† 1 atm ≈ 100 kPa

REFERENCES

Beaume, R. & Coulon, R. 1967 *C.r. hebd. Séanc. Acad. Sci., Paris B* 265, 309.

Blythe, A.R., Lambert, J.D., Petter, P.J. & Spoel, H. 1960 *Proc. R. Soc. Lond. A* 255, 427.

Buckingham, A.D. & Graham, C. 1974 *Proc. R. Soc. Lond A* 336, 275.

Everett, D.H. & Munn, R.J. 1963 *Trans. Faraday Soc.* 59, 2486.

Goodwin, R.D. & Prydz, R. 1972 *J. Res. Nat. Bur. Stand. (U.S.) A* 76, 81.

Hadrich, J. 1975 *Appl. Phys.* 7, 209.

Michels, A. & Hamers, J. 1937 *Physica* 4, 995.

Michels, A., Lebesque, H., Lebesque, L. & de Groot, S.R. 1947 *Physica* 13, 337.

Michels, A. & Botzen, A. 1949 *Physica* 15, 769.

Olson, D. 1975 *J. Chem. Phys.* 63, 474.

Orcutt, R.H. & Cole, R.H. 1967 *J. Chem. Phys.* 46, 697.

Phillips, D. 1920 *Proc. R. Soc. Lond. A* 97, 225.

Sliwinski, P. 1969 *Z. Phys. Chem.* 63, 263.

St-Arnaud, J.M. & Bose, T.K. 1976 *J. Chem. Phys.* 65, 4854.

CHAPTER 3

EXPERIMENTAL METHOD AND APPARATUS

§1. Introduction

Prior to the experiments of Buckingham & Graham (1974) all the determinations of the second refractivity virial coefficient B_R outlined in the previous chapter have been deduced from refractive index measurements made at varying gas pressures. This procedure has suffered from the disadvantage that only a small fraction (approximately 1 part in 10^4 at 500 kPa) of the observed quantity $(n-1)$ is due to gas imperfections, so that small errors in $(n-1)$ or the pressure measurement lead to large errors in B_R.

A new method for the determination of reliable values of B_R by direct measurement of refractive index virial coefficients was described by Buckingham & Graham (1974). Their apparatus has been reassembled and used in this work to extend the range of their measurements and to investigate the wavelength dependence of B_R. We review the principle of operation of this system and give specifications of the apparatus used.

§2. Principle of the method

Consider a beam of light of wavelength λ which is split into two coherent beams, a sample and a reference beam. Suppose that the sample beam is passed through two identical optical cells A and B as in figure 1, and that both emergent beams are in phase when the cells are evacuated.

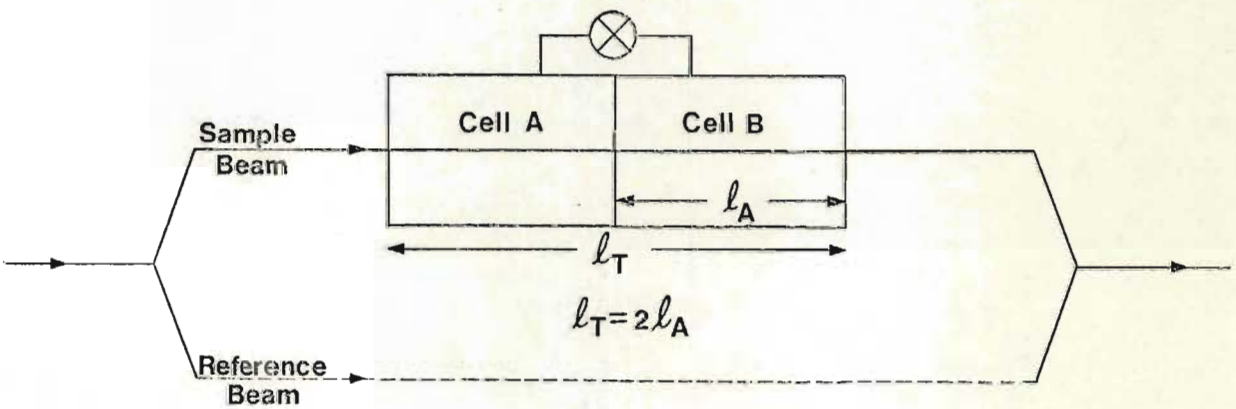

Figure 1. Arrangement of two identical optical cells A and B of path length ℓ_A in a simple decompression experiment to measure refractive index virial coefficients.

If gas is allowed to fill cell A, a phase difference

$$\delta_A = \frac{2\pi \ell_A}{\lambda} (n_1 - 1) \quad , \tag{3.1}$$

results between the sample and reference beams where n_1 is the refractive index of the gas when at equilibrium in cell A. If the same mass of gas were to fill both cells (as after a decompression) the corresponding phase difference compared to the vacuum zero is

$$\delta_B = \frac{2\pi \ell_T}{\lambda} (n_2 - 1) \quad , \tag{3.2}$$

where n_2 is now the refractive index when gas fills both cells at half the original density. The change in phase which would be caused by the decompression of the fixed mass of gas in cell A into cell B is

$$\delta_B - \delta_A = \frac{2\pi \ell_A}{\lambda} \left[2(n_2 - 1) - (n_1 - 1) \right] \quad , \tag{3.3}$$

where $\ell_T = 2\,\ell_A$.

Now, if the quantity $(n - 1)$ were proportional to gas density, $\delta_B - \delta_A$ given by (3.3) would be zero, but departures from proportionality arising from molecular interactions and bulk polarization effects give rise to a non-zero $(\delta_B - \delta_A)$ described by the refractive index virial coefficients $B_n, C_n, \ldots$ defined by

$$(n - 1)V_m = A_n + \frac{B_n}{V_m} + \frac{C_n}{V_m^2} + \ldots \quad , \tag{3.4}$$

where V_m is the molar volume. If this experiment is limited to gas pressures in which a system of molecules may be considered to contain some non-interacting molecules and a proportion of interacting molecular pairs then

$$\delta_B - \delta_A = -\frac{2\pi \ell_A}{\lambda} \frac{B_n}{2V_{m1}^2} \quad , \tag{3.5}$$

where V_{m1} is the molar volume of the gas when it fills cell A. Since the parameters required for the study of short range molecular interactions are the refractivity virial coefficients $B_R, C_R, \ldots$ defined by

$$R_m \equiv \frac{n^2 - 1}{n^2 + 2} V_m = A_R + \frac{B_R}{V_m} + \frac{C_R}{V_m^2} + \ldots \quad , \tag{3.6}$$

(3.4) is used to express R_m in terms of A_n, B_n .... and (3.6) is written as

$$\frac{n^2-1}{n^2+2} V_m = \frac{2}{3} A_n + \left[\frac{2}{3} B_n - \frac{1}{9} A_n^2 \right] \Big/ V_m + \left[\frac{2}{3} C_n - \frac{2}{9} A_n B_n - \frac{4}{27} A_n^3 \right] \Big/ V_m^2 \ , \tag{3.7}$$

to second order in V_m. A comparison of the coefficients of V_m^n in (3.6) and (3.7) shows that

$$A_R = \frac{2}{3} A_n \ , \tag{3.8}$$

$$B_R = \frac{2}{3} B_n - \frac{1}{9} A_n^2 \tag{3.9}$$

and

$$C_R = \frac{2}{3} C_n - \frac{2}{9} A_n B_n - \frac{4}{27} A_n^3 \ . \tag{3.10}$$

Therefore if A_n is measured at low pressure by standard procedures and B_n is measured directly by the decompression experiment described above, B_R may be calculated from (3.9).

In table 1 below known values of B_n at 632.8 nm (Buckingham & Graham 1974) are used to calculate expected values of the fringe shift observed when gas is decompressed from an initial pressure of 500 kPa in a pair of cells each with a length of 0.5 m.

gas	$\frac{10^{12} B_n}{m^6 mol^{-2}}$	$\frac{\delta_B - \delta_A}{rad}$	corresponding number of fringes
Ne	0.33	0.034	0.005
Ar	9.80	1.005	0.160
N_2	8.98	0.921	0.147
CO_2	22.30	2.287	0.364
CH_4	27.05	2.774	0.441
SF_6	94.10	9.650	1.536
CHF_3	23.10	2.369	0.377

Table 1. Estimates of $(\delta_B - \delta_A)$ in a decompression experiment with identical cells with an initial pressure of 500 kPa and length of 0.5 m.

We note that for the above experimental conditions phase changes ranging from 10^{-3} of a fringe to multiples of a fringe may be expected. Most commercially available interferometers have a precision of about 10^{-2} of a fringe which would be inadequate for measurements under the above

conditions. We later describe the design of a Dyson-type interferometer (Dyson 1963; 1968; 1970) with a sensitivity and stability of better than 10^{-4} of a fringe which has been used to obtain precise values of B_n for a range of gases.

§3. The effect of mismatch in the dimensions of the decompression cells : the double decompression technique

In practice it is not possible to construct cells which have *identical* volumes and lengths. We now consider what additional restrictions are implied if *similar* cells are used in the simple decompression experiment.

Consider two similar cells, A and B of volumes

$$V_A = V(1 + \delta) \qquad \text{and} \qquad V_B = V(1 - \delta) \ , \tag{3.11}$$

and lengths

$$\ell_A = \ell(1 + \Delta) \qquad \text{and} \qquad \ell_B = \ell(1 - \Delta) \ , \tag{3.12}$$

where δ and Δ are the deviations from the average volume V and average path length ℓ. Combination of (3.3), (3.4) with (3.11), (3.12) above yields the expression

$$\delta_B - \delta_A = \frac{2\pi\ell}{\lambda}\left[\frac{A_n}{V_{ml}}(\delta - \Delta) + \frac{B_n}{V_{ml}^2}(\delta - \Delta) - \frac{B_n}{2V_{ml}^2} + \cdots\right] \ , \tag{3.13}$$

for the phase change observed when gas decompresses between the similar cells A and B. A comparison of (3.13) with (3.5) for identical cells shows that the ratio

$$\frac{\text{phase change in similar cells}}{\text{phase change in identical cells}}$$

$$= 1 + \frac{A_n}{B_n/V_{ml}}(\Delta - \delta) + 2(\Delta - \delta) + \cdots \ . \tag{3.14}$$

Since the ratio $\dfrac{A_n}{B_n/V_{ml}}$ of the first two terms in the refractive index virial expansion is of the order of 10^4 for a pressure of about 500 kPa at room temperature, it follows from (3.14) that the phase change due to cell defects may be comparable with the change due to B_n in a cell for which $(\Delta - \delta)$ is only about 10^{-4}. Consequently, if B_n is to be evaluated with (3.13) from results of a simple decompression experiment, either $(\Delta - \delta)$ must be known or the volumes and lengths must be matched to better than 1 part in 10^6. However, it has been shown by Buckingham & Graham (1974) that if a

second decompression is performed immediately after the first, the phase changes for the double decompression may be combined to eliminate $(\Delta - \delta)$.

If after the first decompression the valve connecting cells A and B is closed and the cell A is evacuated, then the phase change $(\delta_D - \delta_C)$ observed in decompressing the remaining gas in B into A is

$$(\delta_D - \delta_C) = \frac{2\pi\ell}{\lambda}\left[\frac{A_n(\Delta - \delta)}{V_{m2}} + \frac{B_n}{V_{m2}^2}(\Delta - \delta) - \frac{B_n}{2V_{m2}^2} + \cdots\right], \tag{3.15}$$

where V_{m2} is the molar volume of the gas in cell B after the first decompression.

Substitution of the expression

$$(n - 1) = \frac{A_n}{V_m} + \frac{B_n}{V_m^2} + \cdots \tag{3.16}$$

into (3.13) and (3.15) followed by simplification yields

$$B_n = -\frac{\lambda}{\pi\ell}\left[\frac{\delta_B - \delta_A}{n_1 - 1} + \frac{\delta_D - \delta_C}{n_2 - 1}\right] \Bigg/ \left[\frac{1}{V_{m1}^2(n_1 - 1)} + \frac{1}{V_{m2}^2(n_2 - 1)}\right] + O[(\Delta - \delta)^2], \tag{3.17}$$

where n_1 and n_2 are the refractive indices at the beginning and end of the first decompression. For $V_{m2} \approx 2V_{m1}$ (to within about 0.1%), (3.17) can be written as

$$B_n = -\frac{\lambda}{\pi\ell} V_{m1}^2 \frac{2}{3}[(\delta_B - \delta_A) + 2(\delta_D - \delta_C)] . \tag{3.18}$$

If (3.17) is compared with the expression for the simple decompression using identical cells, namely

$$B_n = -\frac{\lambda}{\pi\ell} V_{m1}^2 (\delta_B - \delta_A)_{\text{identical cells}} , \tag{3.19}$$

we note that the use of similar cells in a *double* decompression experiment results in a combined phase change $\frac{2}{3}[(\delta_B - \delta_A) + 2(\delta_D - \delta_C)]$. Physically this result is meaningful since the contribution from $\frac{A_n}{V_m}$ to the observed phase change in the second expansion of the double-decompression experiment is half of that in the first but of opposite sign, while the contribution from $\frac{B_n}{V_m^2}$ in the second expansion is one-quarter that in the first

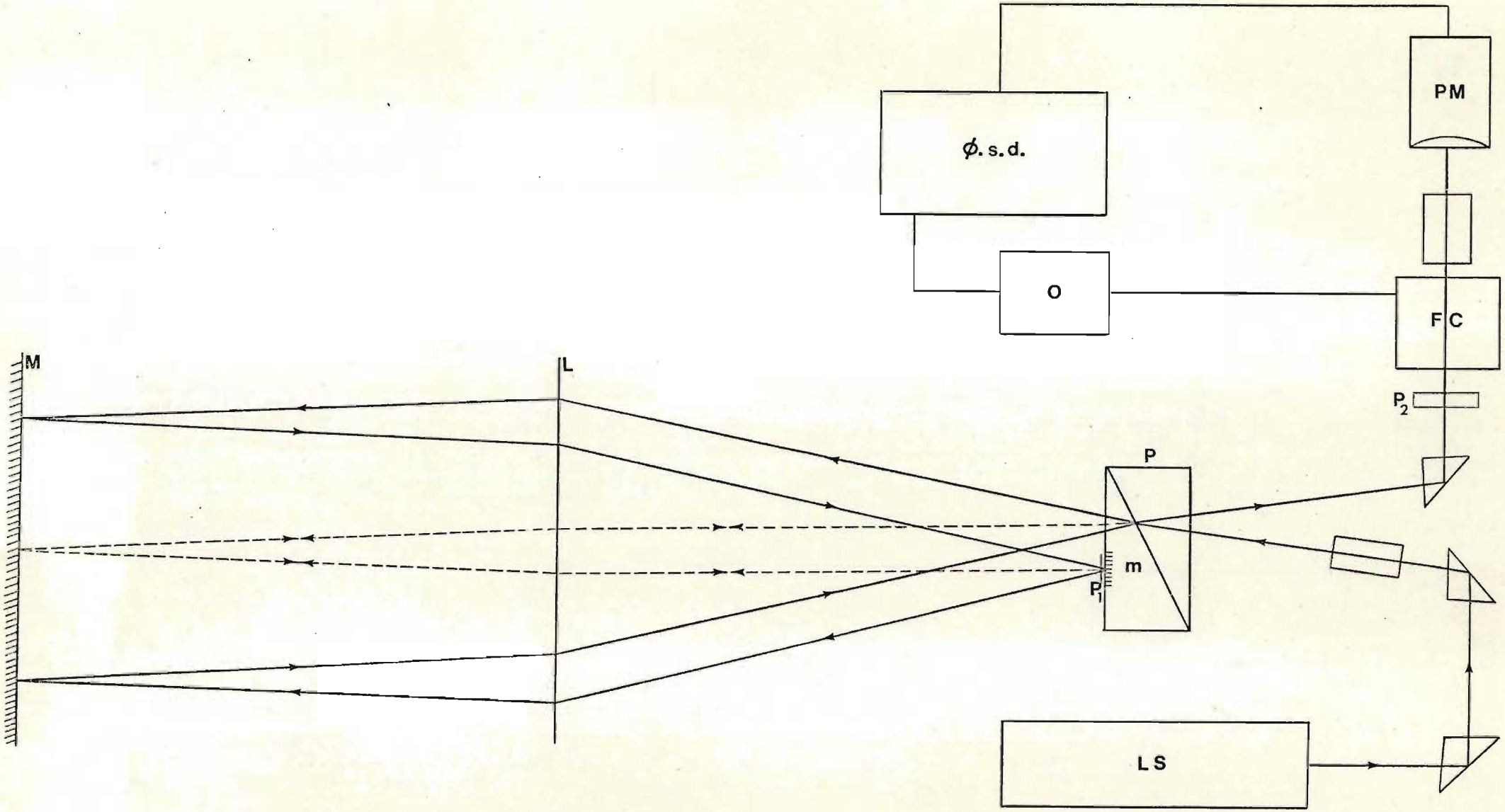

Figure 2. The interferometer and detection system. M, large fused silica mirror; m, small fused silica mirror; L, lens; P_1, P_2, quarter-wave plates; P, Wollaston prism; LS, laser; FC, Faraday modulation solenoid; PM, photomultiplier; φ.s.d., phase-sensitive detector; O, oscillator.

but of the same sign. The combination $(\delta_B - \delta_A) + 2(\delta_D - \delta_C)$ eliminates the A_n term and gives one and a half times the phase change due to B_n using identical cells in a simple decompression experiment.

§4. Interferometric measurement of phase changes on decompression

§§4.1 The interferometer

The Dyson-type polarization interferometer (Dyson 1963; 1968; 1970) shown in figure 2 has been successfully adapted by Buckingham & Graham (1974) to measure phase changes in a decompression experiment. The interferometer produces a single polarized output beam in which the state of polarization varies with the path difference experienced by two beams within the interferometer before they are recombined to interfere. Polarization modulation and phase-sensitive detection techniques have been used to measure changes in the state of polarization of the output beam and a sensitivity and stability of 10^{-4} of a fringe has been achieved consistently.

A laser beam polarized at 45° to the horizontal is split by a Wollaston prism P, into two diverging beams linearly polarized in the horizontal and vertical planes respectively. The prism is at one prime focus of a double convex lens L, and a plane mirror M is placed at the other. The two beams (a reference beam indicated by a broken line and a sample beam indicated by a continuous line) travel parallel to each other after passing through L and are reflected back by M towards a small mirror m near the Wollaston. After reflection at m the reference beam retraces its initial path, and re-enters the Wollaston while the sample beam is reflected backwards and forwards along the path shown before it also re-enters the Wollaston. A quarter-wave plate is placed in front of the small mirror m, as shown, with its fast or slow axis at 45° to the horizontal. Since each beam makes a double traverse of this plate, its effect is that of a half-wave plate which rotates each plane of polarization through 90°. This ensures that the two return beams emerge as a single polarized beam inclined at a small angle (nearly equal to the splitting angle of the Wollaston) to the direction of the incident beam. The output of the interferometer will in general be elliptically polarized with the azimuth of the ellipse at 45° to the horizontal.

The decompression cells A and B and a reference cell R are positioned between the lens L and mirror M. The polarization state of the output beam will then be sensitive to any change in the optical paths in cells A and B which are not counteracted by an equal change of path in the reference cell.

The folded symmetry of the light paths renders the interferometer insensitive to any small movements of the mirror M which do not distort it. In particular, a rotation of the mirror about its central point leaves the path length of the reference beam unchanged while the path length of the sample beam is increased at one point on M and decreased at the other, so that no net path difference is indicated by the interferometer. Lateral movements of M have no effect and translations along the axis affects the path lengths of the sample and reference beams equally.

This remarkable stability makes it suitable for measuring phase changes in our decompression experiment which requires the mechanical operation of a valve connecting cells A and B.

§§4.2 Measurement of path difference by a null-detection method

For some of the gases in our range the path difference expected during decompression will be of the order of 10^{-3} of a fringe (see table 1), for an initial pressure of 500 kPa at room temperature and a path length of 0.5 m, so that precise detection techniques will be necessary. Significant advances have been made in the measurement of small optical path differences by modulation and phase-sensitive detection techniques (Danby 1970).

The output beam of the interferometer will in general be elliptically polarized and since the linearly polarized component beams are equally intense, the axes of the ellipse will be at 45° to the directions of the component vibrations. If a quarter-wave plate is placed in the output beam and oriented with its fast and slow axis along the axes of the ellipse, the beam becomes linearly polarized. The direction of vibration of this beam depends on the phase difference ϕ between the component beams. This direction is determined with an analyser mounted in a divided circle. If the analyser is set for extinction of the linearly polarized beam emerging from the quarter-wave plate and a phase difference ϕ is induced between the interfering beams, the analyser has to be rotated through an angle

$$\theta = \phi/2 \quad , \tag{3.20}$$

to regain extinction.

Measurement of θ resulting from the decompression of gas from A into B is made by a nulling procedure. The analyser is adjusted at the beginning of the experiment for the extinction of the transmitted beam and the setting is noted. Gas is now decompressed from A to B and the analyser is continuously adjusted to maintain extinction. When equilibrium has been

reached the decompression valve is closed and the angle θ is calculated from the final reading on the divided circle.

Precision in the setting of the analyser for extinction is enhanced by a modulation and phase-sensitive detection system shown in figure 2. The linearly polarized beam emerging from the quarter-wave plate is passed through a Faraday modulation cell and an analyser, and a modulated intensity is detected by a photomultiplier. If the analyser is set at an angle γ from the position required for extinction, the transmitted flux I through the analyser is given by Malus' Law as

$$I = I_s + I_o \sin^2\gamma \quad , \tag{3.21}$$

where I_s is a small transmitted intensity arising from the incomplete extinction of the beam due to apparatus imperfections. The Faraday modulation cell is driven by an alternating voltage and superimposes a modulated rotation $\theta_F = \theta_m \sin 2\pi\nu t$ of amplitude θ_m and frequency ν upon the initial rotation γ. The transmitted flux at the photomultiplier becomes

$$I = I_s + I_o \sin^2(\gamma + \theta_F) \quad . \tag{3.22}$$

For small θ_F this may be written in the form

$$I = I_s + I_o\theta_m^2\sin^2 2\pi\nu t \cos^2\gamma + I_o\sin^2\gamma + I_o\theta_m \sin 2\pi\nu t \sin 2\gamma \quad . \tag{3.23}$$

Since the flux intensity I is proportional to the anode current of the photomultiplier, the output from the photomultiplier consists of a d.c. voltage modulated by an a.c. voltage. This signal was fed into an a.c. coupled phase-sensitive detector whose reference frequency was derived from the voltage source driving the Faraday modulation cell.

We note from (3.23) that the terms I_s and $I_o\sin^2\gamma$ give rise to d.c. photomultiplier output voltages which have no effect on the a.c. coupled phase-sensitive detector, while the term $I_o\theta_m^2 \sin^2 2\pi\nu t \cos^2\gamma$ gives rise to a signal of frequency 2ν against a small d.c. background. Since the phase-sensitive detector is tuned to the modulation frequency ν this term makes no contribution to the phase-sensitive detector output. The d.c. output of the phase-sensitive detector therefore arises from the term $I_o\theta_m \sin 2\pi\nu t \sin 2\gamma$ and is proportional to $\sin 2\gamma$. When $\gamma = 0$ or 90°, the output of the phase-sensitive detector is zero and when $\gamma = 45^\circ$ it is a maximum. In order to determine the true zero (i.e. when the plane of the analyser is crossed with respect to the plane of polarization of the emergent beam) the photomultiplier

output is monitored on a d.c. coupled oscilloscope. A zero output from the phase-sensitive detector which is confirmed by a zero output on the oscilloscope indicates unambiguously that $\gamma = 0$ (note γ is the angle of uncrossing). This system enables the analyser to be adjusted with a sensitivity of about 10^{-4} of a fringe or better.

Moreover since $\sin 2\gamma$ is a signed quantity and since the sign of γ depends on whether the optical path is decreasing or increasing, the sense of deflection of the phase-sensitive detector output meter may be used to deduce the sign of B_n. To do this the analyser is set for extinction, a small amount of gas is admitted to the sample cells, and the direction in which the phase-sensitive detector meter deflects for the increase in path is noted.

In measurements of A_n, the sample cells A and B are evacuated and the analyser is set for extinction. Gas is fed slowly into the cells and the output of the phase-sensitive detector is recorded on a strip chart recorder. The total number of complete fringes is determined from the chart and fractions of a fringe are measured by the nulling procedure.

§5. Details of the apparatus

§§5.1 Mounting and housing of the interferometer

The optical components of the interferometer and a Faraday modulation cell were mounted on a 2 m optical bench with standard optical bench fittings capable of vertical and lateral movement. The Wollaston prism P was positioned midway along the bench and the stainless-steel decompression cells and a reference cell were mounted adjacent to each other in the space between the lens L and mirror M. In order to prevent air currents from disturbing the interferometer output, the whole optical system was enclosed. This was achieved by bolting the 2 m bench to an aluminium plate 2.2 m long, 0.36 m wide and 6.0 mm thick. A foam-lined aluminium housing 0.36 m deep was then bolted onto the aluminium plate completely enclosing the interferometer. The system was mounted on three 36 kg adjustable steel feet, two of which were bolted to the base of the large aluminium housing, whilst the third was secured on a heavy protruding aluminium bracket attached to the base-plate at two points near its centre. The three point mounting rested on steel discs placed on a large terazzo-top table supported by brick walls. The laser was mounted on a heavy I-beam section supported by a wing of the table at right-angles to the optical bench.

In order to discuss the apparatus in greater detail, the apparatus is subdivided into three systems :

1. The optical system,
2. the decompression cells and gas handling system,
3. the photomultiplier and phase-sensitive detection system.

§6. The optical system

§§6.1 Introduction

The optical system of the interferometer comprises a number of components whose specifications and design have a marked influence on the performance of the apparatus. The most critical components are the laser light source, the Wollaston prism, the mirror M and the lens. In this section we discuss some of the design considerations and specifications of these components. A procedure for the alignment of the optical system is described.

§§6.2 The laser light source

Buckingham & Graham (1974) found that the interferometer was extremely sensitive to instabilities in the direction of the laser beam. They noted fluctuations of about 10^{-2} to 5×10^{-2} of a fringe while conducting trial measurements with a 1.0 mW Scientifica and Cook B17/SH He-Ne laser, and the same effects were observed with the high stability 8 mW Scientifica and Cook B18/3 He-Ne laser. Further tests with a 5 mW Spectra-Physics model 120 He-Ne laser reduced the instabilities by about a factor of 50 . A possible reason for this improvement is that the plasma tube bore to length ratio of the Spectra-Physics laser is much smaller than the Scientifica and Cook laser and thus limited instabilities in the direction of the beam.

Our measurements of B_R were made at four wavelengths (407.9 nm, 488.0 nm, 514.5 nm and 632.8 nm) in the visible. The first three wavelengths spanned the blue-green spectral range of a 2.5 W Spectra-Physics model 165 Argon Ion laser, while the fourth wavelength is the red spectral line of a 5 mW Spectra-Physics model 120 He-Ne laser. The argon ion laser has a variable power output and was operated between 3 and 5 mW. During our trial measurements troublesome fluctuations occurred if the optics of the argon ion laser were not adjusted for optimum power. Fine adjustments to the beam output power were made with a Spectra-Physics model 404 power meter. No similar fluctuations occurred with the He-Ne laser and a sensitivity of better than 10^{-4} of a fringe was achieved. The long term stability over a 30-minute period

was typically 10^{-3} of a fringe although this approached 10^{-4} of a fringe depending on the amount of activity in or near the laboratory.

§§6.3 The Wollaston prism, mirror M and lens

The calcite Wollaston prism used in our interferometer was designed by Graham (1971) and has an aperture of 1 sq. cm and a prism angle of 5°. His design calculations showed that if a beam with λ = 632.8 nm, polarized at 45° to the horizontal enters the Wollaston obliquely at 0.85° to the normal, then two beams will emerge with an angular separation of 1.75° with one beam emerging normal to the exit face. This angular shear produced a separation of 1.5 cm between beam centres over a distance of 50 cm, so that cells 45 cm long with centres 1.5 cm apart, could be accommodated between the lens L and mirror M. After passing through the interferometer system, the sample and reference beams are recombined by the Wollaston and emerge as a single beam at an angle of 1.71° to the incident beam on the opposite side of the normal. Although the angular separation of the beams is a function of the wavelength of the incident light beam, we note from table 2 that

λ	angle of shear	beam separation
nm	degrees	cm
404.6	1.85	1.61
480.0	1.78	1.55
508.6	1.76	1.54
632.8	1.75	1.50

Table 2. Variation of beam separation with wavelength for a Wollaston to lens distance of 0.5 m.

only small changes resulted in the separation for other wavelengths in the visible. These changes were easily accommodated in cells with an i.d. of 1.2 cm.

It was shown in §§4.1 that the interferometer is insensitive to small movements of the mirror M, provided its shape is unchanged. In an attempt to minimize the effects of thermal distortion of the mirror, we used a fused silica mirror 6 cm in diameter and 1.5 cm thick. The aluminized surface was flat to $\lambda/10$ of the mercury green line. The double convex lens L was 5 cm in diameter with spherical surfaces correct to $\lambda/10$, and with a focal length of 50 cm for 632.8 nm.

§§6.4 The alignment of the optical system

It is essential to follow a systematic alignment procedure to realize the required geometrical arrangement of the interferometer (as shown in figure 2) if frustrating and time-consuming difficulties are to be avoided.

To ensure that the reference beam emerges normal to the exit face of the Wollaston, and travels parallel to the optical bench, it is important to adjust the angle of incidence at the Wollaston to the calculated value. This is achieved by passing the laser beam through light stops which have calculated offsets from the centre of the bench. It is also important to note, that since the reference beam traverses laterally symmetric paths equally offset from the centre of the bench, the point of incidence at the Wollaston must be offset from the bench axis, the amount of offset determining the beam separation. For cells of 1 cm diameter we found a beam separation of 6 mm to be satisfactory, so that the incident beam had to enter the Wollaston 3 mm off axis. The initial alignment arrangement is summarized in the figure below, where the dotted lines indicate the ultimate positions of the mirror M, lens L and Wollaston P.

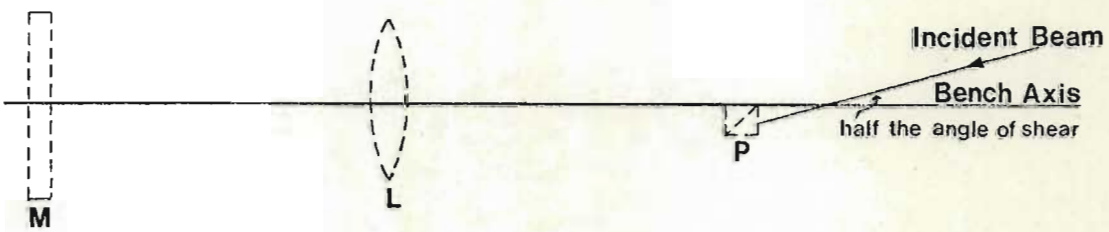

The stops determine the incident angle as well as the beam offset. They must clearly be of equal height above the bench so that the emergent beams lie in a horizontal plane, with the reference beam travelling parallel to axis of the bench. Indeed, a final check that stops have been correctly positioned is made by noting if the reference beam is parallel to the optical bench. This is readily done by mounting a screen on an optical bench saddle, which is moved along the bench : with the Wollaston in position the point of incidence of the reference beam on the screen must remain fixed. If this is not achieved at this stage suitable adjustments *must* be made.

The mirror M is now placed at a distance 2f from the Wollaston, where f is the focal length of the lens. (Note that the lens is not yet in

position.) Careful adjustments of the large mirror are made until the reflected reference beam retraces its outward path, as shown below.

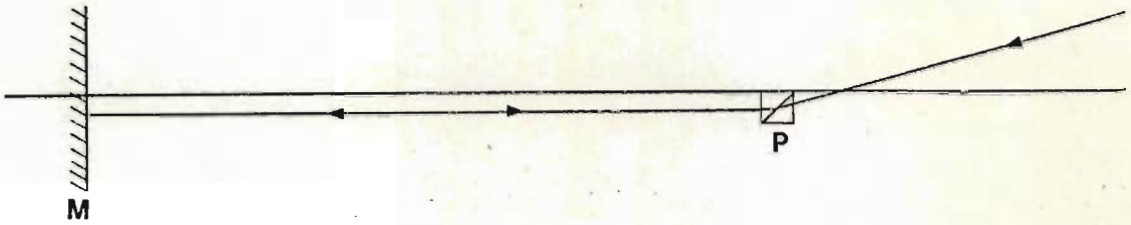

(We found it useful, at this stage, to stop out the sample beam. Rigorous constraints on the reference beam are sufficient to ensure alignment, whilst the unnecessary presence of the sample beam with its multiple traverses of the system usually leads to a confusing array of light spots.)

The lens is now placed in position midway between the Wollaston and mirror, with its principal axis directly above and parallel to the optical bench, at a height equal to that of the laser beams. The small mirror m is positioned next to the Wollaston, and adjusted until the four spots, where

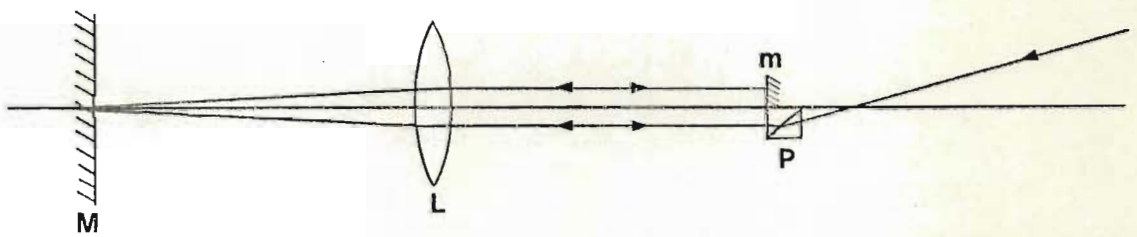

the outward and return reference beams strike the lens, merge into two. If the stop is now removed there should be *three pairs* of spots on the lens and three single spots on the mirror M. When the quarter-wave plate is positioned there should be a single output beam. This beam is now passed through the second quarter-wave plate and an analyser. It is helpful if a screen is positioned after the analyser to allow visual observation of the output beam. The analyser is now adjusted for extinction and the residual intensity is minimized by adjusting the distance of the lens from the mirror. Poor

adjustment of the lens position is recognized by the presence of a series of fine light and dark bands which shift across the diameter of the beam as the beam is moved slightly. As the lens approaches its correct position, the interference bands become wider until the whole diameter of the beam becomes uniformly illuminated. Alignment is now complete. With our optical system we have achieved an extinction ratio of typically 1 in 18.

§7. The decompression cells and gas-handling system

§§7.1 Introduction

In §3. of this chapter we described how in principle the double decompression technique eliminates the need to use identical cells. However, we note from (3.18) that B_n is proportional to the combined phase changes $(\delta_B - \delta_A) + 2(\delta_D - \delta_C)$ observed in a double decompression experiment. $(\delta_B - \delta_A)$ and $(\delta_D - \delta_C)$ each have two components, one due to cell defects and one due to virial effects. Since the contributions due to cell defects are opposite in sign and those due to virial effects have the same sign, we may in principle eliminate cell defects by taking the combination $(\delta_B - \delta_A) + 2(\delta_D - \delta_C)$. However, if the cells are poorly matched the major part of $(\delta_B - \delta_A)$ and $(\delta_D - \delta_C)$ would be due to cell defects and $(\delta_B - \delta_A) + 2(\delta_D - \delta_C)$ is the difference between two large numbers. Errors in $(\delta_B - \delta_A)$ and $(\delta_D - \delta_C)$ could swamp the desired observables. Therefore, it is advisable to use cells which are well matched for precise measurements of B_n in a double decompression experiment.

The cells used in our measurements of B_n were built by Buckingham & Graham (1974) and have lengths which are matched to better than 5 parts in 10^5 (a tolerance of 0.002 cm over a length of 42 cm). To enable compensation for any mismatch in the volumes of the cells, the decompression valve was connected to each cell through an additional valve which was always left open. The volumes of the cells were adjusted by fractionally advancing or withdrawing the stems of the open valves.

§§7.2 Specifications and construction details of the decompression cells

The sample and reference cells consisted of three 321 stainless-steel tubes each 43 cm long, with o.d. 1.58 cm and i.d. 1.16 cm, which were vacuum-brazed into machined stainless-steel end-blocks 8.0 cm wide, 4.5 cm high and 2.5 cm thick. The cells lay side by side almost touching in order to achieve maximum wall thickness. The end-blocks were vacuum-brazed to a base-plate 42 cm long and 6 mm thick. Additional plates were bolted into position on

the top and sides to form a water jacket and to provide extra rigidity. Standard Gyrolok fittings screwed into tapered holes in the end-blocks provided connections for the gas inlet valves at one end, while the decompression valve was connected through the volume-equalizing valves at the other. Hoke packless vacuum valves with non-rotating stems were used and the decompression valve had fine metering capabilities. This allowed fringe shifts to be followed continuously. The faces of the end-blocks were initially machined flat to better than 10^{-3} cm and were then lapped flat to one wavelength of the mercury green line. Glass windows, $2.5 \times 6.0 \times 0.25$ cm, which were flat to $\lambda/10$ were clamped across the three cells at each end by stainless-steel bulkheads. Three holes in each bulkhead which corresponded in size and position to the inner diameters of the three cells allowed the transmission of the interferometer light beams. It is important that the windows of the cells have a very low inherent strain which does not vary with a change in pressure during decompression, since this could affect the polarization state of the output beam and lead to an additional spurious phase change. Pockels glass eliminates this difficulty and only windows of this glass were used. In order to ensure a leak tight seal between the optically flat windows and stainless-steel end-blocks, a thin gasket of Kel-F grease was applied to the metal surface. The window seals and the fittings of the cells were leak tested with a helium leak detector by filling each cell in turn with helium to about 500 kPa and testing for leaks between the cells and to the atmosphere. The cells were only considered suitable for use when no leakage could be detected indicating that the leak rate was less than 10^{-8} cm^3 s^{-1} of helium at s.t.p. During the course of experiments tests were frequently carried out, using the interferometer as a leak detector, to check that there was no leakage between cells and to the atmosphere but no such leakage was ever detected during any of our runs.

Although refractivity virial coefficients do not depend strongly on temperature, it is necessary to temperature control the decompression cells to ensure that the temperatures and therefore dimensions of the cells are the same before and after decompression. Water from a 10 litre reservoir was circulated constantly through two water jackets, one surrounding the cells and the other containing the body and connections of the decompression valve. The circulating water temperature was measured to a tenth of a degree with a Hewlett Packard model 2802A digital thermometer. This temperature was used as a measure of the temperature of the gas in the cells. During a 6 hr period the cell temperature was maintained constant to within 1°C.

window. When operated at the recommended operating voltage of -990 V the tube produced a current amplification of approximately 2×10^6 with a low dark current of 1 nA. The tube was powered by a stabilized high voltage Fluke model 412B d.c. power supply.

The photomultiplier was connected to a Brookdeal FL 355 phase-sensitive detector incorporating a MS 320 phase shifter. The reference signal of the phase-sensitive detector was derived from a Marconi audio oscillator which also powered the Faraday modulation cell. The geometrical and electrical parameters for our Faraday modulation solenoid are summarized in table 3 below. The symbols a_1, a_2 and ℓ are given in figure 4.

a_1 / cm	a_2 / cm	ℓ / cm	power / mW	resistance / Ω	current / mA	number of turns
0.65	1.6	30	180	16	106	6506

Table 3. The electrical and geometrical parameters of the Faraday modulation solenoid.

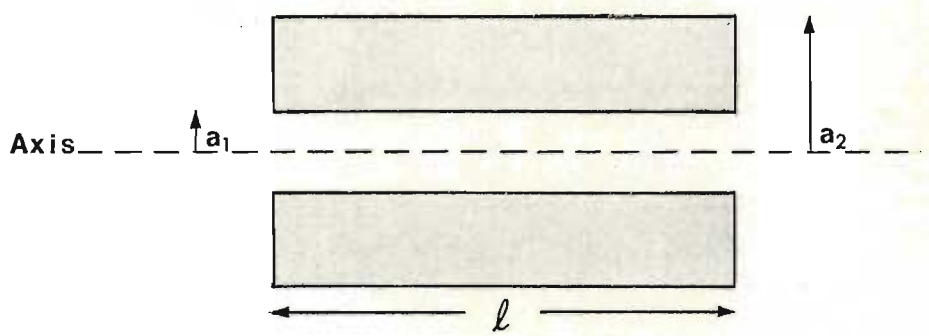

Figure 4. Representation of the solenoid dimensions.

The solenoid was wound with 22 S.W.G. copper wire. An optical cell containing carbon disulphide was placed within the solenoid and for a solenoid current of 106 mA produced a modulation amplitude of 1° for $\lambda = 632.8$ nm.

REFERENCES

Buckingham, A.D. & Graham, C. 1974 *Proc. R. Soc. Lond. A* 336, 275.

Danby, P.C.G. 1970 *Signal recovery using a phase-sensitive detector.* Brookdeal Electronics Limited.

Dyson, J. 1963 *J. Opt. Soc. Am.* 53, 690.

Dyson, J. 1968 *Appl. Opt.* 7, 569.

Dyson, J. 1970 *Interferometry as a measuring tool.* London : Machinery Publishing Company.

Graham, C. 1971 Ph.D. thesis, University of Cambridge.

CHAPTER 4

EXPERIMENTAL TECHNIQUES AND ERRORS

§1. Introduction

In the following sections a detailed analysis is given of the possible errors in measurements of B_n arising from imbalance between the sample cell volumes, gas leaks, surface adsorption of the decompressed gases, cell distortion and uncertainties due to drift of the interferometer output.

§2. Volume matching of the sample cells and errors due to changes in their relative volumes

In §3. of chapter 3 we showed how B_n may be calculated from the initial and final phase changes of a double decompression experiment using the expression

$$B_n = - \frac{\lambda}{\pi \ell} V_{m1}^2 \frac{2}{3} \left[(\delta_B - \delta_A) + 2(\delta_D - \delta_C) \right] , \qquad (4.1)$$

provided the volumes and lengths of the sample cells are well matched. The provision that the lengths of the cells should be well matched was satisfied during construction, by securely mounting the cell tubes between end-blocks which were subsequently machined parallel and then lapped flat to give an overall tolerance in the lengths of 0.002 cm in 42 cm. The cell volumes were matched to an accuracy of about 5 parts in 10^5 by adjusting the volume-equalizing valves according to the following procedure : With the sample cell in position in the interferometer, the analyser was adjusted for extinction of the interferometer output and the direction of rotation of the analyser was noted when air was slowly bled into an evacuated sample cell; this established the response of the phase-sensitive detector to an increase of optical path. Both cells were now evacuated and filtered dry air at atmospheric pressure was allowed to fill cell A. The air was then decompressed into cell B and the phase change was measured by a nulling procedure. The direction of rotation of the analyser was used to establish whether the optical path was increasing or decreasing and hence the relative sizes of the sample cells were deduced with the assumption that virial effects in nitrogen at these low pressures are negligible. After evacuating both cells once more, and filling cell B with air, a similar decompression experiment was performed to confirm the results of the first experiment. The volume mismatch was calculated from the observed phase change and suitable adjustments were made to the volume-equalizing valves by advancing or withdrawing the

valve stems. A further decompression was carried out to establish whether the adjustments had been made correctly. If required ultra fine adjustments to the volumes could be calculated according to the following procedure which does not neglect virial effects. A decompression experiment is carried out with sulphur hexafluoride at a pressure of 250 kPa (since it has a large $A_n = 17.01 \times 10^{-6}\ m^3\ mol^{-1}$ at 632.8 nm) and the initial phase change $(\delta_B - \delta_A)$ and final phase change $(\delta_D - \delta_C)$ are noted. For unmatched cells the phase changes $(\delta_B - \delta_A)$ and $(\delta_D - \delta_C)$ each have two components, one due to cell defects δ_{defect} and one due to virial effects δ_{virial}. The contribution δ_{virial} varies as the inverse square of the initial molar volume and its sign is independent of the relative volumes of the sample cells. The magnitude of δ_{defect} varies as the inverse of the initial molar volume and its sign depends on the relative volumes of the sample cells. For the two decompression experiments we may write,

$$\delta_B - \delta_A = -\delta_{virial} + \delta_{defect}$$

and

$$\delta_D - \delta_C = -\frac{\delta_{virial}}{4} - \frac{\delta_{defect}}{2}\ , \qquad (4.2)$$

and knowing the quantities on the left-hand side of (4.2) solve for δ_{virial} and δ_{defect}. The phase change δ_{defect} may now be used to calculate the volume mismatch and fine adjustments can be made to the volume-equalizing valves. In the absence of cell defects the ratio between the initial and final phase changes should be 4 : 1 .

In practice the 4 : 1 ratio was generally realized at the commencement of a set of readings but shifts were noted in the course of measurements, probably due to wear in the valves. For sample cells of the dimensions used in our experiments, (namely 42 cm long and 1 cm internal diameter), (3.13) may be used to show that if cell A is filled with nitrogen to a pressure of 500 kPa at room temperature and the volume of cell B is altered by 0.002 cm^3 , a shift of 7^o in the observed phase change θ will occur on decompression. This error is proportional to A_n , which for nitrogen is $6.69 \times 10^{-6}\ m^3\ mol^{-1}$ at λ = 632.8 nm; for sulphur hexafluoride with $A_n = 17.01 \times 10^{-6}\ m^3\ mol^{-1}$ the shift in θ would be 18^o .

If the Hoke sample cell valves are closed an additional tenth of a turn, a volume change of 0.002 cm^3 is possible for cells of the above dimensions. It is therefore important to apply the same torque consistently when closing the valves to the sample cells. Furthermore, repeated operation of a sample cell can result in wear of the surfaces of the valve seat and stem. Since

one of the sample cell valves was opened and closed twice as often as the other during decompression experiments, uneven wear resulted and frequent adjustment of the cell volumes was necessary. A similar change in volume can occur if dust particles are forced into a sample cell during filling. Consequently, all gas samples were filtered by passing them through two Hoke sintered metal sieves which removed particles with a diameter of 2 microns and larger.

§3. Errors due to gas leaks in the sample cells

A spurious change in optical path can arise during decompression if gas leaks from the sample cells. For our geometrical arrangement of the sample and reference cells four distinct types of leak are possible, namely:

(a) gas leakage from a pressurized sample cell into the atmosphere,

(b) gas leakage from a pressurized sample cell into the reference cell,

(c) gas leakage into an evacuated sample cell from the atmosphere, and

(d) gas leakage from the reference cell (at atmospheric pressure) into an evacuated sample cell.

Since the reference beam in our interferometer makes a double traverse of the reference cell, the admission of a given mass of gas to this cell will have twice the effect of withdrawing the same mass of gas from one sample cell, and a leak from sample to reference cells has three times the effect of a leak of the same size between a sample cell and the atmosphere. Fortunately, the effects of gas leaks on the interferometer output are easily recognized since even a small leak rate, for example, 10^{-5} cm^3 s^{-1} of methane at a pressure of 500 kPa at room temperature from one of our cells will produce a large spurious phase change of 15° in 300 s. Nevertheless, the fittings of the sample and reference cells and the Kel-F gaskets of the cell windows were rigorously checked at frequent intervals (both under vacuum and pressure) throughout our measurements, to ensure that all leakage was below the sensitivity limit (10^{-8} cm^3 s^{-1} at s.t.p.) of our helium leak detector.

§4. Possible errors due to surface adsorption of gas during decompression

Suppose a pressurized sample of gas at equilibrium is decompressed from one cell into the other which has previously been evacuated. Some of the gas may be adsorbed onto the surface of the second cell resulting in a decrease in the number of free molecules contributing to the optical path. This adsorption may to some extent be compensated by desorption of gas mole-

cules from the surface of the first cell which gives rise to an increase in the number of free molecules. If the amount of gas adsorbed onto the surface of a cell is directly proportional to the pressure, then for a system at equilibrium adsorption and desorption should compensate each other exactly and there will be no error in the observed phase change. Any imbalance between the extents of adsorption and desorption will give rise to a spurious change in optical path.

Buckingham & Graham (1974) using (3.3) and (3.4) of chapter 3 derived the expression

$$\delta_{\text{adsorption}} = -\frac{4\pi\ell}{\lambda}\,\frac{A_n}{V_{m1}}\,\frac{\Delta\mu}{\mu_1}\quad , \tag{4.3}$$

for the phase change due to adsorption in identical cells. Here ℓ is the length of a cell in which there are initially μ_1 free moles of gas and $\Delta\mu$ is the net loss in the number of free moles at equilibrium after decompression. Due to the absence in the literature of adsorption data for stainless-steel at pressuresgreater than 10 kPa, they were unable to evaluate (4.3) for a high pressure (~ 500 kPa) decompression experiment using stainless-steel cells; but the adsorption data for carbon dioxide on silica glass at pressures up to 100 kPa given by Moles (1938) and Hartley, Henry & Whytlaw-Gray (1939) was used to make a rough estimate of the approximate magnitude of errors due to adsorption. Their calculations using (4.3) above and (3.5) of chapter 3 showed that if a silica cell A contains carbon dioxide at a pressure of 200 kPa at 294 K, and 1.45×10^{-8} m^3 m^{-2} of gas at 294 K and 100 kPa is adsorbed onto the walls of cell B after decompression, 3.5% of the observed phase change may be due to adsorption if any compensation from possible desorption is neglected. They noted, however, that for many of the gases studied to pressures of 100 kPa by Moles (1938) and Hartley *et al.* (1939) the adsorption varied approximately linearly with pressure, indicating that compensation by desorption should occur and significantly reduce the percentage error.

Observations of the ratio of the phase changes in the first and second decompressions support the conclusion that either adsorption is negligible or compensation of this type does in fact occur in stainless-steel cells at higher pressures. In table 1 below we list values of B_n for methane and its fluorinated derivatives obtained by the double decompression technique using accurately matched sample cells with λ = 632.8 nm .

gas	initial pressure	temperature	initial phase change	final phase change	ratio	10^{12} B_n
	kPa	K	rad	rad		m^6 mol^{-2}
CH_4	439.02	292.9	3.818	0.880	4.3 : 1	28.20
CH_3F	438.54	296.2	3.058	0.757	4.0 : 1	22.40
CH_2F_2	438.58	296.8	2.028	0.471	4.3 : 1	14.31
CHF_3	438.79	294.7	2.847	0.719	4.0 : 1	21.12
CF_4	432.99	288.4	3.343	0.850	3.9 : 1	25.06

Table 1. Measurements of B_n for methane and its fluorinated derivatives.

The ratio of the initial phase change to the final phase change for each gas is given in column six. For identical sample cells this ratio should be 4 : 1 since the phase change due to virial effects varies as the inverse square of the molar volume. Any imbalance between the compensating effects of adsorption and desorption in a decompression experiment will lead to a loss of gas from the optical path in each decompression, and significant deviations from the ideal 4 : 1 ratio could indicate the presence of surface adsorption effects. The 4 : 1 ratio could, however, be retained even in the presence of uncompensated adsorption effects if the amount of gas adsorbed is *itself* proportional to the inverse square of the molar volume. We note from table 1 that deviations from the 4 : 1 ratio are small, even for the polar gases CH_3F, CH_2F_2 and CHF_3 for which adsorption effects may be expected to be at their greatest. We conclude that adsorption effects are either negligible or compensated, or that adsorption is proportional to the inverse square of the molar volume. To exclude the latter possibility (which would imply uncertainty in the measured B_n values) the surface-to-volume ratio of the cells was artificially increased by about 46% to change the *extent* of adsorption. This was achieved by placing 120 , 3.5 mm diameter stainless-steel ball-bearings inside each sample cell. The volumes were matched by weighing (assuming the density of each ball to be constant) and the cell volumes were accurately matched by the low-pressure matching procedure described in §2. Three measurements of B_n were obtained for each of the gases, methane and trifluoromethane before and after the balls were in position and the averages are summarized in table 2. The detailed measurements are given in table 28.1 of chapter 5.

	CH_4	CHF_3
	$10^{12}\ B_n$ / $m^6\ mol^{-2}$	
without balls in cells	25.32	21.92
with balls in cells	25.21	22.07

Table 2. Measurements of B_n for CH_4 and CHF_3 at a pressure of 439 kPa before and after increasing the surface-to-volume ratio of the sample cells.

We note from table 2 that our measurements of B_n indicate no significant change in the amount of gas adsorbed and we conclude that surface adsorption effects are negligible or compensation occurs.

§5. Errors due to changes in the dimensions of the cells with pressure

Elastic distortion of a sample cell arises whenever there is a pressure gradient across its walls. In a decompression experiment cell B is initially under vacuum and cell A is filled with gas at a high pressure causing its length and volume to increase fractionally. On decompression the gas in cell A should expand into a cell of equal dimensions, but it decompresses into a cell B which is relatively smaller in volume. This results in an increase in optical path which is enhanced by the additional gas forced into the path as the volume of cell A diminishes.

For cylindrical cells the spurious phase change arising from cell distortion depends on the radial deformation of a cell to first order in the distortions (Buckingham & Graham 1974) and is given by the expression

$$\delta_{\text{distortion}} = \frac{4\pi\ell}{\lambda} \frac{A_n}{V_{ml}} \frac{\Delta R_i}{R_i} \quad , \tag{4.4}$$

where ℓ is the undistorted length of a cell, R_i is the internal radius of an unstrained cell and ΔR_i is the change in radius due to an initial absolute pressure P of a gas in a sample cell. There are no errors to first order in the distortion $\Delta\ell$ of the length. If a cylindrical cell of internal and external radii R_i and R_e is subjected to an uniform pressure along its length from within, then in the absence of longitudinal deformation (a condition approximately satisfied due to the effects of the constraining water jacket around the cells) $\Delta R_i/R_i$ is (Landau & Lifshitz 1959)

$$\frac{\Delta R_i}{R_i} = \left[\frac{R_i^2}{(R_e^2 - R_i^2)} \frac{(1+\sigma)(1-2\sigma)}{E} + \frac{R_e^2}{(R_e^2 - R_i^2)} \frac{1+\sigma}{E} \right] P \quad , \qquad (4.5)$$

where E is the Young modulus and σ is the Poisson ratio. In table 3 below we list values of $\Delta R_i/R_i$ and the corresponding $\delta_{distortion}$ for a decompression experiment with stainless-steel cells of length 41.74 cm with various radii at 301 K.

R_i / cm	R_e / cm	wall thickness / cm	$10^6\ \Delta R_i/R_i$	$\delta_{distortion}$ / rad
0.578	0.788	0.21	8.58	0.1494
0.280	0.730	0.50	3.82	0.0663
0.578	1.578	1.00	3.85	0.0670
2.000	3.000	1.00	6.88	0.1197
2.000	4.000	2.00	4.69	0.0817

Table 3. $\delta_{distortion}$ for 321 stainless-steel tubes containing carbon dioxide at an initial pressure of 500 kPa ($E = 2.0 \times 10^{11}$ Pa, $\sigma = 0.3$ and $\lambda = 632.8$ nm).

Values in the first row of table 3 apply to the cells used in our experiments and we note that significant increases in optical path occur even for cells with very thick walls. Since few materials have a Young's modulus greater than that of stainless-steel little improvement could be gained from constructing the cells from another material. Since errors due to cell distortion effects vary linearly with the pressure P while virial effects vary as P^2, there is an advantage to be gained by working at the highest pressures practicable. St-Arnaud & Bose (1976) enjoyed this advantage by carrying out their experiments at pressures ranging from 120 to 180 atm. However, in view of the size of cell distortion effects we have corrected our observed phase changes, allowance being made for the increase in wall thickness where the cell tubes are supported by the end-blocks.

In our interferometer we observe the rotation $\theta = \frac{\delta}{2}$ (see (3.20) of chapter 3) and the value of $(\delta_B - \delta_A) + 2(\delta_D - \delta_C)$ appropriate to (4.1) may be written as

$$(\delta_B - \delta_A) + 2(\delta_D - \delta_C) = 2(\theta_1 + 2\theta_2) + \theta_C \quad , \qquad (4.6)$$

where θ_1 and θ_2 are the observed rotations in the first and second decompressio

and where θ_C is a correction for the effects of cell distortion. For a positive B_n the phase change resulting from virial effects will be in the sense of decreasing optical path and $(\delta_B - \delta_A) + 2(\delta_D + \delta_C)$ is a negative number. Since cell distortion gives rise to an increase in path, the correction θ_C must be a negative number.

For a single decompression experiment the correction θ_A to the observed rotation is

$$\theta_A = -\frac{\delta_{distortion}}{2} = -\frac{2\pi\ell}{\lambda}\,\frac{A_n}{V_{ml}}\,\frac{\Delta R_i}{R_i} \quad . \tag{4.7}$$

In the second decompression of a double decompression experiment the correction is, to a very good approximation, half the value in the first expansion; but since twice the observed rotation in the second decompression is required in (4.6), the total correction θ_C is

$$\theta_C = 2\theta_A \quad . \tag{4.8}$$

§6. Uncertainties in B_n due to drift in the interferometer

If the analyser is set for extinction when a sample cell is filled in preparation for a decompression experiment, adjustment in the direction of decreasing optical path is necessary to maintain extinction. Since leakage of gas from the cells can give rise to this behaviour rigorous leak tests were carried out with the cells alternatively under pressure and vacuum, but no leaks were revealed. The drift rate of the interferometer was largest soon after filling but for all gases diminished with time. For some gases such as neon or argon the drift rate became negligible after about 30 minutes, but for others the drift rate in a 5-minute period was typically between 1° and 3° an hour or more after filling. After the decompression valve had been opened there was usually a rapid change in path followed by a much slower change, which for some gases (neon, argon, methane) dropped to zero 15 to 20 minutes after the valve had been opened. However, for the others drift rates of between 1° and 2° in 5 minutes were evident. For these gases it is difficult to assess precisely which reading to take for the crossed position of the analyser, as it is uncertain whether the drift leads to an observed phase change which is too large or whether the system requires a longer period to equilibrate after decompression. In all our measurements the reading of the analyser position was taken 15 to 20 minutes after the

decompression valve had been fully opened and re-closed. This reading was used in the calculations of B_R. We estimate the effects of drift by the following procedure : If A_1 is the drift occurring in a 5-minute period immediately before the decompression valve was opened and A_2 is the drift in the same period after closing, then we state that the drift for the first decompression is $d_1 = A_1 + A_2$. A similar definition may be stated for d_2, the drift in the second decompression. The quantity $\Delta = (d_1 + 2d_2)$ is then an estimate of the uncertainty in the combined phase charges $(\theta_1 + 2\theta_2)$ in a double decompression due to drift. Average values of Δ have been determined for each gas and the effects $\pm B_\Delta$ of a change $\pm\Delta$ in $(\theta_1 + 2\theta_2)$ are given in chapter 5 for our values of B_R.

REFERENCES

Buckingham, A.D. & Graham, C. 1974 *Proc. R. Soc. Lond. A* 336, 275.

Hartley, G.A.R., Henry, T.H. & Whytlaw-Gray, R. 1939 *Trans. Faraday Soc.* 35, 1452.

Landau, L.D. and Lifshitz, E.M. 1959 *Theory of elasticity*, p. 21. London : Pergamon Press.

Moles, E. 1938 *Bull. Soc. Chim. Belg.* 47, 416.

St-Arnaud, J.M. & Bose, T.K. 1976 *J. Chem. Phys.* 65, 4854.

CHAPTER 5

EXPERIMENTAL RESULTS AND DISCUSSION

§1. Introduction

Measurements of the first and second refractive index virial coefficients A_n and B_n have been carried out at four wavelengths (632.8 nm, 514.5 nm, 488.0 nm and 457.9 nm) in the visible, on the inert gases (excluding B_n for helium), methane and its fluorinated derivatives and the three common gases CO_2 , N_2 and SF_6 . Our experimental results are presented and analysed in this chapter, and derived values of the first and second refractivity virial coefficients A_R and B_R are listed. Literature values are also given where possible for comparison purposes. Expressions used in the calculations are summarized in §3. Experimental results are given in

§ 6. to §14. for the inert gases,
§16. to §25. for methane and its fluorinated derivatives, and
§27. to §32. for CO_2, N_2 and SF_6 .

Summaries of our results are given in §15., §26. and §33. Additional measurements of B_R carried out at different pressures are given in §34. and measurements of B_R obtained using sample cells with an increased surface-to-volume ratio are given in §35. In §36. dispersion plots of our B_R values are presented with a brief discussion. Some limitations of our apparatus are outlined in §37. together with possible improvements.

§2. Purity specifications of the gases

All the gases used in this investigation were obtained from Matheson Gas Products, U.S.A., except for CH_2F_2 which was obtained from E.I. du Pont de Nemours & Co. (INC.), U.S.A. Since this sample was not supplied with a purity specification, a mass spectrometric analysis was undertaken and the cracking patterns were compared with those of McCarthy (1968). This comparison showed that the contamination by other halogenated methanes was less than about 0.1% and the level of contamination by other organic gases was even less. All the gases were used without further purification except for filtering to remove dust particles. In table 1.1 the minimum purity is given for each gas as specified by the manufacturer.

gas	supplier	grade	stated minimum purity %	nature of main impurities
He	Matheson	high purity	99.995	H_2O 12 p.p.m., Ne 14 p.p.m., N_2 14 p.p.m.
Ne	Matheson	prepurified	99.99	not stated
Ar	Matheson	prepurified	99.998	O_2 4-5 p.p.m., N_2 6-7 p.p.m.
Kr	Matheson	research	99.995	Xe < 0.0025% (by vol.), N_2 < 0.0025% (by vol.)
Xe	Matheson	research	99.995	Kr 50 p.p.m. (by vol.), hydrocarbons 10 p.p.m. (by vol.)
CH_4	Matheson	ultra high purity	99.97	N_2 40-50 p.p.m., C_2H_6 20-30 p.p.m., CO_2 40-50 p.p.m.
CH_3F	Matheson	standard	99.0	SiF_4, $(CH_3)_2O$
CH_2F_2	du Pont de Nemours	-	-	-
CHF_3	Matheson	standard	98.0	other halogenocarbons 0.9% (by wt.), H_2O 25 p.p.m.
CF_4	Matheson	standard	99.7	H_2O 15 p.p.m. (by wt.) max., air 1½% (by vol.) max.
CO_2	Matheson	Coleman instrument	99.99	not stated
N_2	Matheson	prepurified	99.997	O_2 0.0008%, Ar 0.0010%
SF_6	Matheson	standard	99.9	air 0.04 %, CF_4 0.05%

Table 1.1 Minimum purity of gases.

§3. A summary of the expressions used to calculate A_R and B_R from the observed measurements

All our B_n values were obtained by the double decompression technique described in §3. of chapter 3 where it was shown that

$$B_n = -\frac{\lambda}{\pi \ell} V_{m1}^2 \frac{2}{3} [(\delta_B - \delta_A) + 2(\delta_D - \delta_C)] \quad , \qquad (5.1)$$

for well matched cells. Here ℓ is twice the geometrical length of a sample cell. In our experiments we observed the rotation of the plane of polarization θ resulting from a phase change δ on decompression. Since $\theta = \frac{\delta}{2}$ (see (3.20) of chapter 3) the value of $(\delta_B - \delta_A) + 2(\delta_D - \delta_C)$ appropriate to (5.1) may be written as

$$(\delta_B - \delta_A) + 2(\delta_D - \delta_C) = 2(\theta_1 + 2\theta_2) \quad ,$$

where θ_1 and θ_2 are the observed rotations in the first and second decompressions. As discussed in §5. of chapter 4 there is need to add a correction θ_c to allow for the effects of cell distortion so that

$$(\delta_B - \delta_A) + 2(\delta_D - \delta_C) = 2(\theta_1 + 2\theta_2) + \theta_c \quad . \qquad (5.2)$$

We note from §5. of chapter 4 that for a positive B_n the rotations θ_1 and θ_2 will be in the sense of decreasing optical path and are negative numbers. The effect of cell distortion is a spurious increase in optical path and the correction θ_c must be a negative number. From (4.8) of chapter 4 we write

$$\theta_c = - \frac{4\pi\ell}{\lambda} \frac{A_n}{V_{m1}} \cdot \frac{\Delta R_i}{R_i} \quad , \qquad (5.3)$$

where ℓ is the geometrical length of a sample cell and $\Delta R_i/R_i$ is the fractional increase in the internal radius given by (4.5) of chapter 4, namely

$$\frac{\Delta R_i}{R_i} = \left[\frac{R_i^2}{R_e^2 - R_i^2} \frac{(1+\sigma)(1-2\sigma)}{E} + \frac{R_e^2}{R_e^2 - R_i^2} \frac{1+\sigma}{E} \right] P \quad . \qquad (5.4)$$

In this expression σ is the Poisson ratio, E is the Young modulus and P is the absolute pressure of gas in a cell of internal radius R_i and external radius R_e. We note from §5. of chapter 4 that (5.4) above is applicable to cylindrical tubes of uniform wall thickness whose length is unchanged during radial deformation. Since the cell tubes were brazed into stainless-steel end-blocks which were bolted to 0.6 cm thick aluminium plates that formed the water jacket, longitudinal deformation was minimal and to a good approximation negligible. However, the effective thickness of the tubes was much greater where they were fixed to the end-blocks. Our cells have R_i = 0.578 cm and R_e = 0.788 cm and were mounted side by side in a horizontal plane with their walls almost touching. For end-blocks 8.0 cm wide, 4.5 cm high and 2.5 cm thick, a total length of 5.0 cm of each tube has an average wall thickness on three sides of about 1.5 cm, while the wall between the sample and reference cells is of varying thickness with a minimum thickness of about 0.4 cm. An attempt has been made to adjust the correction θ_c due to cell distortion for the extra wall thickness at the tube ends. Equation (5.4) was evaluated with the standard tube dimensions and also with R_i = 0.578 cm and R_e = 1.878 cm, that is, a tube with the equivalent internal radius but with a wall thickness of 1.3 cm. For stainless-steel tubes of grade 321, $E = 2.0 \times 10^{11}$ Pa and $\sigma = 0.3$. If (5.4) is evaluated with these values, $\frac{\Delta R_i}{R_i} = 1.710 \times 10^{-11}$ P for the standard tube and $\frac{\Delta R_i}{R_i} = 0.7452 \times 10^{-11}$ P for the tube ends within the end-blocks where P is in Pascal. If the above values of $\frac{\Delta R_i}{R_i}$ are weighted in proportion to the supported and unsupported tube lengths, we calculate an effective $\frac{\Delta R_i}{R_i} = 1.594 \times 10^{-11}$ P. This value has been used in all calculations of θ_c.

The molar volume V_{m1} in (5.1) was calculated for each gas from the measured temperature and pressure with the truncated virial equation

$$PV_m = RT\left(1 + \frac{B_p}{V_m}\right) \quad . \tag{5.5}$$

The second pressure virial coefficients B_p for the gases investigated were extracted from a compilation by Dymond and Smith (1969), whose reference numbers to the original data for each gas are given in table 1.2 .

gas	reference numbers of Dymond and Smith (1969)
He	6a
Ne	6a
Ar	4a
Kr	1
Xe	2a
CH_4	5
CH_3F	2
CH_2F_2	2
CHF_3	3
CF_4	2
CO_2	3
N_2	7
SF_6	4

Table 1.2 Source of second pressure virial coefficients.

Substitution of V_m (calculated from (5.5)), and $(\delta_B - \delta_A) + 2(\delta_D - \delta_C) = 2(\theta_1 + 2\theta_2) + \theta_c$ from (5.2) in (5.1) allows the calculation of B_n. B_R is related to A_n and B_n by the expression

$$B_R = \frac{2}{3} B_n - \frac{1}{9} A_n^2 \quad , \tag{5.6}$$

given in (3.9) of chapter 3.

The experimental procedure to measure A_n has been described in §§4.2 of chapter 3 and in essence is as follows. The reference cell is closed and the sample cells A and B are evacuated. With the analyser set for extinction gas is slowly bled into cells A and B; and the number of fringes is recorded on a strip chart recorder. If K fringes are observed the phase change is

$$K2\pi = \frac{2\pi L}{\lambda}(n - 1) \quad , \tag{5.7}$$

where L is the geometrical path length in the medium. Since the light beam makes a double traverse through each sample cell, the path length is four times the geometrical length of one sample cell. A_n is evaluated from

$$(n-1)V_m = A_n + \frac{B_n}{V_m} \quad , \tag{5.8}$$

where B_n is known, and where V_m is calculated from the final pressure and temperature of the gas with (5.5). Finally, the first refractivity virial coefficient A_R is evaluated with the expression

$$A_R = \frac{2}{3} A_n \quad , \tag{5.9}$$

given in (3.8) of chapter 3.

§4. Measurements of A_n and A_R

For each of the gases investigated tables of data for A_n and A_R precede the tables of data for B_n and B_R. Where possible literature values are listed for comparison purposes. The refractive index data of Cuthbertson & Cuthbertson (1909; 1910; 1913; 1920; 1932), Ramaswamy (1935; 1936) and Watson & Ramaswamy (1936) were not given at our particular wavelengths in the original papers and appropriate values of A_R were calculated from dispersion data given by these workers.

In our measurements several hundred fringes were recorded and phase changes were measured to better than 10^{-2} of a fringe. The error resulting from this measurement is generally negligible ($\sim \pm 0.001\%$) and in the most unfavourable case, namely helium, is about $\pm 0.01\%$. Pressure measurements were determined with an accuracy of $\pm 0.05\%$ with a capacitance manometer while the temperature of the sample cells was measured to $0.1^{\circ}C$ with a digital thermometer. The standard deviation of the A_R values is in general better than 0.1%. If all the uncertainties given above are summed the estimated uncertainty in the measurements of A_n and A_R is at most $\pm 0.2\%$.

Values of A_n have been obtained from the values of $(n-1)V_m$ where a small correction due to B_n has been applied in accordance with (5.8). Although the precision of the experiment does not justify the presentation of five or six significant figures in $(n-1)V_m$ and A_n, the values for these quantities are given to five or six significant figures to illustrate the effects of B_n. In the tables of mean values of A_n and A_R the precision is in accordance with that attainable with this interferometer.

The length of the geometrical path within the medium for these measurements was 1.6696 m. Our own values of A_n were used in the calculations of B_R.

§5. Measurements of B_n and B_R

The procedure for the calculation of B_R is outlined in §3. The quoted estimated uncertainty in our derived B_R values is obtained by taking the sum of three uncertainties, namely the standard deviation, the variation in B_R for a ±30% error in the correction θ_c for cell distortion and an uncertainty $\pm B_\Delta$ in B_R due to drift estimated as described in §6. of chapter 4. The standard deviation, and B_Δ are given separately for each gas while the uncertainty in the correction for cell distortion (~ 0.2 m^6 mol^{-2}) is incorporated in the combined uncertainty. Literature values are quoted where possible and are drawn from table 1 of chapter 2.

Although A_n and A_R measurements are presented for helium in tables 2.1 and 2.2, no accompanying B_n measurements are given since measurements on this gas were outside the range of sensitivity of our apparatus with the present cells.

The geometrical path length within the medium for our measurements of B_n was 0.83480 m, namely twice the geometrical length of one sample cell.

§§5.1 Summary of symbols used in the tables of results of B_n and B_R

θ_1 is the rotation of the plane of polarization of the interferometer output beam in the first decompression of a double decompression experiment when the interfering sample and reference beams undergo a phase change $(\delta_B - \delta_A) = 2\theta_1$. For a positive B_n value, this phase change due to virial effects is in the direction of decreasing optical path and $(\delta_B - \delta_A)$ and hence θ_1 are negative numbers.

θ_2 is the analogue of θ_1 for the second decompression of a double decompression experiment.

θ_c is the correction to $(\theta_1 + 2\theta_2)$ for the effects of cell distortion and is given by (5.3) and (5.4). Cell distortion gives rise to a spurious increase in optical path on decompression so that the correction θ_c which must be added to $(\theta_1 + 2\theta_2)$ is a negative number.

B_Δ is an estimate of the uncertainty in B_R due to the uncertainty Δ in $(\theta_1 + 2\theta_2)$ due to drift. The quantity Δ is estimated according to the procedure given in §6. of chapter 4.

MEASUREMENTS OF A_R AND B_R FOR THE INERT GASES

§6. Measurements of A_n and A_R for helium (He)

Our detailed measurements used to calculate A_n and A_R for helium are given in table 2.1 , and mean values of A_n and A_R are summarized in table 2.2 . Since B_n was not determined for this gas, A_n was obtained directly from $(n-1)V_m$ where the effects of B_n in the expression

$$(n - 1)V_m = A_n + \frac{B_n}{V_m}$$

have been omitted. This approximation will have a negligible effect on the A_R values for helium.

λ / nm	$10^6 A_n$ / $m^3\ mol^{-1}$	$10^6 A_R$ / $m^3\ mol^{-1}$	$\pm 10^6 \times$ s.d. / $m^3\ mol^{-1}$	literature values $10^6 A_R$ / $m^3\ mol^{-1}$	references
632.8	0.7302	0.5202	0.0003	0.5214	Cuthbertson & Cuthbertson 1913; 1932
514.5	0.7829	0.5219	0.0001	0.5231	Cuthbertson & Cuthbertson 1913; 1932
488.0	0.7840	0.5227	0.0003	0.5237	Cuthbertson & Cuthbertson 1913; 1932
457.9	0.7849	0.5233	0.0001	0.5244	Cuthbertson & Cuthbertson 1913; 1932

Table 2.2 Mean values of A_n and A_R for helium.

N E O N

λ / nm	final pressure / kPa	final pressure / cm Hg(0°C)	T / K	$10^2 V_m$ / $m^3\ mol^{-1}$	number of fringes	$10^6(n-1)V_m$ / $m^3\ mol^{-1}$	$10^6 A_n$ / $m^3\ mol^{-1}$	$10^6 A_R$ / $m^3\ mol^{-1}$
632.8	132.93	99.705	289.8	1.8135	218.031	1.4986	1.4986	0.99909
	134.41	100.82	290.4	1.7972	219.998	1.4985	1.4985	0.99903
	127.17	95.387	290.7	1.9014	208.014	1.4991	1.4991	0.99940
514.5	130.31	97.739	294.0	1.8768	260.020	1.5038	1.5038	1.0025
	131.61	98.720	294.6	1.8619	262.014	1.5034	1.5034	1.0022
	131.75	98.822	295.0	1.8625	261.993	1.5037	1.5037	1.0025
488.0	122.38	91.796	292.6	1.9864	259.108	1.5044	1.5044	1.0029
	134.43	100.83	292.9	1.8101	284.048	1.5029	1.5029	1.0019
	138.01	103.52	293.5	1.7691	291.000	1.5047	1.5047	1.0031
457.9	133.83	100.39	294.6	1.8311	300.005	1.5066	1.5066	1.0044
	133.94	100.47	294.9	1.8314	300.077	1.5072	1.5072	1.0045
	134.45	100.85	294.9	1.8245	301.035	1.5064	1.5064	1.0042

Table 3.1 Measurements of A_n and A_R for neon.

§7. Measurements of A_n and A_R for neon (Ne)

Our detailed measurements used to calculate A_n and A_R for neon are given in table 3.1 , and mean values of A_n and A_R are summarized in table 3.2 .

λ / nm	$10^6 A_n$ / $m^3\ mol^{-1}$	$10^6 A_R$ / $m^3\ mol^{-1}$	$\pm 10^6 \times$ s.d. / $m^3\ mol^{-1}$	literature values $10^6 A_R$ / $m^3\ mol^{-1}$	references
632.8	1.4988	0.9992	0.0002	1.003	Buckingham & Graham 1974
				1.002	Cuthbertson & Cuthbertson 1913; 1932
514.5	1.5036	1.0024	0.0002	1.005	Cuthbertson & Cuthbertson 1913; 1932
488.0	1.5039	1.0027	0.0007	1.006	Cuthbertson & Cuthbertson 1913; 1932
457.9	1.5067	1.0044	0.0002	1.007	Cuthbertson & Cuthbertson 1913; 1932

Table 3.2 Mean values of A_n and A_R for neon.

N E O N

λ / nm	initial pressure / kPa	T / K	$10^3 V_{ml}$ / $m^3\ mol^{-1}$	$-\theta_1$ / degrees	$-\theta_2$ / degrees	$-(\theta_1+2\theta_2)$ / degrees	$-\theta_c$ / degrees	$10^{12} B_n$ / $m^6\ mol^{-2}$	$10^{12} B_R$ / $m^6\ mol^{-2}$
632.8	507.18	291.1	4.7826	-0.83	0.64	0.45	1.20	0.211	-0.109
	507.47	290.1	4.7635	-0.77	-0.27	-1.31	1.20	-0.012	-0.257
	507.07	292.6	4.8084	-0.33	0.61	0.89	1.20	0.271	-0.069
	507.31	291.2	4.7830	-0.57	-0.24	-1.05	1.20	-0.021	-0.236
	507.08	292.5	4.8066	-0.03	0.70	1.37	1.20	0.333	-0.028
457.9	507.83	293.0	4.8077	-0.43	0.97	1.51	1.66	0.297	-0.055
	507.46	294.1	4.8293	-0.63	1.57	2.51	1.66	0.394	0.010
	507.26	294.7	4.8410	-2.63	0.14	-2.35	1.66	-0.067	-0.298

Table 4.1 Measurements of B_n and B_R for neon.

§8. Measurements of B_n and B_R for neon (Ne)

Our detailed measurements used to calculate B_n and B_R for neon are given in table 4.1 , and mean values of B_n and B_R are summarized in table 4.2 . Measurements of B_n for neon were carried out at only two wavelengths, namely 632.8 nm and 457.9 nm since the phase change on decompression was just within the sensitivity limit of our apparatus. Nevertheless, the sign of B_R was determined and upper and lower limits were set on the numerical value.

λ / nm	$10^{12}\ B_n$ / $m^6\ mol^{-2}$	$10^{12}\ B_R$ / $m^6\ mol^{-2}$	$\pm 10^{12} \times$ s.d. / $m^6\ mol^{-2}$	$\pm 10^{12}\ B_\Delta$ / $m^6\ mol^{-2}$	$\pm 10^{12} \times$ estimated uncertainty / $m^6\ mol^{-2}$	literature values $10^{12}\ B_R$ / $m^6\ mol^{-2}$
632.8	0.165	-0.14	0.10	0.01	0.14	-0.06 ± 0.14
457.9	0.202	-0.11	0.16	0.01	0.20	-

Table 4.2 Mean values of B_n and B_R for neon.

ARGON

λ / nm	final pressure / kPa	final pressure / cm Hg(0°C)	T / K	$10^2 V_m$ / $m^3\ mol^{-1}$	number of fringes	$10^6(n-1)V_m$ / $m^3\ mol^{-1}$	$10^6 A_n$ / $m^3\ mol^{-1}$	$10^6 A_R$ / $m^3\ mol^{-1}$
632.8	83.779	62.841	290.5	2.8808	576.028	6.2895	6.2892	4.1928
	84.071	63.060	291.6	2.8817	576.006	6.2912	6.2909	4.1939
	84.902	63.683	292.0	2.8578	581.026	6.2934	6.2931	4.1954
514.5	54.063	40.551	292.6	4.4976	457.012	6.3341	6.3339	4.2226
	53.536	40.156	292.9	4.5466	452.024	6.3331	6.3329	4.2219
	53.506	40.134	293.4	4.5568	450.993	6.3329	6.3328	4.2218
488.0	55.571	41.680	297.2	4.4444	489.004	6.3523	6.3521	4.2347
	50.470	37.860	297.3	4.8955	444.016	6.3533	6.3531	4.2354
	51.607	38.710	297.2	4.7859	454.025	6.3512	6.3510	4.2340
457.9	74.214	55.666	292.1	3.2703	709.015	6.3592	6.3590	4.2393
	60.431	45.328	292.9	4.0276	575.941	6.3618	6.3616	4.2411
	68.009	51.012	293.4	3.5848	647.104	6.3621	6.3618	4.2412

Table 5.1 Measurements of A_n and A_R for argon.

§9. Measurements of A_n and A_R for argon (Ar)

Our detailed measurements used to calculate A_n and A_R for argon are given in table 5.1 , and mean values of A_n and A_R are summarized in table 5.2 .

λ / nm	$10^6 A_n$ / $m^3\ mol^{-1}$	$10^6 A_R$ / $m^3\ mol^{-1}$	$\pm 10^6 \times$ s.d. / $m^3\ mol^{-1}$	literature values $10^6 A_R$ / $m^3\ mol^{-1}$	references
632.8	6.291	4.194	0.001	4.207	Buckingham & Graham 1974
				4.203	Cuthbertson & Cuthbertson 1910; 1913
				4.195	Dalgarno & Kingston 1960
514.5	6.333	4.222	0.001	4.232	Cuthbertson & Cuthbertson 1910; 1913
488.0	6.352	4.235	0.001	4.242	Cuthbertson & Cuthbertson 1910; 1913
457.9	6.361	4.241	0.001	4.255	Cuthbertson & Cuthbertson 1910; 1913

Table 5.2 Mean values of A_n and A_R for argon .

ARGON

λ / nm	initial pressure / kPa	T / K	$10^3 V_{ml}$ / $m^3\ mol^{-1}$	$-\theta_1$ / degrees	$-\theta_2$ / degrees	$-(\theta_1+2\theta_2)$ / degrees	$-\theta_c$ / degrees	$10^{12} B_n$ / $m^6\ mol^{-2}$	$10^{12} B_R$ / $m^6\ mol^{-2}$
632.8	473.33	295.6	5.1755	39.23	9.60	58.43	4.35	9.44	1.90
	473.36	295.8	5.1788	35.00	15.74	56.48	4.35	9.16	1.71
	473.01	292.3	5.1204	39.17	10.07	59.31	4.41	9.38	1.85
	472.81	294.3	5.1577	39.53	9.00	57.53	4.35	9.25	1.77
	472.86	295.5	5.1762	35.50	8.20	51.90	4.35	8.46	1.24
	473.06	292.9	5.1304	35.80	8.77	53.34	4.41	8.53	1.29
	472.73	292.3	5.1234	35.77	9.00	53.77	4.41	8.57	1.32
	474.54	293.8	5.1304	35.40	9.80	55.00	4.41	8.78	1.46
514.5	473.33	293.5	5.1382	41.70	16.70	75.10	5.44	9.71	2.02
	473.47	295.1	5.1651	39.13	14.64	68.41	5.41	8.99	1.54
	473.78	295.4	5.1671	36.53	13.20	62.93	5.41	8.32	1.10
488.0	472.28	297.5	5.2209	36.90	18.34	73.58	5.61	9.35	1.75
	472.61	294.5	5.1639	36.10	16.17	68.44	5.71	8.56	1.22
	472.02	296.4	5.2042	40.43	16.94	74.31	5.66	9.38	1.77
457.9	472.25	293.8	5.1554	45.20	16.00	77.20	6.07	9.00	1.50
	472.16	294.7	5.1723	47.30	15.17	77.64	6.07	9.10	1.57
	473.86	292.1	5.1076	46.83	16.00	78.83	6.19	9.01	1.51

Table 6.1 Measurements of B_n and B_R for argon.

§10. Measurements of B_n and B_R for argon (Ar)

Our detailed measurements used to calculate B_n and B_R for argon are given in table 6.1 , and mean values of B_n and B_R are summarized in table 6.2 .

λ / nm	$10^{12}\ B_n$ / $m^6\ mol^{-2}$	$10^{12}\ B_R$ / $m^6\ mol^{-2}$	$\pm 10^{12} \times$ s.d. / $m^6\ mol^{-2}$	$\pm 10^{12}\ B_\Delta$ / $m^6\ mol^{-2}$	$\pm 10^{12} \times$ estimated uncertainty / $m^6\ mol^{-2}$	literature values $10^{12}\ B_R$ / $m^6\ mol^{-2}$
632.8	8.94	1.57	0.27	0.18	0.58	2.16 ± 0.34
514.5	9.01	1.55	0.46	0.15	0.74	-
488.0	9.10	1.58	0.31	0.15	0.69	-
457.9	9.04	1.53	0.04	0.13	0.32	-

Table 6.2 Mean values of B_n and B_R for argon.

KRYPTON

λ / nm	final pressure / kPa	final pressure / cm Hg(0°C)	T / K	$10^2 V_m$ / $m^3\ mol^{-1}$	number of fringes	$10^6(n-1)V_m$ / $m^3\ mol^{-1}$	$10^6 A_n$ / $m^3\ mol^{-1}$	$10^6 A_R$ / $m^3\ mol^{-1}$
632.8	54.865	41.153	288.4	4.3642	576.051	9.5285	9.5279	6.3520
	58.726	44.049	289.4	4.0917	615.690	9.5481	9.5476	6.3650
	54.249	40.069	290.5	4.4461	566.990	9.5545	9.5540	6.3693
514.5	40.625	30.472	292.2	5.9739	524.001	9.6463	9.6459	6.4306
	40.723	30.545	292.5	5.9657	524.065	9.6343	9.6339	6.4226
	40.860	30.648	292.8	5.9517	525.981	9.6469	9.6465	6.4310
488.0	35.712	26.786	296.8	6.9040	479.981	9.6857	9.6854	6.4569
	37.784	28.341	296.7	6.5226	508.013	9.6851	9.6848	5.4565
	36.585	27.442	296.7	6.7365	491.920	9.6858	9.6855	6.4570
457.9	32.693	24.522	294.6	7.4858	473.024	9.7113	9.7110	6.4740
	34.950	26.215	294.4	6.9972	505.992	9.7102	9.7099	6.4733
	34.448	25.839	296.7	7.0967	499.031	9.7128	9.7125	6.4750

Table 7.1 Measurements of A_n and A_R for krypton.

§11. Measurements of A_n and A_R for krypton (Kr)

Our detailed measurements of A_n and A_R for krypton are given in table 7.1 , and mean values of A_n and A_R are summarized in table 7.2 .

$\frac{\lambda}{nm}$	$\frac{10^6 A_n}{m^3\ mol^{-1}}$	$\frac{10^6 A_R}{m^3\ mol^{-1}}$	$\frac{\pm 10^6 \times s.d.}{m^3\ mol^{-1}}$	literature values $\frac{10^6 A_R}{m^3\ mol^{-1}}$	references
632.8	9.543	6.362	0.009	6.349	Cuthbertson & Cuthbertson 1910
				6.349	Dalgarno & Kingston 1960
514.5	9.642	6.428	0.005	6.408	Cuthbertson & Cuthbertson 1910
488.0	9.685	6.457	0.001	6.428	Cuthbertson & Cuthbertson 1910
457.9	9.711	6.474	0.001	6.454	Cuthbertson & Cuthbertson 1910

Table 7.2 Mean values of A_n and A_R for krypton.

KRYPTON

λ / nm	initial pressure / kPa	T / K	$10^3 V_{ml}$ / $m^3\ mol^{-1}$	$-\theta_1$ / degrees	$-\theta_2$ / degrees	$-(\theta_1+2\theta_2)$ / degrees	$-\theta_c$ / degrees	$10^{12} B_n$ / $m^6\ mol^{-2}$	$10^{12} B_R$ / $m^6\ mol^{-2}$
632.8	471.85	293.9	5.1235	116.30	28.90	174.10	6.65	26.64	7.64
	471.94	295.3	5.1477	109.70	24.67	159.04	6.65	24.65	6.31
	472.36	295.6	5.1485	108.00	19.14	146.28	6.65	22.76	5.05
	473.15	293.3	5.0985	105.43	28.50	162.43	6.70	24.69	6.34
	472.23	294.6	5.1319	106.40	27.67	161.74	6.65	24.93	6.50
	472.74	295.3	5.1388	114.00	22.60	159.20	6.65	24.59	6.28
	472.30	295.3	5.1437	102.13	23.60	149.33	6.65	23.17	5.33
	473.64	291.3	5.0572	111.83	24.64	171.11	6.76	25.54	6.91
	473.62	293.3	5.1042	110.10	26.00	162.10	6.70	24.69	6.34
	472.81	291.7	5.0734	111.47	22.20	155.87	6.76	23.50	5.55
514.5	438.86	294.3	5.5205	114.90	20.90	156.70	7.16	22.80	4.87
	438.84	294.7	5.5285	111.37	21.17	153.71	7.10	22.44	4.63
	438.87	294.8	5.5299	112.83	26.80	166.43	7.10	24.23	5.82
488.0	438.30	295.9	5.5586	109.43	17.87	145.17	7.51	20.42	3.19
	438.31	296.6	5.5720	106.93	24.80	156.53	7.51	22.05	4.28
	438.43	298.0	5.5977	119.70	23.17	166.04	7.45	23.54	5.27
	369.55	297.0	6.6281	79.57	19.87	119.31	5.31	23.70	5.38
457.9	437.54	291.2	5.4772	128.37	30.00	188.37	8.14	23.95	5.49
	437.07	293.2	5.5218	124.10	30.00	184.10	8.02	23.80	5.39
	437.02	294.6	5.5498	130.23	28.00	186.23	8.02	24.31	5.73

Table 8.1 Measurements of B_n and B_R for krypton.

§12. Measurements of B_n and B_R for krypton (Kr)

Our detailed measurements used to calculate B_n and B_R for krypton are given in table 8.1 , and mean values of B_n and B_R are summarized in table 8.2 .

$\frac{\lambda}{nm}$	$\frac{10^{12}\ B_n}{m^6\ mol^{-2}}$	$\frac{10^{12}\ B_R}{m^6\ mol^{-2}}$	$\frac{\pm 10^{12}\ \text{s.d.}}{m^6\ mol^{-2}}$	$\frac{\pm 10^{12}\ B_\Delta}{m^6\ mol^{-2}}$	$\frac{\pm 10^{12} \times \text{estimated uncertainty}}{m^6\ mol^{-2}}$	literature values $\frac{10^{12}\ B_R}{m^6\ mol^{-2}}$
632.8	24.52	6.23	0.76	0.59	1.55	-
514.5	23.16	5.11	0.63	0.56	1.39	-
488.0	22.06	4.28	1.10	0.57	1.87	-
457.9	24.02	5.54	0.17	0.50	0.80	-

Table 8.2 Mean values of B_n and B_R for krypton.

XENON

λ / nm	final pressure / kPa	final pressure / cm Hg(0°C)	T / K	$10^2 V_m$ / $m^3\ mol^{-1}$	number of fringes	$10^6(n-1)V_m$ / $m^3\ mol^{-1}$	$10^6 A_n$ / $m^3\ mol^{-1}$	$10^6 A_R$ / $m^3\ mol^{-1}$
632.8	26.697	20.025	288.2	8.9603	457.000	15.520	15.519	10.346
	30.660	22.997	289.8	7.8439	523.000	15.548	15.547	10.365
	30.190	22.645	290.4	7.9828	514.000	15.552	15.551	10.367
514.5	24.303	18.229	294.5	10.060	508.896	15.777	15.776	10.517
	25.232	18.926	294.7	9.6960	527.958	15.775	15.774	10.516
	24.473	18.357	294.9	10.004	511.919	15.781	15.781	10.520
488.0	21.568	16.178	297.1	11.438	473.944	15.845	15.844	10.563
	21.649	16.238	297.7	11.419	474.125	15.824	15.824	10.549
	21.449	16.089	298.0	11.536	470.012	15.848	15.848	10.565
457.9	14.577	10.934	292.7	16.679	348.034	15.920	10.919	10.613
	16.629	12.473	292.8	14.624	396.924	15.920	10.919	10.613
	19.662	14.748	293.0	12.375	496.081	15.920	10.919	10.613

Table 9.1 Measurements of A_n and A_R for xenon.

§13. Measurements of A_n and A_R for xenon (Xe)

Our detailed measurements used to calculate A_n and A_R for xenon are given in table 9.1 , and mean values of A_n and A_R are summarized in table 9.2 .

λ / nm	$10^6 A_n$ / $m^3\ mol^{-1}$	$10^6 A_R$ / $m^3\ mol^{-1}$	$\pm 10^6 \times$ s.d. / $m^3\ mol^{-1}$	literature values $10^6 A_R$ / $m^3\ mol^{-1}$	references
632.8	15.539	10.359	0.012	10.38	Dalgarno & Kingston 1960
				10.38	Cuthbertson & Cuthbertson 1910
514.5	15.777	10.518	0.002	10.52	Cuthbertson & Cuthbertson 1910
488.0	15.839	10.559	0.009	10.56	Cuthbertson & Cuthbertson 1910
457.9	15.919	10.613	0.001	10.63	Cuthbertson & Cuthbertson 1910

Table 9.2 Mean values of A_n and A_R for xenon.

XENON

λ / nm	initial pressure / kPa	T / K	$10^3 V_{ml}$ / $m^3\ mol^{-1}$	$-\theta_1$ / degrees	$-\theta_2$ / degrees	$-(\theta_1+2\theta_2)$ / degrees	$-\theta_c$ / degrees	$10^{12} B_n$ / $m^6\ mol^{-2}$	$10^{12} B_R$ / $m^6\ mol^{-2}$
632.8	266.32	292.9	9.0062	119.17	22.27	163.71	3.50	76.14	23.93
	266.21	292.1	8.9830	123.00	23.27	169.54	3.50	78.39	25.43
	267.00	291.0	8.9209	132.27	22.60	177.47	3.50	80.87	27.09
	266.84	291.0	8.9263	128.80	29.84	168.48	3.50	76.95	24.47
	266.37	293.4	9.0195	120.20	21.97	164.14	3.50	76.56	24.21
	263.24	290.5	8.9305	130.23	22.47	175.17	3.50	80.01	26.51
	267.21	289.8	8.8752	120.60	26.00	172.60	3.55	77.91	25.11
	267.35	288.0	8.8128	129.96	26.27	182.50	3.55	81.14	27.26
514.5	262.30	294.9	9.0702	115.04	34.50	184.04	4.30	70.74	19.51
	266.25	292.6	8.9976	110.00	34.22	178.44	4.35	67.56	17.38
	266.20	295.1	9.0801	111.00	34.90	180.80	4.30	69.67	18.79
488.0	266.22	295.8	9.1017	124.60	24.24	173.08	4.53	63.72	14.60
	266.59	293.5	9.0147	127.43	23.84	175.11	4.58	63.23	14.28
	266.13	294.7	9.0693	115.43	24.10	179.63	4.58	65.60	15.86
457.9	265.49	295.7	9.1239	125.57	32.50	190.57	4.87	66.10	15.91
	265.03	297.8	9.2078	135.73	29.54	194.81	4.81	68.76	17.68
	265.61	298.4	9.2070	114.00	34.94	183.94	4.81	65.00	15.18

Table 10.1 Measurements of B_n and B_R for xenon.

§14. Measurements of B_n and B_R for xenon (Xe)

Our detailed measurements used to calculate B_n and B_R for xenon are given in table 10.1 , and mean values of B_n and B_R are summarized in table 10.2 .

λ / nm	$10^{12}\ B_n$ / $m^6\ mol^{-2}$	$10^{12}\ B_R$ / $m^6\ mol^{-2}$	$\pm 10^{12} \times$ s.d. / $m^6\ mol^{-2}$	$\pm 10^{12}\ B_\Delta$ / $m^6\ mol^{-2}$	$\pm 10^{12} \times$ estimated uncertainty / $m^6\ mol^{-2}$	literature values $10^{12}\ B_R$ / $m^6\ mol^{-2}$
632.8	78.50	25.50	1.31	1.23	2.85	-
514.5	69.32	18.56	1.01	1.03	2.36	-
488.0	64.18	14.91	0.84	0.98	2.14	-
457.9	66.62	16.26	1.29	0.93	2.55	-

Table 10.2 Mean values of B_n and B_R for xenon.

§15. Summary of our A_R and B_R values for inert gases

§§15.1 A_R values for the inert gases

λ / nm	$10^6 A_R/m^3\ mol^{-1}$				
	He	Ne	Ar	Kr	Xe
632.8	0.5202 ±0.0003	0.9992 ±0.0002	4.194 ±0.001	6.362 ±0.009	10.359 ±0.012
514.5	0.5219 ±0.0001	1.0024 ±0.0002	4.222 ±0.001	6.428 ±0.005	10.518 ±0.002
488.0	0.5227 ±0.0003	1.0027 ±0.0007	4.235 ±0.001	6.457 ±0.001	10.559 ±0.009
457.9	0.5233 ±0.0001	1.0044 ±0.0002	4.241 ±0.001	6.474 ±0.001	10.613 ±0.001

Table 10.3 Dispersion of the A_R values for the inert gases; the quoted uncertainties are standard deviations.

§§15.2 B_R values for some of the inert gases

λ / nm	$10^{12} B_R^*/m^6\ mol^{-2}$			
	Ne	Ar	Kr	Xe
632.8	-0.14 ± 0.14	1.57 ± 0.58	6.23 ± 1.55	25.50 ± 2.85
514.5	-	1.55 ± 0.74	5.11 ± 1.39	18.56 ± 2.36
488.0	-	1.58 ± 0.69	4.28 ± 1.87	14.91 ± 2.14
457.9	-0.11 ± 0.20	1.53 ± 0.32	5.54 ± 0.80	16.26 ± 2.55

* These values are shown graphically in §§36.1 on page 79.

Table 10.4 Dispersion of the B_R values for some of the inert gases; the quoted uncertainties are deduced as described in §5.

MEASUREMENTS OF A_R AND B_R FOR METHANE AND ITS FLUORINATED DERIVATIVES

§16. Measurements of A_n and A_R for methane (CH_4)

Our detailed measurements used to calculate A_n and A_R for methane are given in table 11.1 , and mean values of A_n and A_R are summarized in table 11.2 .

λ / nm	$10^6 A_n$ / $m^3\ mol^{-1}$	$10^6 A_R$ / $m^3\ mol^{-1}$	$\pm 10^6 \times$ s.d. / $m^3\ mol^{-1}$	literature values $10^6 A_R$ / $m^3\ mol^{-1}$	references
632.8	9.853	6.569	0.003	6.600	Buckingham & Graham 1974
				6.57	Buckingham & Orr 1969
				6.537	Cuthbertson & Cuthbertson 1920
				6.553	St-Arnaud & Bose 1976
				6.564	Watson & Ramaswamy 1936
514.5	9.959	6.639	0.001	6.603	Cuthbertson & Cuthbertson 1920
				6.632	Watson & Ramaswamy 1936
488.0	9.980	6.654	0.001	6.626	Cuthbertson & Cuthbertson 1920
				6.654	Watson & Ramaswamy 1936
457.9	10.023	6.682	0.003	6.656	Cuthbertson & Cuthbertson 1920
				6.684	Watson & Ramaswamy 1936

Table 11.2 Mean values of A_n and A_R for methane.

METHANE

λ / nm	initial pressure / kPa	T / K	$10^3 V_{ml}$ / $m^3\ mol^{-1}$	$-\theta_1$ / degrees	$-\theta_2$ / degrees	$-(\theta_1+2\theta_2)$ / degrees	$-\theta_c$ / degrees	$10^{12} B_n$ / $m^6\ mol^{-2}$	$10^{12} B_R$ / $m^6\ mol^{-2}$
632.8	438.85	294.9	5.5409	128.83	13.97	156.77	5.91	28.04	7.91
	439.02	292.9	5.5012	109.37	25.30	159.97	5.95	28.20	8.01
	438.63	294.8	5.5420	93.97	25.00	143.97	5.91	25.85	6.44
	437.82	295.9	5.5736	93.13	24.24	141.61	5.90	25.72	6.36
	437.96	296.1	5.5757	96.30	22.47	141.24	5.90	25.68	6.33
	438.67	292.7	5.5018	105.70	23.94	153.58	5.94	27.11	7.29
	438.55	295.6	5.5592	96.53	30.17	156.87	5.88	28.24	8.04
	438.40	296.3	5.5747	131.90	13.87	159.64	5.87	28.70	8.35
	439.30	294.6	5.5296	124.77	13.44	151.65	5.93	27.05	7.25
	438.89	295.4	5.5500	132.03	14.64	161.31	5.90	28.92	8.50
	438.18	296.0	5.5708	129.20	15.60	160.40	5.87	28.97	8.53
	438.29	296.0	5.5695	128.63	15.54	159.71	5.87	28.84	8.44
	438.55	293.6	5.5194	127.27	15.47	158.21	5.92	28.08	7.93
	438.12	296.6	5.5832	129.17	16.10	160.37	5.86	29.09	8.61
	437.91	296.6	5.5858	128.47	15.14	158.75	5.87	28.84	8.44
514.5	438.51	290.7	5.4640	113.37	33.00	179.37	7.45	25.46	5.96
	438.92	291.4	5.4917	107.60	38.94	185.48	7.45	26.56	6.69
	438.67	294.1	5.5279	110.16	30.67	181.50	7.45	26.35	6.54
488.0	438.81	290.9	5.4641	128.13	47.94	224.01	7.85	29.98	8.92
	438.89	292.2	5.4884	128.23	46.00	220.23	7.85	29.75	8.76
	438.73	293.2	5.5099	127.33	47.50	222.33	7.79	30.25	9.10
457.9	472.95	296.8	5.1726	117.77	30.90	179.57	6.82	28.00	7.88
	473.31	295.2	5.1399	114.17	29.50	173.17	6.87	26.71	7.02
	473.17	296.3	5.1611	120.00	27.60	175.20	6.84	27.23	7.36

Table 12.1 Measurements of B_n and B_R for methane.

§17. Measurements of B_n and B_R for methane (CH_4)

Our detailed measurements used to calculate B_n and B_R for methane are given in table 12.1 , and mean values of B_n and and B_R are summarized in table 12.2 .

$\frac{\lambda}{nm}$	$\frac{10^{12}\ B_n}{m^6\ mol^{-2}}$	$\frac{10^{12}\ B_R}{m^6\ mol^{-2}}$	$\frac{\pm 10^{12} \times s.d.}{m^6\ mol^{-2}}$	$\frac{\pm 10^{12}\ B_\Delta}{m^6\ mol^{-2}}$	$\frac{\pm 10^{12} \times \text{estimated uncertainty}}{m^6\ mol^{-2}}$	literature values $\frac{10^{12}\ B_R}{m^6\ mol^{-2}}$
632.8	27.78	7.76	0.83	0.28	1.32	7.15 ± 0.35 6.60 ± 0.38
514.5	26.12	6.40	0.39	0.22	0.83	5.5 ± 1.0 (546.0 nm)
488.0	29.99	8.93	0.17	0.20	0.57	-
457.9	27.30	7.04	0.33	0.24	0.78	-

Table 12.2 Mean values of B_n and B_R for methane.

FLUOROMETHANE

λ / nm	final pressure / kPa	final pressure / cm Hg(0°C)	T / K	$10^2 V_m$ / $m^3\ mol^{-1}$	number of fringes	$10^6(n-1)V_m$ / $m^3\ mol^{-1}$	$10^6 A_n$ / $m^3\ mol^{-1}$	$10^6 A_R$ / $m^3\ mol^{-1}$
632.8	52.485	39.367	297.5	4.6918	557.819	9.9194	9.9190	6.6127
	40.611	30.461	297.0	6.0595	431.905	9.9193	9.9189	6.6126
	43.238	32.431	297.6	5.7017	458.905	9.9170	9.9167	6.6111
514.5	26.941	20.207	293.0	9.0196	357.960	9.9493	9.9497	6.6328
	35.247	26.438	293.6	6.9029	468.000	9.9552	9.9550	6.6366
	34.848	26.139	294.0	6.9918	462.046	9.9551	9.9549	6.6366
488.0	33.535	25.154	293.4	7.2514	470.082	9.9633	9.9631	6.6421
	43.347	32.513	293.4	5.6051	608.906	9.9757	9.9754	6.6503
	33.955	25.469	293.0	7.1516	476.968	9.9701	9.9699	6.6466
457.9	39.617	29.716	289.9	6.0607	598.978	9.9561	9.9559	6.6372
	49.612	36.537	290.7	4.9389	736.004	9.9693	9.9690	6.6460
	37.183	27.890	291.5	6.4950	560.011	9.9766	9.9764	6.6509

Table 13.1 Measurements of A_n and A_R for fluoromethane.

§18. Measurements of A_n and A_R for fluoromethane (CH_3F)

Our detailed measurements used to calculate A_n and A_R for fluoromethane are given in table 13.1 , and mean values of A_n and A_R are summarized in table 13.2 .

λ / nm	$10^6 A_n$ / $m^3\ mol^{-1}$	$10^6 A_R$ / $m^3\ mol^{-1}$	$\pm 10^6 \times$ s.d. / $m^3\ mol^{-1}$	literature values $10^6 A_R$ / $m^3\ mol^{-1}$	references
632.8	9.918	6.612	0.001	6.57	Buckingham & Orr 1969
				6.652	Ramaswamy 1936
514.5	9.953	6.635	0.002	6.709	Ramaswamy 1936
488.0	9.970	6.646	0.004	6.728	Ramaswamy 1936
457.9	9.967	6.645	0.007	6.754	Ramaswamy 1936

Table 13.2 Mean values of A_n and A_R for fluoromethane.

F L U O R O M E T H A N E

λ / nm	initial pressure / kPa	T / K	$10^3 V_{ml}$ / $m^3\ mol^{-1}$	$-\theta_1$ / degrees	$-\theta_2$ / degrees	$-(\theta_1+2\theta_2)$ / degrees	$-\theta_c$ / degrees	$10^{12} B_n$ / $m^6\ mol^{-2}$	$10^{12} B_R$ / $m^6\ mol^{-2}$
632.8	438.54	296.2	5.3946	87.60	21.70	131.00	6.12	22.40	4.01
	438.12	298.2	5.4417	83.93	18.07	120.07	6.05	20.97	3.05
	438.71	294.8	5.3515	94.73	21.00	136.73	6.17	22.98	4.39
	438.83	292.6	5.3171	95.90	18.30	132.50	6.20	22.02	3.75
	446.26	295.6	5.2857	114.50	17.34	149.18	6.34	24.04	5.33
	438.22	297.4	5.4210	123.33	5.00	133.33	6.07	23.00	4.41
	438.60	294.6	5.3597	115.63	14.47	144.57	6.15	24.31	5.28
514.5	438.92	294.2	5.3471	85.87	16.44	118.75	7.62	16.49	-0.012
	440.30	290.8	5.2587	82.50	15.07	112.64	7.73	15.20	-0.875
	440.20	290.8	5.2845	74.60	21.84	118.28	7.73	16.06	-0.299
488.0	439.53	290.6	5.2640	91.07	15.57	122.21	8.19	15.63	-0.623
	439.57	291.9	5.2905	82.33	15.45	113.23	8.14	14.71	-1.24
	439.42	289.0	5.2318	102.17	9.27	120.71	8.25	15.28	-0.856
	439.27	290.8	5.2721	79.53	16.64	112.81	8.14	14.55	-1.34
	439.13	292.8	5.3152	86.30	14.00	114.30	8.08	14.97	-1.06
457.9	439.10	293.9	5.3174	104.50	22.87	150.24	8.56	18.25	1.13
	439.08	290.1	5.2592	98.63	26.00	150.63	8.71	17.91	0.900
	439.04	291.6	5.2909	96.37	29.07	154.51	8.65	18.56	1.33
	439.48	290.0	5.2517	101.25	26.30	153.85	8.71	18.22	1.11

Table 14.1 Measurements of B_n and B_R for fluoromethane.

§19. Measurements of B_n and B_R for fluoromethane (CH_3F)

Our detailed measurements used to calculate B_n and B_R for fluoromethane are given in table 14.1 , and mean values of B_n and B_R are summarized in table 14.2 .

λ / nm	$10^{12}\ B_n$ / $m^6\ mol^{-2}$	$10^{12}\ B_R$ / $m^6\ mol^{-2}$	$\pm 10^{12} \times$ s.d. / $m^6\ mol^{-2}$	$\pm 10^{12}\ B_\Delta$ / $m^6\ mol^{-2}$	$\pm 10^{12} \times$ estimated uncertainty / $m^6\ mol^{-2}$	literature values $10^{12}\ B_R$ / $m^6\ mol^{-2}$
632.8	22.82	+4.32	0.82	0.78	1.80	-
514.5	15.92	-0.40	0.44	0.64	1.28	7 ± 100 (546.0 nm)
488.0	15.03	-1.02	0.29	0.60	1.09	-
457.9	18.24	+1.12	0.18	0.60	0.88	-

Table 14.2 Mean values of B_n and B_R for fluoromethane.

D I F L U O R O M E T H A N E

λ / nm	final pressure: kPa	final pressure: cm Hg(0°C)	T / K	$10^2 V_m$ / $m^3\ mol^{-1}$	number of fringes	$10^6(n-1)V_m$ / $m^3\ mol^{-1}$	$10^6 A_n$ / $m^3\ mol^{-1}$	$10^6 A_R$ / $m^3\ mol^{-1}$
632.8	54.626	40.973	298.5	4.5109	595.832	10.1869	10.1866	6.7911
	39.589	29.694	290.5	6.0701	442.000	10.1689	10.1686	6.7791
	44.450	33.213	293.0	5.4677	491.000	10.1751	10.1749	6.7833
514.5	35.151	26.366	291.9	6.8691	485.030	10.2670	10.2669	6.8446
	36.441	27.334	293.0	6.6501	501.000	10.2668	10.2667	6.8445
	37.856	28.395	293.4	6.4092	519.967	10.2696	10.2695	6.8463
488.0	34.469	25.854	293.4	7.0425	500.042	10.2929	10.2928	6.8619
	35.356	26.520	293.7	6.8719	512.543	10.2947	10.2946	6.8630
	37.702	28.279	294.0	6.4490	546.083	10.2934	10.2933	6.8622
457.9	30.606	22.957	288.2	7.7924	482.005	10.3015	10.3014	6.8675
	38.303	28.730	288.9	6.2350	603.008	10.3114	10.3113	6.8742
	37.106	27.832	289.9	6.4601	581.980	10.3111	10.3110	6.8740

Table 15.1 Measurements of A_n and A_R for difluoromethane.

§20. Measurements of A_n and A_R for difluoromethane (CH_2F_2)

Our detailed measurements used to calculate A_n and A_R for difluoromethane are given in table 15.1 , and mean values of A_n and A_R are summarized in table 15.2 .

$\frac{\lambda}{nm}$	$\frac{10^6 A_n}{m^3\ mol^{-1}}$	$\frac{10^6 A_R}{m^3\ mol^{-1}}$	$\frac{\pm 10^6 \times s.d.}{m^3\ mol^{-1}}$	literature values $\frac{10^6 A_R}{m^3\ mol^{-1}}$	references
632.8	10.177	6.785	0.006	-	-
514.5	10.268	6.845	0.001	-	-
488.0	10.294	6.862	0.006	-	-
457.9	10.308	6.872	0.004	-	-

Table 15.2 Mean values of A_n and A_R for difluoromethane.

D I F L U O R O M E T H A N E

λ / nm	initial pressure / kPa	T / K	$10^3 V_{m1}$ / $m^3\ mol^{-1}$	$-\theta_1$ / degrees	$-\theta_2$ / degrees	$-(\theta_1+2\theta_2)$ / degrees	$-\theta_c$ / degrees	$10^{12} B_n$ / $m^6\ mol^{-2}$	$10^{12} B_R$ / $m^6\ mol^{-2}$
632.8	445.83	296.2	5.1738	54.80	11.67	78.14	6.64	12.74	-3.01
	438.96	294.6	5.2250	55.97	15.74	87.45	6.47	14.39	-1.91
	438.58	296.8	5.2781	58.10	13.50	85.10	6.40	14.31	-1.97
	440.92	295.8	5.2291	58.10	18.80	95.70	6.50	15.70	-1.04
	438.99	295.2	5.2378	63.57	15.34	94.25	6.46	15.51	-1.17
	438.63	296.8	5.2785	59.63	7.34	74.31	6.40	12.63	-3.09
	438.72	294.2	5.2189	67.30	10.40	88.10	6.48	14.46	-1.86
514.5	438.15	294.1	5.2223	32.57	19.27	71.11	8.02	9.851	-5.15
	438.23	293.3	5.2036	37.80	14.70	67.20	8.08	9.303	-5.51
	438.35	293.8	5.2133	42.77	12.24	67.25	8.07	9.341	-5.49
488.0	438.38	294.8	5.2350	38.60	15.00	68.60	8.48	9.145	-5.68
	438.56	291.8	5.1659	36.00	14.87	65.74	8.59	8.587	-6.05
	438.51	294.2	5.2195	37.63	14.07	66.77	8.48	8.877	-5.85
457.9	438.93	290.4	5.1299	32.90	14.10	61.10	9.22	7.520	-6.79
	439.04	291.3	5.1489	37.30	10.30	57.90	9.22	7.228	-6.99
	439.54	288.8	5.0865	31.07	17.14	65.35	9.34	7.849	-6.57

Table 16.1 Measurements of B_n and B_R for difluoromethane.

§21. Measurements of B_n and B_R for difluoromethane (CH_2F_2)

Our detailed measurements used to calculate B_n and B_R for difluoromethane are given in table 16.1 , and mean values of B_n and B_R are summarized in table 16.2 .

λ / nm	$10^{12}\ B_n$ / $m^6\ mol^{-2}$	$10^{12}\ B_R$ / $m^6\ mol^{-2}$	$\pm 10^{12} \times$ s.d. / $m^6\ mol^{-2}$	$\pm 10^{12}\ B_\Delta$ / $m^6\ mol^{-2}$	$\pm 10^{12} \times$ estimated uncertainty / $m^6\ mol^{-2}$	literature values $10^{12}\ B_R$ / $m^6\ mol^{-2}$
632.8	14.25	-2.01	0.80	0.87	1.87	-
514.5	9.50	-5.38	0.20	0.73	1.13	-
488.0	8.87	-5.86	0.19	0.70	1.09	-
457.9	7.53	-6.78	0.21	0.65	1.06	-

Table 16.2 Mean values of B_n and B_R for difluoromethane.

TRIFLUOROMETHANE

λ / nm	final pressure / kPa	final pressure / cm Hg(0°C)	T / K	$10^2 V_m$ / $m^3\ mol^{-1}$	number of fringes	$10^6(n-1)V_m$ / $m^3\ mol^{-1}$	$10^6 A_n$ / $m^3\ mol^{-1}$	$10^6 A_R$ / $m^3\ mol^{-1}$
632.8	63.168	47.381	290.3	3.8014	731.021	10.5323	10.5318	7.0212
	61.919	46.444	290.9	3.8856	715.041	10.5302	10.5297	7.0198
	61.269	45.957	291.6	3.9376	706.065	10.5372	10.5367	7.0245
514.5	46.229	34.675	293.2	5.2540	655.049	10.6056	10.6052	7.0701
	44.835	33.629	293.3	5.4198	635.014	10.6057	10.6054	7.0703
	40.491	30.371	293.4	6.0053	573.004	10.6039	10.6035	7.0690
488.0	50.524	37.897	292.6	4.7957	758.010	10.6252	10.6248	7.0831
	34.216	25.702	292.8	7.0849	512.974	10.6228	10.6225	7.0817
	33.545	25.161	292.9	7.2401	502.014	10.6236	10.6233	7.0822
457.9	56.749	42.573	289.0	4.2137	920.980	10.6431	10.6427	7.0951
	78.983	59.243	289.8	3.0310	1280.94	10.6482	10.6475	7.0983
	56.144	42.113	290.3	4.2793	907.000	10.6458	10.6443	7.0962

Table 17.1 Measurements of A_n and A_R for trifluoromethane.

§22. Measurements of A_n and A_R for trifluoromethane (CHF_3)

Our detailed measurements used to calculate A_n and A_R for trifluoromethane are given in table 17.1 , and mean values of A_n and A_R are summarized in table 17.2 .

λ / nm	$10^6 A_n$ / $m^3\ mol^{-1}$	$10^6 A_R$ / $m^3\ mol^{-1}$	$\pm 10^6 \times$ s.d. / $m^3\ mol^{-1}$	literature values $10^6 A_R$ / $m^3\ mol^{-1}$	references
632.8	10.533	7.022	0.002	7.06	Bridge & Buckingham 1966
				7.052	Buckingham & Graham 1974
				7.07	Buckingham & Orr 1969
				7.020	Ramaswamy 1936
514.5	10.605	7.070	0.001	7.065	Ramaswamy 1936
488.0	10.624	7.082	0.001	7.080	Ramaswamy 1936
457.9	10.645	7.097	0.002	7.100	Ramaswamy 1936

Table 17.2 Mean values of A_n and A_R for trifluoromethane.

TRIFLUOROMETHANE

λ / nm	initial pressure / kPa	T / K	$10^3 V_{ml}$ / $m^3\ mol^{-1}$	$-\theta_1$ / degrees	$-\theta_2$ / degrees	$-(\theta_1+2\theta_2)$ / degrees	$-\theta_c$ / degrees	$10^{12} B_n$ / $m^6\ mol^{-2}$	$10^{12} B_R$ / $m^6\ mol^{-2}$
632.8	452.20	297.0	5.2761	106.10	18.87	143.84	6.83	23.86	3.58
	439.07	295.9	5.4166	99.80	9.54	118.88	6.46	20.65	1.44
	438.60	295.6	5.4169	100.17	14.00	128.17	6.45	22.18	2.46
	438.79	294.7	5.3944	81.57	20.60	122.77	6.49	21.12	1.75
	438.79	295.5	5.4066	80.93	20.97	122.87	6.47	21.23	1.83
	438.58	295.5	5.4111	82.60	25.37	133.34	6.46	22.98	3.00
	438.28	289.5	5.2800	90.43	26.37	143.17	6.65	24.45	3.31
	439.02	291.2	5.3188	85.53	21.44	128.41	6.59	21.44	1.97
	439.52	289.5	5.2768	87.43	25.74	138.91	6.65	22.76	2.84
	439.39	291.3	5.3171	82.77	28.57	139.91	6.59	23.25	3.18
514.5	438.81	293.7	5.3738	97.87	33.50	164.87	8.08	22.80	2.70
	438.92	293.9	5.3771	96.43	33.47	163.37	8.08	22.63	2.59
	439.60	290.5	5.2971	100.73	30.50	161.73	8.19	21.77	2.02
488.0	439.56	292.0	5.3281	107.83	29.44	166.71	8.59	21.55	1.83
	439.90	289.4	5.2700	106.33	29.40	165.13	8.71	20.91	1.40
	439.44	291.2	5.3134	101.67	30.70	163.07	8.65	20.99	1.45
457.9	438.47	288.0	5.2587	114.10	35.54	185.18	9.28	21.85	1.98
	438.45	290.3	5.3071	119.30	30.54	180.38	9.22	21.69	1.87
	439.54	287.5	5.2351	112.23	38.84	189.91	9.34	22.19	2.20
	439.20	289.4	5.2790	113.47	34.00	181.47	9.28	21.60	1.81

Table 18.1 Measurements of B_n and B_R for trifluoromethane.

§23. Measurements of B_n and B_R for trifluoromethane (CHF_3)

Our detailed measurements used to calculate B_n and B_R for trifluoromethane are given in table 18.1 , and mean values of B_n and B_R are summarized in table 18.2 .

λ / nm	$10^{12}\ B_n$ / $m^6\ mol^{-2}$	$10^{12}\ B_R$ / $m^6\ mol^{-2}$	$\pm 10^{12} \times$ s.d. / $m^6\ mol^{-2}$	$\pm 10^{12}\ B_\Delta$ / $m^6\ mol^{-2}$	$\pm 10^{12} \times$ estimated uncertainty / $m^6\ mol^{-2}$	literature values $10^{12}\ B_R$ / $m^6\ mol^{-2}$
632.8	22.39	2.54	0.75	0.39	1.35	3.4 ± 1.1
514.5	22.40	2.44	0.37	0.31	0.89	-
488.0	21.15	1.56	0.24	0.30	0.75	-
457.9	21.83	1.97	0.17	0.28	0.66	-

Table 18.2 Mean values of B_n and B_R for trifluoromethane.

TETRAFLUOROMETHANE

λ / nm	final pressure / kPa	final pressure / cm Hg(0^{o}C)	T / K	$10^{2}\,V_m$ / $m^3\,mol^{-1}$	number of fringes	$10^{6}(n-1)V_m$ / $m^3\,mol^{-1}$	$10^{6}\,A_n$ / $m^3\,mol^{-1}$	$10^{6}\,A_R$ / $m^3\,mol^{-1}$
632.8	58.657	43.997	290.8	4.1120	690.001	10.7535	10.7529	7.1686
	57.376	43.036	291.8	4.2186	673.033	10.7611	10.7605	7.1736
	62.774	47.085	292.9	3.8696	734.026	10.7655	10.7648	7.1765
514.5	34.856	26.145	291.5	6.9429	505.019	10.8049	10.8045	7.2030
	35.287	26.468	291.9	6.8675	511.021	10.8146	10.8142	7.2095
	37.606	28.207	292.3	6.4523	544.008	10.8166	10.8162	7.2108
488.0	32.514	24.388	290.5	7.4180	499.007	10.8194	10.8190	7.2127
	34.074	25.558	291.3	7.0986	521.171	10.8133	10.8130	7.2087
	37.352	28.017	291.9	6.4872	571.069	10.8282	10.8278	7.2185
457.9	42.245	31.687	289.2	5.6814	696.007	10.8450	10.8446	7.2297
	40.740	30.558	289.8	5.9035	670.014	10.8489	10.8485	7.2323
	42.220	31.651	290.3	5.7097	693.017	10.8521	10.8516	7.2345

Table 19.1 Measurements of A_n and A_R for tetrafluoromethane.

§24. Measurements of A_n and A_R for tetrafluoromethane (CF_4)

Our detailed measurements used to calculate A_n and A_R for tetrafluoromethane are given in table 19.1 , and mean values of A_n and A_R are summarized in table 19.2 .

λ / nm	$10^6 A_n$ / $m^3\ mol^{-1}$	$10^6 A_R$ / $m^3\ mol^{-1}$	$\pm 10^6 \times$ s.d. / $m^3\ mol^{-1}$	literature values $10^6 A_R$ / $m^3\ mol^{-1}$	references
632.8	10.759	7.173	0.004	7.19	Buckingham & Orr 1969
				7.335	Ramaswamy 1935
				6.735	Watson & Ramaswamy 1936
514.5	10.811	7.208	0.004	7.371	Ramaswamy 1935
				6.769	Watson & Ramaswamy 1936
488.0	10.820	7.213	0.005	7.383	Ramaswamy 1935
				6.781	Watson & Ramaswamy 1936
457.9	10.848	7.232	0.002	7.400	Ramaswamy 1935
				6.796	Watson & Ramaswamy 1936

Table 19.2 Mean values of A_n and A_R for tetrafluoromethane.

TETRAFLUOROMETHANE

λ / nm	initial pressure / kPa	T / K	$10^3 V_{m1}$ / $m^3\ mol^{-1}$	$-\theta_1$ / degrees	$-\theta_2$ / degrees	$-(\theta_1+2\theta_2)$ / degrees	$-\theta_c$ / degrees	$10^{12} B_n$ / $m^6\ mol^{-2}$	$10^{12} B_R$ / $m^6\ mol^{-2}$
632.8	432.99	288.4	5.4377	95.77	24.34	144.45	6.50	25.06	3.84
	439.75	290.8	5.4021	99.13	29.39	157.91	6.64	26.96	5.11
	439.78	290.2	5.3903	97.23	30.40	158.03	6.66	26.87	5.05
	438.54	297.9	5.5578	81.10	28.10	137.30	6.44	24.93	3.76
	438.31	299.0	5.5825	86.60	25.70	138.00	6.41	25.27	3.98
	438.74	297.3	5.5427	93.33	20.60	134.53	6.46	24.32	3.35
	438.71	298.9	5.5754	121.73	14.87	151.47	6.42	27.56	5.51
	438.94	296.5	5.5175	120.68	15.24	151.16	6.50	26.95	5.10
	441.91	299.6	5.5481	108.53	14.57	137.67	6.50	24.39	3.40
	439.01	292.6	5.4462	94.83	23.44	141.71	6.57	24.69	3.60
	438.22	292.6	5.4461	109.83	18.92	147.67	6.55	25.68	4.26
514.5	440.40	292.2	5.4211	122.97	39.07	201.11	8.19	28.08	5.73
	439.80	291.7	5.4187	113.77	36.74	187.25	8.19	26.19	4.48
	440.21	289.9	5.3779	110.47	35.64	181.75	8.25	25.08	3.74
488.0	438.71	293.8	5.4740	119.37	39.60	198.57	8.54	26.87	4.91
	438.07	291.5	5.4363	127.13	35.54	198.21	8.54	26.46	4.63
	437.71	293.1	5.4726	116.93	39.10	195.13	8.48	26.41	4.60
457.9	439.21	290.7	5.4066	121.32	44.00	209.32	9.22	25.95	4.23
	439.58	288.5	5.4494	114.87	43.50	201.87	9.17	25.46	3.90
	439.34	290.7	5.4044	126.80	43.80	214.40	9.22	26.54	4.62

Table 20.1 Measurements of B_n and B_R for tetrafluoromethane.

§25. Measurements of B_n and B_R for tetrafluoromethane (CF_4)

Our detailed measurements used to calculate B_n and B_R for tetrafluoromethane are given in table 20.1 , and mean values of B_n and B_R are summarized in table 20.2 .

λ / nm	$10^{12}\ B_n$ / $m^6\ mol^{-2}$	$10^{12}\ B_R$ / $m^6\ mol^{-2}$	$\pm 10^{12} \times$ s.d. / $m^6\ mol^{-2}$	$\pm 10^{12}\ B_\Delta$ / $m^6\ mol^{-2}$	$\pm 10^{12}$ estimated uncertainty / $m^6\ mol^{-2}$	literature values $10^{12}\ B_R$ / $m^6\ mol^{-2}$
632.8	25.70	4.27	0.78	0.38	1.38	-
514.5	26.45	4.65	1.01	0.30	1.53	-
488.0	26.58	4.71	0.17	0.28	0.67	-
457.9	25.98	4.25	0.36	0.26	0.84	-

Table 20.2 Mean values of B_n and B_R for tetrafluoromethane.

§26. Summary of our A_R and B_R values for methane and its fluorinated derivatives

§§26.1 A_R values for methane and its fluorinated derivatives

λ/nm	$10^6 A_R/m^3\ mol^{-1}$				
	CH_4	CH_3F	CH_2F_2	CHF_3	CF_4
632.8	6.569 ±0.003	6.612 ±0.001	6.785 ±0.006	7.022 ±0.002	7.173 ±0.004
514.5	6.639 ±0.001	6.635 ±0.002	6.845 ±0.001	7.070 ±0.001	7.208 ±0.004
488.0	6.654 ±0.001	6.646 ±0.004	6.862 ±0.006	7.082 ±0.001	7.213 ±0.005
457.9	6.682 ±0.003	6.645 ±0.007	6.872 ±0.004	7.097 ±0.002	7.232 ±0.002

Table 20.3 Dispersion of the A_R values for methane and its fluorinated derivatives; the quoted uncertainties are standard deviations.

§§26.2 B_R values for methane and its fluorinated derivatives

λ/nm	$10^{12} B_R^*/m^6\ mol^{-2}$				
	CH_4	CH_3F	CH_2F_2	CHF_3	CF_4
632.8	7.76 ± 1.32	+4.32 ± 1.80	-2.01 ± 1.87	2.54 ± 1.35	4.27 ± 1.38
514.5	6.40 ± 0.83	-0.40 ± 1.28	-5.38 ± 1.13	2.44 ± 0.89	4.65 ± 1.53
488.0	8.93 ± 0.57	-1.02 ± 1.09	-5.86 ± 1.09	1.56 ± 0.75	4.71 ± 0.67
457.9	7.04 ± 0.78	+1.12 ± 0.88	-6.78 ± 1.06	1.97 ± 0.66	4.27 ± 0.84

* These values are shown graphically in §§36.1 on page 79.

Table 20.4 Dispersion of the B_R values for methane and its fluorinated derivatives; the quoted uncertainties are deduced as described in §5.

CARBON DIOXIDE

λ / nm	final pressure / kPa	final pressure / cm Hg(0°C)	T / K	$10^2 V_m$ / $m^3\ mol^{-1}$	number of fringes	$10^6(n-1)V_m$ / $m^3\ mol^{-1}$	$10^6 A_n$ / $m^3\ mol^{-1}$	$10^6 A_R$ / $m^3\ mol^{-1}$
632.8	71.210	53.412	297.5	3.4611	753.878	9.8894	9.8888	6.5925
	67.769	50.831	298.6	3.6511	714.027	9.8808	9.8802	6.5868
	67.165	50.378	298.6	3.6840	707.948	9.8851	9.8845	6.5897
514.5	40.722	30.545	298.7	6.0854	535.981	10.0510	10.0508	5.7005
	41.954	31.469	298.9	5.9103	551.958	10.0529	10.0526	6.7017
	49.985	37.492	298.8	4.9570	657.964	10.0506	10.0503	6.7002
488.0	37.151	27.866	293.8	6.5615	524.966	10.0680	10.0678	6.7118
	37.410	28.060	294.3	6.5272	527.956	10.0724	10.0722	6.7148
	36.943	27.710	294.6	6.6166	520.933	10.0745	10.0743	6.7162
457.9	27.640	20.732	290.7	8.7401	420.985	10.0911	10.0909	6.7273
	31.933	23.952	291.2	7.5679	486.020	10.0876	10.0876	6.7249
	31.995	23.999	291.8	7.5687	486.059	10.0894	10.0892	6.7261

Table 21.1 Measurements of A_n and A_R for carbon dioxide.

§27. Measurements of A_n and A_R for carbon dioxide (CO_2)

Our detailed measurements used to calculate values of A_n and A_R for carbon dioxide are given in table 21.1 , and mean values of A_n and A_R are summarized in table 21.2 .

λ / nm	$10^6 A_n$ / $m^3\ mol^{-1}$	$10^6 A_R$ / $m^3\ mol^{-1}$	$\pm 10^6 \times$ s.d. / $m^3\ mol^{-1}$	literature values $10^6 A_R$ / $m^3\ mol^{-1}$	references
632.8	9.885	6.590	0.003	6.63	Bridge & Buckingham 1966
				6.650	Buckingham & Graham 1974
				6.649	Cuthbertson & Cuthbertson 1920
				6.613	Watson & Ramaswamy 1936
514.5	10.051	6.701	0.001	6.704	Cuthbertson & Cuthbertson 1920
				6.668	Watson & Ramaswamy 1936
488.0	10.071	6.714	0.002	6.723	Cuthbertson & Cuthbertson 1920
				6.686	Watson & Ramaswamy 1936
457.9	10.089	6.726	0.001	6.748	Cuthbertson & Cuthbertson 1920
				6.712	Watson & Ramaswamy 1936

Table 21.2 Mean values of A_n and A_R for carbon dioxide.

CARBON DIOXIDE

λ / nm	initial pressure / kPa	T / K	$10^3 V_{ml}$ / $m^3\ mol^{-1}$	$-\theta_1$ / degrees	$-\theta_2$ / degrees	$-(\theta_1+2\theta_2)$ / degrees	$-\theta_c$ / degrees	$10^{12} B_n$ / $m^6\ mol^{-2}$	$10^{12} B_R$ / $m^6\ mol^{-2}$
632.8	438.18	296.8	5.5032	89.33	16.80	122.93	6.01	21.92	3.76
	437.71	296.2	5.4974	107.67	11.27	130.01	6.01	23.07	4.53
	437.20	298.8	5.5558	105.77	13.20	132.17	5.94	23.93	5.10
	438.53	295.5	5.4725	105.77	13.87	133.51	6.05	23.46	4.78
	437.84	295.3	5.4775	105.17	17.67	140.51	6.02	24.68	5.60
514.5	439.29	295.2	5.4573	88.30	17.80	123.90	7.56	17.87	0.688
	438.94	296.9	5.4954	75.93	24.07	124.07	7.51	18.13	0.865
	438.89	296.2	5.4821	76.10	23.04	122.18	7.51	17.79	0.635
488.0	438.79	295.6	5.4715	90.50	21.64	133.78	9.91	18.37	0.976
	439.27	296.7	5.4871	83.33	26.07	135.47	9.91	18.61	1.14
	439.50	296.6	5.4822	92.73	20.27	133.27	9.91	18.37	0.979
457.9	439.30	292.5	5.4030	87.97	28.94	145.85	8.59	18.32	0.901
	439.05	289.4	5.3448	97.70	30.40	158.50	8.65	19.40	1.63
	438.82	291.8	5.3954	89.87	30.60	151.07	8.59	18.88	1.28

Table 22.1 Measurements of B_n and B_R for carbon dioxide.

§28. Measurements of B_n and B_R for carbon dioxide (CO_2)

Our detailed measurements used to calculate values of B_n and B_R for carbon dioxide are given in table 22.1 , and mean values of B_n and B_R are summarized in table 22.2 .

λ / nm	$10^{12}\ B_n$ / $m^6\ mol^{-2}$	$10^{12}\ B_R$ / $m^6\ mol^{-2}$	$\pm 10^{12} \times$ s.d. / $m^6\ mol^{-2}$	$\pm 10^{12}\ B_\Delta$ / $m^6\ mol^{-2}$	$\pm 10^{12} \times$ estimated uncertainty / $m^6\ mol^{-2}$	literature values $10^{12}\ B_R$ / $m^6\ mol^{-2}$
632.8	23.41	4.75	0.68	0.42	1.30	3.2 ± 1.6
514.5	17.93	0.729	0.12	0.33	0.66	0.4 ± 0.36 (546.1 nm)
488.0	18.45	1.03	0.09	0.32	0.66	-
457.9	18.87	1.27	0.36	0.29	0.85	-

Table 22.2 Mean values of B_n and B_R for carbon dioxide.

NITROGEN

λ / nm	final pressure / kPa	final pressure / cm Hg (0°C)	T / K	$10^2 V_m$ / $m^3\ mol^{-1}$	number of fringes	$10^6 (n-1) V_m$ / $m^3\ mol^{-1}$	$10^6 A_n$ / $m^3\ mol^{-1}$	$10^6 A_R$ / $m^3\ mol^{-1}$
632.8	73.671	55.259	294.2	3.3197	530.008	6.6686	6.6684	4.4456
	82.109	61.588	294.2	2.9781	591.005	6.6709	6.6706	4.4471
	68.204	51.158	294.1	3.5841	491.017	6.6702	6.6699	4.4466
514.5	55.058	41.289	297.0	4.4839	485.994	6.7152	6.7150	4.4767
	53.947	40.465	297.1	4.5777	475.959	6.7142	6.7140	4.4759
	54.351	40.767	296.8	4.5392	479.989	6.7141	6.7139	4.4759
488.0	52.785	39.593	294.8	4.6423	496.001	6.7301	6.7299	4.4866
	49.104	36.832	295.1	4.9954	460.968	6.7305	6.7304	4.4869
	46.931	35.202	295.5	5.2338	440.011	6.7312	6.7310	4.4873
457.9	45.316	33.990	294.2	5.3966	456.039	6.7496	6.7495	4.4997
	46.048	34.540	294.3	5.3125	463.226	6.7491	6.7489	4.4993
	45.523	34.146	294.2	5.3719	458.133	6.7496	6.7495	4.4997

Table 23.1 Measurements of A_n and A_R for nitrogen.

§29. Measurements of A_n and A_R for nitrogen (N_2)

Our detailed measurements used to calculate A_n and A_R for nitrogen are given in table 23.1 , and mean values of A_n and A_R are summarized in table 23.2 .

λ / nm	$10^6 A_n$ / $m^3\ mol^{-1}$	$10^6 A_R$ / $m^3\ mol^{-1}$	$\pm 10^6 \times$ s.d. / $m^3\ mol^{-1}$	literature values $10^6 A_R$ / $m^3\ mol^{-1}$	references
632.8	6.670	4.446	0.001	4.457	Cuthbertson & Cuthbertson 1909
				4.46	Bridge & Buckingham 1966
				4.460	Buckingham & Graham 1974
514.5	6.714	4.476	0.001	4.488	Cuthbertson & Cuthbertson 1909
488.0	6.730	4.487	0.001	4.498	Cuthbertson & Cuthbertson 1909
457.9	6.749	4.500	0.001	4.512	Cuthbertson & Cuthbertson 1909

Table 23.2 Mean values of A_n and A_R for nitrogen.

NITROGEN

λ / nm	initial pressure / kPa	T / K	$10^3 V_{ml}$ / $m^3\ mol^{-1}$	$-\theta_1$ / degrees	$-\theta_2$ / degrees	$-(\theta_1+2\theta_2)$ / degrees	$-\theta_c$ / degrees	$10^{12} B_n$ / $m^6\ mol^{-2}$	$10^{12} B_R$ / $m^6\ mol^{-2}$
632.8	472.74	291.9	5.1269	32.93	11.34	55.61	4.65	8.893	0.986
	473.25	290.7	5.1001	38.93	9.50	57.93	4.69	9.145	1.15
	473.06	291.8	5.1223	30.07	10.20	50.47	4.66	8.123	0.472
	473.61	288.9	5.0640	31.33	11.47	54.27	4.72	8.493	0.719
	472.58	290.6	5.1055	29.47	11.67	52.81	4.68	8.412	0.665
	472.43	292.2	5.1357	29.63	10.30	50.23	4.65	8.127	0.475
	473.31	289.8	5.0834	31.90	10.80	53.50	4.70	8.447	0.687
514.5	473.00	296.3	5.2026	32.97	14.14	61.25	5.67	8.270	0.504
	473.10	296.5	5.2048	29.47	14.54	58.55	5.67	7.943	0.286
	473.59	294.4	5.5059	31.13	14.24	60.61	5.39	9.131	1.08
488.0	473.35	296.2	5.1969	32.40	21.04	74.48	6.02	9.413	1.29
	473.06	297.2	5.2178	31.47	19.20	69.87	6.02	8.943	0.929
	473.08	295.6	5.1892	35.07	16.00	67.07	6.02	8.523	0.649
457.9	472.94	290.1	5.0928	40.87	18.87	78.61	6.53	8.974	0.921
	472.67	291.6	5.1223	37.93	18.44	74.81	6.53	8.669	0.718
	472.53	293.2	5.1546	43.63	18.24	80.11	6.47	9.346	1.11

Table 24.1 Measurements of B_n and B_R for nitrogen.

§30. Measurements of B_n and B_R for nitrogen (N_2)

Our detailed measurements used to calculate B_n and B_R for nitrogen are given in table 24.1 , and mean values of B_n and B_R are summarized in table 24.2 .

λ / nm	$10^{12}\ B_n$ / $m^6\ mol^{-2}$	$10^{12}\ B_R$ / $m^6\ mol^{-2}$	$\pm 10^{12} \times$ s.d. / $m^6\ mol^{-2}$	$\pm 10^{12}\ B_\Delta$ / $m^6\ mol^{-2}$	$\pm 10^{12} \times$ estimated uncertainty / $m^6\ mol^{-2}$	literature values $10^{12}\ B_R$ / $m^6\ mol^{-2}$
632.8	8.52	0.74	0.25	0.26	0.65	1.0 ± 0.31
514.5	8.45	0.62	0.41	0.23	0.78	-
488.0	8.96	0.96	0.32	0.21	0.68	-
457.9	9.00	0.92	0.20	0.19	0.43	-

Table 24.2 Mean values of B_n and B_R for nitrogen.

SULPHUR HEXAFLUORIDE

λ / nm	final pressure		T / K	$10^2 V_m$ / $m^3\ mol^{-1}$	number of fringes	$10^6(n-1)V_m$ / $m^3\ mol^{-1}$	$10^6 A_n$ / $m^3\ mol^{-1}$	$10^6 A_R$ / $m^3\ mol^{-1}$
	kPa	cm Hg(0°C)						
632.8	66.731	50.053	298.4	3.6894	1212.92	16.9604	16.9580	11.3054
	41.249	30.940	290.0	5.8146	768.008	16.9253	16.9239	11.2826
	41.473	31.108	292.8	5.8397	765.998	16.9539	16.9525	11.3017
514.5	25.481	19.113	294.4	9.5755	577.992	17.0552	17.0545	11.3696
	26.478	19.861	294.7	9.2233	600.034	17.0543	17.0535	11.3690
	28.649	21.489	295.0	8.5311	649.000	17.0617	17.0608	11.3739
488.0	24.300	18.227	296.1	10.1009	579.012	17.0944	17.0936	11.3957
	27.581	20.688	296.7	8.9141	655.977	17.0912	17.0902	11.3935
	25.278	18.960	297.1	9.7424	600.130	17.0890	17.0880	11.3921
457.9	27.217	20.415	289.9	8.8245	706.020	17.0870	17.0861	11.3907
	26.757	20.070	290.5	8.9955	692.991	17.0967	17.0958	11.3972
	27.574	20.683	290.9	8.7402	712.983	17.0906	17.0897	11.3915

Table 25.1 Measurements of A_n and A_R for sulphur hexafluoride.

§31. Measurements of A_n and A_R for sulphur hexafluoride (SF_6)

Our detailed measurements used to calculate A_n and A_R for sulphur hexafluoride are given in table 25.1 , and mean values of A_n and A_R are summarized in table 25.2 .

λ / nm	$10^6 A_n$ / $m^3\ mol^{-1}$	$10^6 A_R$ / $m^3\ mol^{-1}$	$\pm 10^6 \times$ s.d. / $m^3\ mol^{-1}$	literature values $10^6 A_R$ / $m^3\ mol^{-1}$	references
632.8	16.945	11.297	0.012	11.34	Buckingham & Graham 1974
				11.27	Watson & Ramaswamy 1936
514.5	17.056	11.371	0.003	11.33	Watson & Ramaswamy 1936
488.0	17.091	11.394	0.002	11.34	Watson & Ramaswamy 1936
457.9	17.091	11.394	0.002	11.37	Watson & Ramaswamy 1936

Table 25.2 Mean values of A_n and A_R for sulphur hexafluoride.

SULPHUR HEXAFLUORIDE

λ / nm	initial pressure / kPa	T / K	$10^3 V_{ml}$ / $m^3\ mol^{-1}$	$-\theta_1$ / degrees	$-\theta_2$ / degrees	$-(\theta_1+2\theta_2)$ / degrees	$-\theta_c$ / degrees	$10^{12} B_n$ / $m^6\ mol^{-2}$	$10^{12} B_R$ / $m^6\ mol^{-2}$
632.8	246.76	292.0	9.5335	131.05	23.84	178.73	3.32	92.90	30.33
	246.68	293.0	9.5730	123.17	23.04	169.25	3.31	88.79	27.29
	245.83	290.2	9.5056	113.90	24.75	163.40	3.32	84.58	24.49
	267.39	292.1	8.7783	138.10	23.54	185.18	3.91	93.49	30.43
	265.34	297.9	9.0414	169.07	9.34	187.75	3.76	87.90	26.70
	266.10	295.4	8.9309	169.57	9.54	188.65	3.82	86.20	25.56
	266.56	293.6	8.8558	171.37	12.80	196.97	3.86	88.44	27.06
	266.09	297.1	8.9881	130.70	29.07	188.84	3.80	87.38	26.35
514.5	266.08	292.8	8.8444	139.60	32.84	205.28	4.76	75.01	17.68
	265.82	294.0	8.8937	142.60	33.64	209.88	4.76	77.50	19.34
	265.78	292.8	8.8550	140.33	33.24	207.81	4.76	76.09	18.40
	266.34	295.7	8.9325	144.10	32.77	209.64	4.74	78.09	19.73
	266.85	293.5	8.8414	143.33	37.14	217.61	4.80	79.37	20.59
	266.45	295.8	8.9316	144.13	29.44	203.01	4.74	75.66	18.11
488.0	265.42	296.5	8.9908	148.23	46.34	240.91	4.93	86.05	24.92
	265.80	294.6	8.9143	150.57	45.94	242.45	4.98	85.14	24.31
	265.42	297.3	9.0175	150.33	45.97	242.27	4.93	87.04	25.57
	266.34	294.8	8.9023	163.97	36.47	236.90	5.02	83.02	22.89
457.9	266.76	254.34	8.7200	162.07	46.14	254.35	5.44	80.27	21.06
	267.60	248.64	8.6652	166.77	40.94	248.65	5.50	77.54	19.24
	267.32	251.26	8.7386	156.20	47.53	251.26	5.44	79.65	20.65

Table 26.1 Measurements of B_n and B_R for sulphur hexafluoride.

§32. Measurements of B_n and B_R for sulphur hexafluoride (SF_6)

Our detailed measurements used to calculate B_n and B_R for sulphur hexafluoride are given in table 26.1 , and mean values of B_n and B_R are summarized in table 26.2 .

λ / nm	$10^{12}\ B_n$ / $m^6\ mol^{-2}$	$10^{12}\ B_R$ / $m^6\ mol^{-2}$	$\pm 10^{12} \times$ s.d. / $m^6\ mol^{-2}$	$\pm 10^{12}\ B_\Delta$ / $m^6\ mol^{-2}$	$\pm 10^{12} \times$ estimated uncertainty / $m^6\ mol^{-2}$	literature values $10^{12}\ B_R$ / $m^6\ mol^{-2}$
632.8	88.71	27.28	2.11	2.72	5.18	29 ± 5.4
514.5	77.71	19.48	1.26	2.07	4.68	-
488.0	86.08	24.93	0.63	2.01	2.99	-
457.9	79.15	20.32	0.95	1.79	3.08	-

Table 26.2 Mean values of B_n and B_R for sulphur hexafluoride.

§33. Summary of our A_R and B_R values for carbon dioxide, nitrogen and sulphur hexafluoride

§§33.1 A_R values for carbon dioxide, nitrogen and sulphur hexafluoride

λ / nm	$10^6 A_R/m^3\ mol^{-1}$		
	CO_2	N_2	SF_6
632.8	6.590 ± 0.003	4.446 ± 0.001	11.297 ± 0.012
514.5	6.701 ± 0.001	4.476 ± 0.001	11.371 ± 0.003
488.0	6.714 ± 0.002	4.487 ± 0.001	11.394 ± 0.002
457.9	6.726 ± 0.001	4.500 ± 0.001	11.392 ± 0.002

Table 26.3 Dispersion of the A_R values for carbon dioxide, nitrogen and sulphur hexafluoride; the quoted uncertainties are standard deviations.

§§33.2 B_R values for carbon dioxide, nitrogen and sulphur hexafluoride

λ / nm	$10^{12} B_R^*/m^6\ mol^{-2}$		
	CO_2	N_2	SF_6
632.8	4.75 ± 1.30	0.74 ± 0.65	27.28 ± 5.18
514.5	0.729 ± 0.66	0.62 ± 0.78	19.48 ± 4.68
488.0	1.03 ± 0.66	0.96 ± 0.68	24.93 ± 2.99
457.9	1.27 ± 0.85	0.92 ± 0.43	20.23 ± 3.08

* These values are shown graphically in §§36.1 on page 79.

Table 26.4 Dispersion of the B_R values for carbon dioxide, nitrogen and sulphur hexafluoride; the quoted uncertainties are deduced as described in §5.

§34. Measurements of B_R at different pressures

Values of B_R for methane, trifluoromethane and sulphur hexafluoride were determined at a range of pressures as indicated in table 27.1 below.

gas	mean pressure	$10^{12}\ B_n$	$10^{12}\ B_R$	$\pm 10^{12} \times$ s.d.	$\pm 10^{12}\ B_\Delta$	$\pm 10^{12} \times$ estimated uncertainty
	kPa	$m^6\ mol^{-2}$	$m^6\ mol^{-2}$	$m^6\ mol^{-2}$	$m^6\ mol^{-2}$	$m^6\ mol^{-2}$
CH_4	368.89	25.64	6.31	0.75	0.39	1.35
	403.77	26.31	6.75	0.63	0.32	1.15
	438.48	27.78	7.76 †	0.83	0.28	1.32
	473.13	27.31	7.42	0.43	0.24	0.87
CHF_3	369.42	22.51	2.68	0.04	0.56	0.76
	404.33	24.31	3.88	0.19	0.45	0.85
	440.22	22.39	2.54 †	0.75	0.39	1.35
	474.20	23.03	3.03	0.88	0.32	1.41
SF_6	258.84	88.71	27.28 †	2.11	2.72	5.18
	335.25	89.54	27.79	0.24	1.61	2.29
	403.56	89.53	27.79	2.29	1.07	3.70

† Obtained from table 12.2 for CH_4, table 18.2 for CHF_3 and table 26.2 for SF_6.

Table 27.1 Mean values of B_n and B_R as a function of pressure at room temperature for $\lambda = 632.8$ nm.

The detailed measurements used to calculate B_n and B_R for these gases are given in tables 27.2 , 27.3 and 27.4 . We note from the above summary that the values of B_R for methane, trifluoromethane and sulphur hexafluoride show no systematic dependence on the initial pressure in a double decompression experiment within experimental error. This indicates that C_R makes a negligible contribution and that the observed rotations θ_1 and θ_2 are determined by B_n only. This range of gases was chosen since it incorporates a polar gas trifluoromethane and two non-polar gases whose B_n values are easily measured, even at low pressures.

METHANE

initial pressure / kPa	T / K	$10^3 V_{m1}$ / $m^3\ mol^{-1}$	$-\theta_1$ / degrees	$-\theta_2$ / degrees	$-(\theta_1+2\theta_2)$ / degrees	$-\theta_c$ / degrees	$10^{12} B_n$ / $m^6\ mol^{-2}$	$10^{12} B_R$ / $m^6\ mol^{-2}$
369.16	294.5	6.5864	65.70	16.40	98.50	4.18	25.01	5.89
368.68	296.7	6.6458	67.30	15.14	97.57	4.14	25.22	6.03
369.01	297.0	6.6466	67.13	14.77	96.67	4.14	25.00	5.88
368.72	295.5	6.6174	75.47	15.74	106.95	4.16	27.32	7.42
404.03	297.0	6.0667	85.43	19.74	124.91	4.97	26.84	7.10
403.86	293.4	5.9936	87.13	20.77	128.67	5.03	26.97	7.19
403.62	293.6	6.0015	78.27	20.00	118.27	5.02	24.93	5.83
403.56	297.0	6.0737	85.67	18.67	123.01	4.96	26.50	6.88
472.95	296.8	5.1726	117.77	30.90	179.57	6.82	28.00	7.88
473.31	295.2	5.1399	114.17	29.50	173.17	6.87	26.71	7.02
473.17	296.3	5.1611	120.00	27.60	175.20	6.84	27.23	7.36

Table 27.2 Measurements of B_n and B_R for methane at different pressures for λ = 632.8 nm.

T R I F L U O R O M E T H A N E

initial pressure / kPa	T / K	$10^3 V_{m1}$ / $m^3\ mol^{-1}$	$-\theta_1$ / degrees	$-\theta_2$ / degrees	$-(\theta_1+2\theta_2)$ / degrees	$-\theta_c$ / degrees	$10^{12} B_n$ / $m^6\ mol^{-2}$	$10^{12} B_R$ / $m^6\ mol^{-2}$
369.36	291.3	6.3619	59.83	17.20	94.23	4.63	22.47	2.65
369.64	289.7	6.3184	60.10	18.00	96.10	4.66	22.59	2.73
369.27	291.8	6.3760	60.70	16.57	93.84	4.62	22.47	2.66
404.51	288.1	5.7203	78.60	23.30	125.20	5.61	24.04	3.70
404.32	290.3	5.7724	77.60	23.44	124.47	5.59	24.33	3.90
404.24	291.4	5.7979	77.60	23.80	125.20	5.56	24.68	4.13
404.24	289.3	5.7514	78.23	23.17	124.57	5.60	24.18	3.79
474.31	289.1	4.8677	111.43	31.34	174.10	7.79	24.20	3.80
474.09	291.3	4.9102	101.74	24.24	150.24	7.68	21.38	1.93
474.23	289.4	4.8739	107.87	34.64	177.15	7.73	24.66	4.12
474.10	290.7	4.9004	95.57	29.17	153.91	7.73	21.79	2.20
474.33	288.5	4.8547	102.63	30.37	163.37	7.79	22.65	2.77
474.12	290.3	4.8925	104.23	31.37	166.97	7.73	23.48	3.33

Table 27.3 Measurements of B_n and B_R for trifluoromethane at different pressures for λ = 632.8 nm.

S U L P H U R H E X A F L U O R I D E

initial pressure / kPa	T / K	$10^3 V_{ml}$ / $m^3\ mol^{-1}$	$-\theta_1$ / degrees	$-\theta_2$ / degrees	$-(\theta_1+2\theta_2)$ / degrees	$-\theta_c$ / degrees	$10^{12} B_n$ / $m^6\ mol^{-2}$	$10^{12} B_R$ / $m^6\ mol^{-2}$
336.63	296.3	7.0184	277.00	20.34	317.67	6.15	89.56	27.81
334.67	297.7	7.0986	269.00	19.77	308.53	6.05	89.19	27.55
334.46	298.7	7.1300	275.43	16.71	308.86	6.02	89.88	28.02
403.59	295.5	5.7837	409.30	39.17	487.64	8.96	93.27	30.28
403.53	297.6	5.8320	393.13	22.17	437.47	8.88	85.24	24.92
403.55	294.5	5.7614	400.93	32.70	466.33	8.99	88.59	27.16
403.55	297.8	5.8357	409.07	29.00	467.07	8.88	91.01	28.77

Table 27.4 Measurements of B_n and B_R for sulphur hexafluoride at different pressures for λ = 632.8 nm.

gas	initial pressure / kPa	T / K	$10^3 V_{ml}$ / $m^3\ mol^{-1}$	$-\theta_1$ / degrees	$-\theta_2$ / degrees	$-(\theta_1+2\theta_2)$ / degrees	$-\theta_c$ / degrees	$10^{12} B_n$ / $m^6\ mol^{-2}$	$10^{12} B_R$ / $m^6\ mol^{-2}$
CH_4*	438.66	296.1	5.5667	85.20	28.71	142.62	5.73	25.84	6.44
	438.31	297.9	5.6060	80.23	28.54	137.31	5.73	25.26	6.05
	438.44	298.7	5.6200	85.13	24.64	134.41	5.73	24.87	5.79
CH_4†	438.22	295.0	5.5509	93.50	22.78	139.06	5.73	25.08	5.93
	438.19	297.3	5.5960	94.73	22.87	140.47	5.73	25.72	6.36
	427.98	297.8	5.6084	92.20	21.37	134.94	5.67	24.84	5.77
CHF_3*	437.98	295.6	5.4236	88.43	17.77	123.77	6.44	21.54	2.03
	438.33	296.5	5.4367	89.93	18.94	127.81	6.30	22.28	2.53
	437.80	298.6	5.4873	89.97	16.74	123.55	6.30	21.95	2.30
CHF_3†	438.56	298.0	5.4649	86.57	18.07	122.71	6.30	21.65	2.11
	438.73	298.1	5.4651	90.93	14.67	120.27	6.30	21.24	1.84
	438.58	296.0	5.4233	94.37	18.70	131.77	6.30	22.83	2.89
	438.08	297.3	5.4569	92.27	18.14	128.55	6.30	22.56	2.72

Table 28.1 Measurements of B_n and B_R for methane (CH_4) and trifluoromethane (CHF_3) before* and after† increasing the surface-to-volume ratio of the sample cells by 46% using stainless-steel balls (λ = 632.8 nm).

§35. Measurements of B_n and B_R before and after increasing the surface-to-volume ratio of the sample cells

In §4. of chapter 4 the effects of adsorption on our B_R values was discussed and we concluded that the effects of adsorption are either negligible or that compensation by simultaneous desorption occurs. The B_n and B_R values which are referred to in that discussion are given below in table 28.2. These values were obtained before and after increasing the surface-to-volume ratio of the cells by 46% using stainless-steel balls. The detailed

gas	$10^{12}\ B_n$ / $m^6\ mol^{-2}$	$10^{12}\ B_R$ / $m^6\ mol^{-2}$	$\pm 10^{12} \times$ s.d. / $m^6\ mol^{-2}$	$\pm 10^{12}\ B_\Delta$ / $m^6\ mol^{-2}$	$\pm 10^{12} \times$ estimated uncertainty / $m^6\ mol^{-2}$
CH_4*	25.32	6.09	0.27	0.25	0.72
CH_4†	25.21	6.02	0.31	0.27	0.78
CHF_3*	21.92	2.29	0.125	0.41	0.87
CHF_3†	22.07	2.39	0.50	0.41	1.12

Table 28.2 Measurements of B_n and B_R for methane (CH_4) and trifluoromethane (CHF_3) before* and after † increasing the surface-to-volume ratio of the sample cells by 46% (λ = 632.8 nm).

measurements used to calculate these B_n and B_R values are given in table 28.1.

§36. Discussion of our B_R values

§§36.1 Wavelength dependence of B_R

In tables 10.4 , 20.4 and 26.4 (which appear on pages 55, 66 and 73) B_R values have been presented for our range of samples as a function of wavelength and dispersion plots of this data are given in graphs 1, 2 and 3. A striking feature of these graphs is the irregular variation in B_R from 457.9 to 514.5 nm, although for some gases namely Ar, CH_2F_2 , CF_4 and N_2 the variations are less pronounced. It should be emphasized that similar variations may also be present in the wavelength range 514.5 to 632.8 nm and the drawing of a straight line between these wavelength values is unjustified and possibly misleading. On discovering this irregular behaviour of B_R with wavelength further measurements were undertaken on SF_6 at 488.0 nm, 514.7 nm and 632.8 nm and Kr at 632.8 nm and 488.0 nm in an attempt to establish whether these variations were real rather than due to experimental error. However, for both these gases no significant discrepancies between these measurements and those carried out earlier were evident. We have found no reason to attribute the dispersion to a systematic instrumental effect, and note that the absence of anomalous dispersion in A_R supports this view. Our measurements were carried out in no set order and our B_R values at 632.8 nm were calculated from measurements which were accumulated over several months. Further measurements of B_R in the wavelength range 514.5 to 632.8 nm would be helpful in the understanding of the wavelength dependence of B_R for our range of samples. This wavelength range is conveniently spanned with a krypton ion laser.

§§36.2 Variation of B_R within a molecular series

Another interesting feature of the measurements is the unevenness in B_R for the molecular series CH_4 to CF_4 and we note that the anomalous behaviour of these samples has been reported in other effects. Denbigh (1940) reported much larger differences between calculated and observed polarizabilities for molecules containing fluorine than for others, typically 4% compared with 0.7% . Krugh & Bernheim (1969) in their n.m.r. investigation of the structure of molecules oriented by nematic liquids found disagreement with microwave results for CH_3F . Light scattering measurements by Bridge & Buckingham (1966) revealed low anisotropies in the polarizability for the fluoromethanes which they attributed to inaccessible d-orbitals. Also

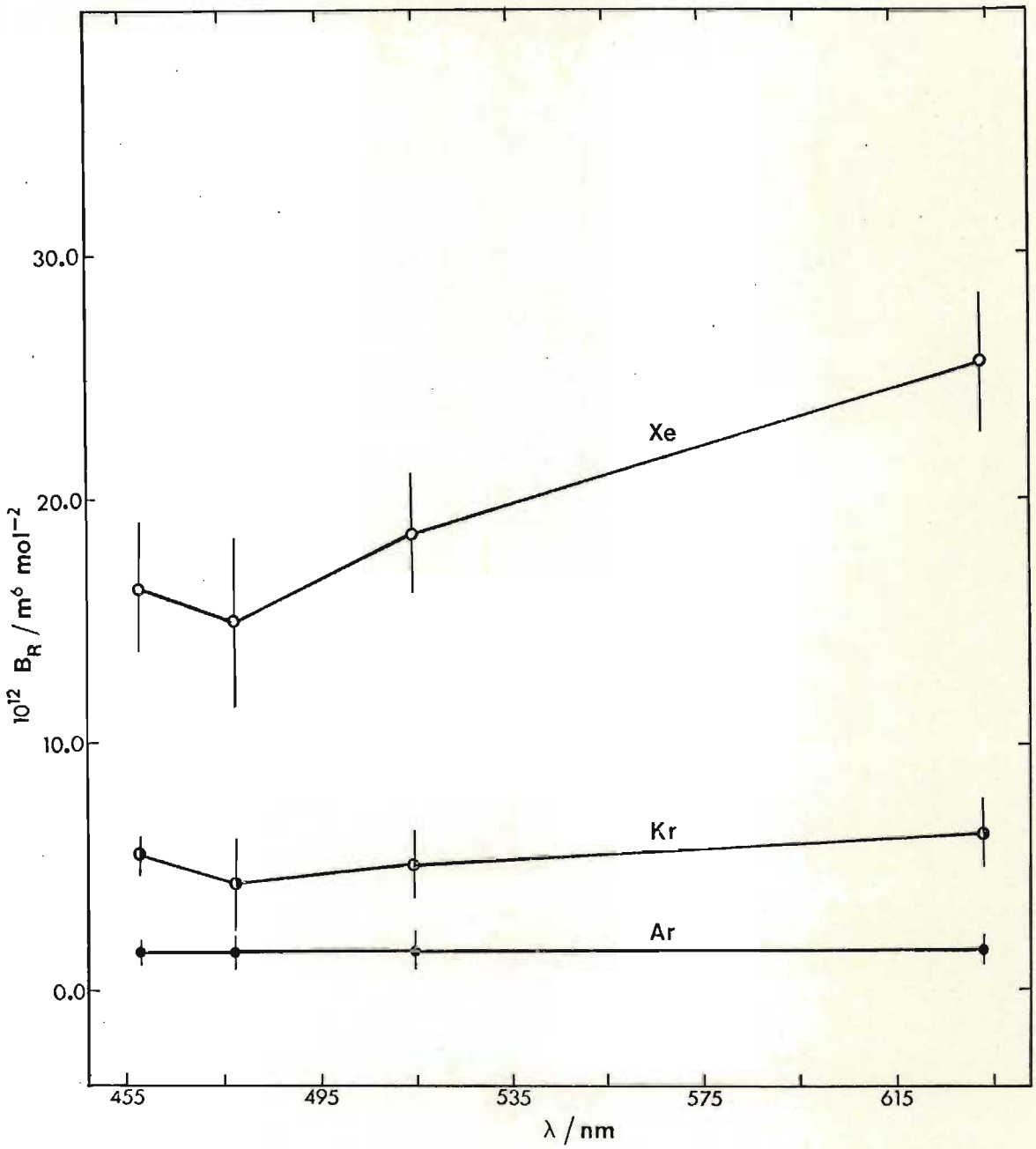

Graph 1. Dispersion of the B_R values for Ar, Kr and Xe (the B_R values for Ne have been omitted from the graph). The vertical bars show the estimated uncertainties in the measurements.

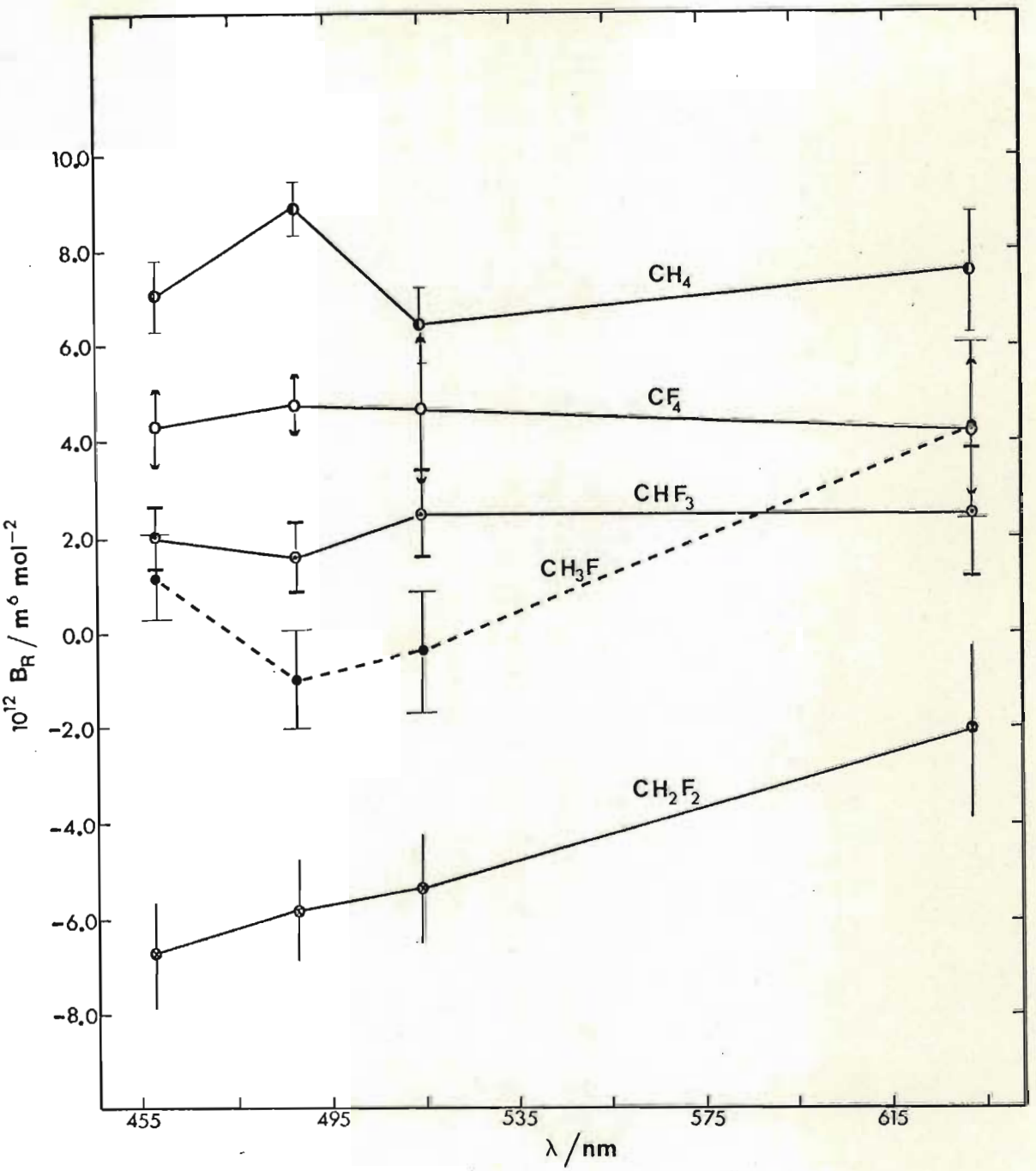

Graph 2. Dispersion of the B_R values for methane and its fluorinated derivatives. The vertical bars show the estimated uncertainties in the measurements.

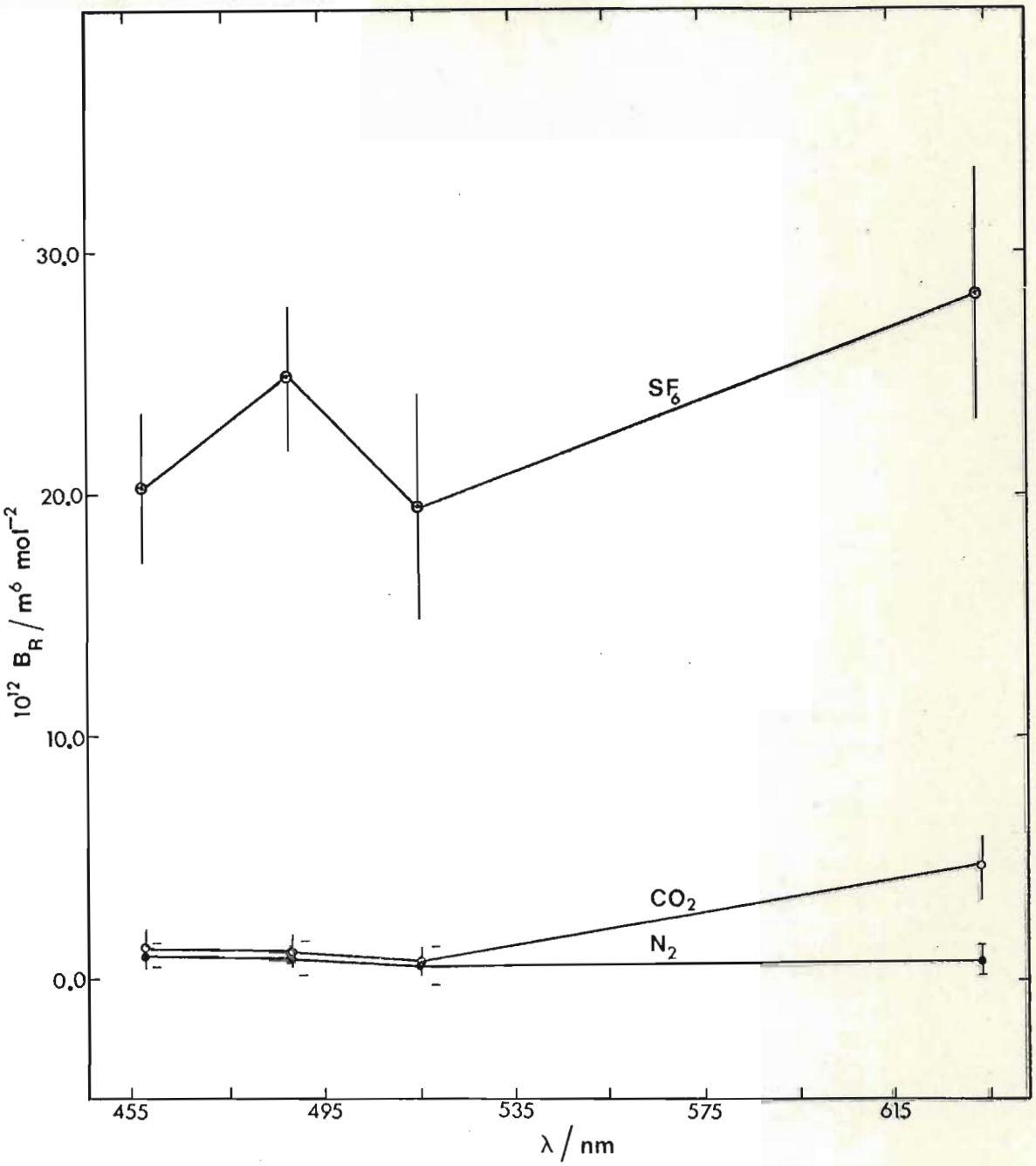

Graph 3. Dispersion of the B_R values for CO_2, N_2 and SF_6. The vertical bars show the estimated uncertainties in the measurements and for N_2 have been shifted to the right-hand side for clarity.

measurements of the Faraday effect of Burns, Hampton & Raab (1977) revealed considerable unevenness in the Verdet constants for the molecular series CH_4 to CF_4 with the Verdet constants of CH_2F_2 and CHF_3 being nearly equal and that of CF_4 being the smallest in the series. We note that no similar unevenness is present in the series Ne to Xe in which B_R increases with increasing molecular diameter.

§37. Some limitations of our apparatus

The chief sources of error in our values of B_R are drift, uncertainties due to cell distortion and relative changes in the decompression cell volumes. Since contributions to the interferometer output arising from cell distortion or volume instability are linear in the starting pressure, whilst effects due to B_R vary as the square of this pressure, the relative importance of errors arising from uncertainties or instabilities in the cell volumes may be substantially reduced by working at high pressures. Measurements at high pressures would have the added advantage of enhanced rotations, so that precise measurements of larger quantities would further increase the precision.

A major problem in the adaptation of our present system for use at higher pressures is the development of a reliable and durable gas seal between the windows and the cells. The present decompression cells were operated at about 500 kPa, but we have been reluctant to increase the pressure substantially for fear of fracturing the 2.5 mm thick Pockels glass windows which are proving to be almost irreplaceable. It is not known at what pressures the thin Kel-F gaskets will prove unreliable, but Graham (1971) suggests the use of indium gaskets with thicker bulkheads may be successful. St-Arnaud & Bose (1976) have successfully used commercially built stainless-steel cells by Aminco. Their cells had been pressure tested to about 32 000 kPa by the supplier. No details are given as to how the windows were kept in position except that their quartz windows were 1.75 cm thick. Their measurements of B_n for methane were conducted at pressures ranging from 12 000 to 18000 kPa and they report, surprisingly, that no contributions from C_n were evident.

A major incentive for the improvement of sensitivity is that accurate measurements on helium (which holds a position of theoretical importance) may become practicable.

REFERENCES

Bridge, N.J. & Buckingham, A.D. 1966 *Proc. R. Soc. Lond. A* 295, 334.

Buckingham, A.D. & Orr, B.J. 1969 *Trans. Faraday Soc.* 65, 673.

Burns, R.C., Hampton, I. & Raab, R.E. 1977 *J. Chem. Soc. Faraday Trans. II*, 73, 958.

Cuthbertson, C. & Cuthbertson, M. 1909 *Proc. R. Soc. Lond. A* 83, 151; 171; 1910 *Proc. R. Soc. Lond. A* 88, 13; 1920 *Proc. R. Soc. Lond. A* 97, 152; 1932 *Proc. R. Soc. Lond. A* 135, 40.

Cuthbertson, C. & Cuthbertson, M. 1913 *Phil. Trans. R. Soc. Lond. A* 213, 1.

Dalgarno, A. & Kingston, A.E. 1960 *Proc. R. Soc. Lond. A* 259, 424.

Denbigh, K.G. 1940 *Trans. Faraday Soc.* 36, 936.

Dymond, J.H. & Smith, E.B. *The virial coefficients of gases.* Oxford : Clarendon Press.

Graham, C. 1971 Ph.D. thesis, University of Cambridge.

Krugh, T.R. & Bernheim, R.A. 1969 *J. Amer. Chem. Soc.* 91, 2385; 1970 *J. Chem. Phys.* 52, 4942.

McCarthy, E.R. 1968 *Org. Mass Spectrometry* 1, 81.

Ramaswamy, K.L. 1935 *Proc. Indian Acad. Sci. A* 2, 639; 1936 *Proc. Indian Acad. Sci. A* 4, 675.

St-Arnaud & Bose, T.K. 1976 *J. Chem. Phys.* 68, 4854.

Watson, R.E. & Ramaswamy, K.L. 1936 *Proc. R. Soc. Lond. A* 156, 144.

CHAPTER 6

MOLECULAR THEORY OF THE SECOND REFRACTIVITY VIRIAL COEFFICIENT B_R

§1. Introduction

In this chapter a formal derivation is given of the phenomenological expression for the second refractivity virial coefficient

$$B_R = \frac{N_A^2}{3\varepsilon_o \Omega}\int (\tfrac{1}{2}\alpha_{12}(\tau) - \alpha_o) \exp(-U_{12}(\tau)/kT)\, d\tau \quad , \tag{6.1}$$

which was presented in the introductory chapter. Here $\alpha_{12}(\tau)$ is the mean pair polarizability of an isolated molecule and $U_{12}(\tau)$ is the intermolecular potential energy of the pair of molecules 1, 2 when in the relative configuration τ .

If B_R is to be calculated the quantities $(\tfrac{1}{2}\alpha_{12}(\tau) - \alpha_o)$ and $U_{12}(\tau)$ must be evaluated and the integration in (6.1) performed. Although there is no general theory of each of these quantities applicable to all molecules for all separations, expressions are derived in terms of multipole moments and polarizabilities of an isolated molecule. This is equivalent to taking the wave functions of an interacting pair as the product of isolated-molecule wave functions. Although this simplification is satisfactory at long range difficulties arise when the charge distributions in the colliding molecules begin to overlap. In this region *ab initio* quantum mechanical calculations may be necessary. These calculations, however, have only been attempted on the simplest molecular systems because they are complicated and require a considerable amount of computing time. Quantum mechanical calculations are beyond the scope of this investigation. In the absence of a better approach we use the isolated-molecule expressions for $(\tfrac{1}{2}\alpha_{12}(\tau) - \alpha_o)$, which are rigorously correct only for large intermolecular separations, to describe both long and short range interactions.

§2. A statistical mechanical expression for B_R

The theory of the second refractivity virial coefficient B_R has been given by Buckingham (1956). This treatment is closely related to the theory of the second dielectric virial coefficient B_ε given by Buckingham & Pople (1955a). Indeed, expressions for B_R are obtained by evaluating B_ε in the limit of a high frequency optical field and by the use of the relationship

$$n^2 = \varepsilon_r \mu_r \quad , \tag{6.2}$$

where ε_r is the dielectric constant and μ_r is the relative permeability.

We consider an assembly of N identical molecules comprising a dielectric sample in a static external field $\underset{\sim}{E}_o$. The electric displacement $\underset{\sim}{D}_i$ within the medium is related to the macroscopic internal field $\underset{\sim}{E}_i$ by the equation

$$\underset{\sim}{D}_i = \varepsilon_o \underset{\sim}{E}_i + \underset{\sim}{P}_i \quad , \tag{6.3}$$

where $\underset{\sim}{P}_i$ is the dipole moment per unit volume. Since $\underset{\sim}{D}_i = \varepsilon_o \varepsilon_r \underset{\sim}{E}_i$, it follows from (6.3) that

$$\varepsilon_o(\varepsilon_r - 1) = \frac{\underset{\sim}{P}_i}{\underset{\sim}{E}_i} \quad . \tag{6.4}$$

For a statistical mechanical treatment of B_ε the macroscopic internal field $\underset{\sim}{E}_i$, which itself is an averaged quantity, must be expressed in terms of $\underset{\sim}{E}_o$. This is simply achieved if we choose a spherical sample where

$$\underset{\sim}{E}_i = \frac{3}{\varepsilon_r + 2} \underset{\sim}{E}_o \quad . \tag{6.5}$$

The factor $\frac{1}{\varepsilon_r + 2}$ in (6.5) implies an internal field which is smaller than the applied field, arising from bulk polarization effects in which the applied field is partially cancelled by induced surface charge. Combination of (6.4) and (6.5) yields

$$\frac{\varepsilon_r - 1}{\varepsilon_r + 2} = \frac{1}{3\varepsilon_o} \left(\frac{\underset{\sim}{P}_i}{\underset{\sim}{E}_o} \right). \tag{6.6}$$

In most experimental situations saturation effects are negligible and $\frac{\underset{\sim}{P}_i}{\underset{\sim}{E}_o}$ may be evaluated in the limit of zero field and we write

$$\frac{\varepsilon_r - 1}{\varepsilon_r + 2} V_m = \frac{1}{3\varepsilon_o} \lim_{E_o \to 0} \frac{\underset{\sim}{\bar{M}}(\underset{\sim}{E}_o)}{\underset{\sim}{E}_o} = \frac{1}{3\varepsilon_o} \left(\frac{\partial \underset{\sim}{\bar{M}}}{\partial \underset{\sim}{E}_o} \right)_{E_o = 0} , \tag{6.7}$$

where $\underset{\sim}{\bar{M}}(\underset{\sim}{E}_o) = \underset{\sim}{P}_i V_m$ is the total dipole moment of one mole of dielectric.

The classical equilibrium statistical mechanical expression for $\bar{M}$ is

$$\underset{\sim}{\bar{M}}(\underset{\sim}{E}_o) = \frac{\int [\underset{\sim}{M}(\tau, \underset{\sim}{E}_o) \cdot \underset{\sim}{e}] \exp[-(V(\tau) - \underset{\sim}{M}(\tau, \underset{\sim}{E}_o) \cdot \underset{\sim}{E}_o)/kT] \, d\tau}{\int \exp[-(V(\tau) - \underset{\sim}{M}(\tau, \underset{\sim}{E}_o) \cdot \underset{\sim}{E}_o)/kT] \, d\tau} , \tag{6.8}$$

where $\underset{\sim}{M}(\tau, \underset{\sim}{E}_o)$ is the total molar moment when the configuration of the molecules is τ and the external field is $\underset{\sim}{E}_o$. $V(\tau)$ is the intermolecular potential energy and $\underset{\sim}{e}$ is a unit vector in the direction of $\underset{\sim}{E}_o$.

If (6.8) is differentiated with respect to E_o and then E_o is set equal to zero, we obtain

$$\left(\frac{\partial \bar{\underset{\sim}{M}}}{\partial E_o}\right)_{E_o=0} = \left\langle \frac{\partial \underset{\sim}{M}(\tau,E_o)}{\partial E_o} \cdot \underset{\sim}{e} \right\rangle + \frac{1}{kT} \left\langle [\underset{\sim}{M}(\tau,0) \cdot \underset{\sim}{e}][\underset{\sim}{M}(\tau,0) \cdot \underset{\sim}{e}] \right\rangle$$

$$- \frac{1}{kT} \left\langle \underset{\sim}{M}(\tau,0) \cdot \underset{\sim}{e} \right\rangle \left\langle \underset{\sim}{M}(\tau,0) \cdot \underset{\sim}{e} \right\rangle \quad , \tag{6.9}$$

where the brackets $\langle\ \rangle$ are used to denote statistical averages of the system in the absence of the field $\underset{\sim}{E}_o$. For an isotropic sample, $\underset{\sim}{e}$ is parallel to $\underset{\sim}{E}_o$ and

$$\left\langle [\underset{\sim}{M}(\tau,0) \cdot \underset{\sim}{e}][\underset{\sim}{M}(\tau,0) \cdot \underset{\sim}{e}] \right\rangle = \frac{1}{3} \left\langle M(\tau,0)^2 \right\rangle$$

and

$$\left\langle \underset{\sim}{M}(\tau,0) \cdot \underset{\sim}{e} \right\rangle = 0 \quad . \tag{6.10}$$

Substitution of (6.9) into (6.7) followed by the use of (6.10) yields

$$\frac{\varepsilon_r - 1}{\varepsilon_r + 2} V_m = \frac{1}{3\varepsilon_o}\left[\left\langle \frac{\partial [\underset{\sim}{M}(\tau,\underset{\sim}{E}_o)] \cdot \underset{\sim}{e}}{\partial E_o} \right\rangle + \frac{1}{3kT} \left\langle M(\tau,0)^2 \right\rangle \right], \tag{6.11}$$

and since all molecules in the medium are identical, this can be written as

$$\frac{\varepsilon_r - 1}{\varepsilon_r + 2} V_m = \frac{N_A}{3\varepsilon_o}\left[\left\langle \frac{\partial \underset{\sim}{\mu}^{(1)}}{\partial E_o} \cdot \underset{\sim}{e} \right\rangle + \frac{1}{3kT} \sum_{i=1}^{N_A} \left\langle \underset{\sim}{\mu}_1 \cdot \underset{\sim}{\mu}_i \right\rangle \right], \tag{6.12}$$

where $\underset{\sim}{\mu}_i$ is the dipole moment of an individual molecule i and where N has been put equal to Avogadro's number N_A.

The two terms on the right-hand side of (6.12) may be given the following physical interpretations : the first arises from the polarizing action of the external field which distorts the molecules, while the second temperature dependent contribution arises from the tendency of the permanent or induced dipoles of a molecule to align themselves with $\underset{\sim}{E}_o$.

For an alternating applied field $\mathscr{E}_o$ at optical frequencies, the molecules are unable to follow the alternations of the field and the temperature-dependent term in (6.12) is zero.

Then at optical frequencies (6.12) can be written as,

$$\frac{\varepsilon_r(\omega) - 1}{\varepsilon_r(\omega) + 2} V_m = \frac{N_A}{3\varepsilon_o} \left\langle \frac{\partial \underset{\sim}{\mu}^{(1)}}{\partial \mathscr{E}_o} \cdot \underset{\sim}{e} \right\rangle \quad , \tag{6.13}$$

and the introduction of the refractive index n using (6.2) ($\mu_r \approx 1$ for a gas) yields

$$\frac{n^2 - 1}{n^2 + 2} V_m = \frac{N_A}{3\varepsilon_o} \left\langle \frac{\partial \underset{\sim}{\mu}^{(1)}}{\partial \mathscr{E}_o} : \underset{\sim}{e} \right\rangle \quad . \tag{6.14}$$

It follows from (1.2) of chapter 1 and (6.14) above that the first refractivity virial coefficient A_R is given by

$$A_R = \lim_{V_m \to \infty} \frac{n^2 - 1}{n^2 + 2} V_m = \frac{N_A \alpha_o}{3\varepsilon_o} \quad , \tag{6.15}$$

and that

$$B_R = \lim_{V_m \to \infty} \left[(R_m - A_R) V_m \right] = \lim_{V_m \to \infty} \frac{N_A}{3\varepsilon_o} \left[\left\langle \frac{\partial \underset{\sim}{\mu}^{(1)}}{\partial \mathscr{E}_o} \cdot \underset{\sim}{e} - \alpha_o \right\rangle V_m \right] . \tag{6.16}$$

The probability of interaction $P(\tau_i)$ of a single molecule i with another molecule 1, having co-ordinates τ_i in the range $d\tau_i$ near molecule 1 is

$$P(\tau_i) = \frac{1}{\Omega V_m} \text{ expt } (-U_{1i}/kT)\, d\tau_i \quad , \tag{6.17}$$

where U_{1i} is their intermolecular potential energy and where

$$\Omega V_m = \int d\tau_i \quad . \tag{6.18}$$

In a molar sample, molecule i may interact with $N_A - 1 \approx N_A$ equivalent molecules and summing over these probabilities gives

$$B_R = \frac{N_A^2}{3\varepsilon_o \Omega} \int \left[\frac{1}{2} \frac{\partial (\underset{\sim}{\mu}^{(1)} + \underset{\sim}{\mu}^{(2)})}{\partial \mathscr{E}_o} \cdot \underset{\sim}{e} - \alpha_o \right] \exp \left[-U_{12}(\tau)/kT \right] d\tau \quad . \tag{6.19}$$

This equation is an alternative form of (6.1) studied in chapter 1.

Since useful relationships exist between refractivity virial coefficients and dielectric virial coefficients, it is helpful to define the first and second dielectric virial coefficients A_ε and B_ε . If the total polarization ${}_TP$ of a gas is expanded in inverse powers of the molar volume V_m ,

$${}_TP = \frac{\varepsilon_r - 1}{\varepsilon_r + 2} V_m = A_\varepsilon + \frac{B_\varepsilon}{V_m} + \cdots \quad , \tag{6.20}$$

(6.12) and (6.20) may be used to show that

$$A_\varepsilon = \frac{N_A}{3\varepsilon_o} \left(\alpha_o + \frac{\mu_o^2}{3kT} \right) \quad , \tag{6.21}$$

and that

$$B_\varepsilon = \frac{N_A^2}{3\varepsilon_o \Omega} \int \left\{ \left[\frac{1}{2} \frac{\partial(\underset{\sim}{\mu}^{(1)} + \underset{\sim}{\mu}^{(2)})}{\partial E_o} \cdot \underset{\sim}{e} - \alpha_o \right] + \frac{1}{3kT} \left[\frac{1}{2}(\underset{\sim}{\mu}^{(1)} + \underset{\sim}{\mu}^{(2)})^2 - \mu_o^2 \right] \right\} \exp(-U_{12}(\tau)/kT)\, d\tau \,. \tag{6.22}$$

The quantities μ_o and $(\underset{\sim}{\mu}^{(1)} + \underset{\sim}{\mu}^{(2)})$ are respectively the permanent dipole moment of an isolated molecule and the total dipole moment of the interacting pair of molecules 1, 2 in a relative configuration τ. α_o is the static field polarizability of an isolated molecule.

If (6.19) and (6.22) for B_R and B_ε are compared, B_ε contains an extra temperature-dependent term $\frac{1}{3kT}[\frac{1}{2}(\underset{\sim}{\mu}^{(1)} + \underset{\sim}{\mu}^{(2)})^2 - \mu_o^2]$ which represents deviations from the independent molecule orientation term $\frac{\mu_o^2}{3kT}$ in A_ε arising from pair interactions. It is important to note that the existence of multipole moments of any order on molecule 2 may induce a dipole moment on molecule 1 and give a non-zero contribution to B_ε. For example a quadrupole moment of a non-polar molecule like carbon dioxide may induce a dipole moment on a neighbouring molecule, producing a non-zero moment in the pair. In this case the temperature-dependent term in B_ε accounts for the orientation of these transient dipole moments by the external field. At optical frequencies no such orientation occurs and this term has no part in B_R.

The remaining terms in B_R and B_ε which arise from the distortion of molecules are similar in form but differ numerically because of the frequency dependence of molecular polarizabilities.

In the next section we develop an expression for $\left(\frac{1}{2} \frac{\partial(\underset{\sim}{\mu}^{(1)} + \underset{\sim}{\mu}^{(2)})}{\partial \mathscr{E}_o} \cdot \underset{\sim}{e} - \alpha_o \right)$ on the basis of the long range approximation introduced at the beginning of this chapter. It is helpful in this derivation to write

$$\left(\frac{1}{2} \frac{\partial(\underset{\sim}{\mu}^{(1)} + \underset{\sim}{\mu}^{(2)})}{\partial \mathscr{E}_o} \cdot \underset{\sim}{e} - \alpha_o \right) = \left(\frac{\partial \mu_\alpha^{(1)}}{\partial \mathscr{E}_o} e_\alpha - \alpha_o \right) .$$

§3. Expressions for $\left(\frac{\partial \mu_\alpha^{(1)}}{\partial \mathscr{E}_o} e_\alpha - \alpha_o \right)$

Forms of the above expression have been given by Buckingham (1956), Kielich (1962) and Graham (1971). In this development we review the treatment of Graham (1971) which is the more general.

The induced dipole moment $\mu_\alpha^{(1)}$ for molecule 1 for weak fields can be written as

$$\mu_\alpha^{(1)}(\mathscr{E}_o) = \alpha_{\alpha\beta}^{(1)}(\mathscr{E}_{o\beta} + \mathscr{F}_\beta^{(1)}) \quad , \tag{6.23}$$

where $\alpha_{\alpha\beta}^{(1)}$ is the polarizability tensor of molecule 1. This tensor describes the way in which the charge distribution of molecule 1 responds to the applied field $\mathscr{E}_{o\beta}$, and the oscillating field $\mathscr{F}_\beta^{(1)}$ due to the presence of molecule 2. However, for polar molecules the field $F_\alpha^{(1)}$ at molecule 1 due to the permanent moments of 2 may be very strong, resulting in a modification of the effective polarizability. Equation (6.23) then becomes (Buckingham 1967)

$$\mu_\alpha^{(1)} = (\alpha_{\alpha\beta}^{(1)} + \beta_{\alpha\beta\gamma}^{(1)} F_\gamma^{(1)} + \frac{1}{2}\gamma_{\alpha\beta\gamma\delta} F_\gamma^{(1)} F_\delta^{(1)} + \ldots.)(\mathscr{E}_{o\beta} + \mathscr{F}_\beta^{(1)}) \quad , \tag{6.24}$$

where $\beta_{\alpha\beta\gamma}$ and $\gamma_{\alpha\beta\gamma\delta}$ are hyperpolarizability tensors which have been discussed by Buckingham & Pople (1955b) and by Buckingham & Orr (1967). The first term in brackets may be regarded as a differential polarizability $\alpha_{\alpha\beta}^{(1)'}$.

In addition to the modification of the polarizability by electric fields it is necessary to consider field-gradient effects. A permanent moment of molecule 2 may give rise to a field gradient $F_{\alpha\beta}^{(1)}$ at molecule 1. This may be described by the addition of a term $\phi_{\alpha\beta,\gamma\delta} F_{\gamma\delta}^{(1)}$ to the differential polarizability. Also the field gradient $\mathscr{E}_{o\alpha\beta}$ of the applied field and the field gradient $\mathscr{F}_{\alpha\beta}^{(1)}$ at 1 due to the oscillating moments on 2 may induce an additional dipole moment on 1, described by the molecular property tensor $A_{\alpha,\beta\gamma}$ of Buckingham (1967). Since the wavelength of light in the visible is large compared to molecular dimensions, we may neglect $\mathscr{E}_{o\alpha\beta}$. Equation (6.24) can then be written as

$$\mu_\alpha^{(1)}(\mathscr{E}_o) = (\alpha_{\alpha\beta}^{(1)} + \beta_{\alpha\beta\gamma} F_\gamma^{(1)} + \tfrac{1}{2}\gamma_{\alpha\beta\gamma\delta}^{(1)} F_\gamma^{(1)} F_\delta^{(1)} + \phi_{\alpha\beta,\gamma\delta}^{(1)} F_{\gamma\delta}^{(1)} + \cdots)(\mathscr{E}_{o\beta} + \mathscr{F}_\beta^{(1)})$$

$$+ \frac{1}{3} A_{\alpha,\beta\gamma}^{(1)} \mathscr{G}_{\beta\gamma}^{(1)} + \ldots. \quad . \tag{6.25}$$

The oscillating dipole moment of molecule 2, $\mu_\alpha^{(2)}$, may be represented by an analogous expression.

T-tensors (Buckingham 1967) may be used to describe the field $E_\alpha^{(1)}$ and field gradient $E_{\alpha\beta}^{(1)}$ at the origin of molecule 1 arising from a dipole moment $\mu_\alpha^{(2)}$ on molecule 2. We write

$$E_\alpha^{(1)} = T_{\alpha\beta}^{(1)} \mu_\beta^{(2)} \quad \text{and} \quad E_{\alpha\beta}^{(1)} = T_{\alpha\beta\gamma}^{(1)} \mu_\gamma^{(2)} \tag{6.26}$$

where, if $\underset{\sim}{R}$ is a vector from the origin of 1 to 2

$$T^{(1)}_{\alpha\beta} = \frac{1}{4\pi\varepsilon_o} \nabla_\alpha \nabla_\beta R^{-1} = \frac{1}{4\pi\varepsilon_o} (3R_\alpha R_\beta - R^2\delta_{\alpha\beta})R^{-5} \tag{6.27}$$

and

$$T^{(1)}_{\alpha\beta\gamma} = -\frac{1}{4\pi\varepsilon_o} \nabla_\alpha \nabla_\beta \nabla_\gamma R^{-1}$$

$$= \frac{3}{4\pi\varepsilon_o} [5R_\alpha R_\beta R_\gamma - R^2(R_\alpha \delta_{\beta\gamma} + R_\beta \delta_{\gamma\alpha} + R_\gamma \delta_{\alpha\beta})] R^{-7} . \tag{6.28}$$

Also $T^{(1)}_{\alpha\beta\gamma} = (-1)^n T^{(2)}_{\alpha\beta\gamma}$, where n is the order of the tensor, since the vector from 1 to 2 is minus the vector from 2 to 1.

The use of (6.26) allows the oscillating field $\mathscr{F}^{(1)}_\beta$ at molecule 1 to be written as

$$\mathscr{F}^{(1)}_\beta = T^{(1)}_{\beta\gamma} \mu^{(2)}_\gamma (\mathscr{E}_o) \quad , \tag{6.29}$$

where the effects of oscillating quadrupoles and higher multipoles have been neglected. Combination of (6.29) and the analogue of (6.25) for molecule 2 yields,

$$\mathscr{F}^{(1)}_\beta = T^{(1)}_{\beta\gamma} \alpha^{(2)'}_{\gamma\delta} \mathscr{E}_{o\delta} + T^{(1)}_{\beta\gamma} \alpha^{(2)'}_{\gamma\delta} T^{(2)}_{\delta\varepsilon} \alpha^{(1)'}_{\varepsilon\phi} \mathscr{E}_{o\phi} + \frac{1}{3} T^{(1)}_{\beta\gamma} A^{(2)}_{\gamma,\delta\varepsilon} T^{(2)}_{\delta\varepsilon\phi} \alpha^{(1)'}_{\phi\eta} \mathscr{E}_{o\eta} , \tag{6.30}$$

where $\alpha^{(i)'}_{\alpha\beta}$ is the differential polarizability of molecule i. By using (6.25) and (6.26) as a basis for interpretation, a simple physical understanding of each term in (6.30) may be gained. The first term represents the oscillating field at molecule 1 due to a dipole moment $\alpha^{(2)'}_{\gamma\delta} \mathscr{E}_{o\delta}$ at molecule 2 induced by the applied light wave field $\mathscr{E}_{o\delta}$. The second term represents the action of the applied field $\mathscr{E}_{o\phi}$ which induces a dipole moment $\alpha^{(1)'}_{\varepsilon\phi} \mathscr{E}_{o\phi}$ in molecule 1 whose field $T^{(2)}_{\delta\varepsilon} \alpha^{(1)'}_{\varepsilon\phi} \mathscr{E}_{o\phi}$ at molecule 2 induces a dipole moment $\alpha^{(2)'}_{\gamma\delta} T^{(2)}_{\delta\varepsilon} \alpha^{(1)'}_{\varepsilon\phi} \mathscr{E}_{o\phi}$ which in turn generates an additional field $T^{(1)}_{\beta\gamma} \alpha^{(2)'}_{\gamma\delta} T^{(2)}_{\delta\varepsilon} \alpha^{(1)'}_{\varepsilon\phi} \mathscr{E}_{o\phi}$ at molecule 1. The third term in $\mathscr{F}^{(1)}_\beta$ describes how a dipole moment $\alpha^{(1)}_{\phi\eta} \mathscr{E}_{o\eta}$, induced by $\mathscr{E}_{o\eta}$ on molecule 1 gives rise to a field gradient $T^{(2)}_{\delta\varepsilon\phi} \alpha^{(1)'}_{\phi\eta} \mathscr{E}_{o\eta}$ at molecule 2, whose induced dipole moment $\frac{1}{3} A^{(2)}_{\gamma,\delta\varepsilon} T^{(2)}_{\delta\varepsilon\phi} \alpha^{(1)'}_{\phi\eta} \mathscr{E}_{o\eta}$ produces a field $\frac{1}{3} T^{(1)}_{\beta\gamma} A^{(2)}_{\gamma,\delta\varepsilon} T^{(2)}_{\delta\varepsilon\phi} \alpha^{(1)'}_{\phi\eta} \mathscr{E}_{o\eta}$ at molecule 1.

It is difficult to know after how many terms the series of (6.30) should be terminated since little is known about the rate of convergence of the contributing terms. Graham (1971) has arbitrarily truncated after terms which have ten or more suffices thereby retaining all terms considered by Buckingham (1956) and Kielich (1962) together with some additional terms which may be important. Since we do likewise (6.30) reduces to

$$\mathcal{F}^{(1)}_{\beta} = T^{(1)}_{\beta\gamma}\,\alpha^{(2)\prime}_{\gamma\delta}\,\mathcal{E}_{o\delta} + T^{(1)}_{\beta\gamma}\,\alpha^{(2)\prime}_{\gamma\delta}\,T^{(2)}_{\delta\varepsilon}\,\alpha^{(1)\prime}_{\varepsilon\phi}\,\mathcal{E}_{o\phi} \quad , \tag{6.31}$$

and substitution of the expression

$$\alpha^{(i)\prime}_{\alpha\beta} = (\alpha^{(i)}_{\alpha\beta} + \beta^{(i)}_{\alpha\beta\gamma}F^{(i)}_{\gamma} + \tfrac{1}{2}\,\gamma^{(i)}_{\alpha\beta\gamma\delta}F^{(i)}_{\gamma}F^{(i)}_{\delta} + \phi^{(i)}_{\alpha\beta,\gamma\delta}F^{(i)}_{\gamma\delta}) \quad , \tag{6.32}$$

for the differential polarizability $\alpha^{(i)\prime}_{\alpha\beta}$ into (6.31) yields

$$\begin{aligned}\mathcal{F}^{(1)}_{\beta} &= T^{(1)}_{\beta\gamma}\,\alpha^{(2)}_{\gamma\delta}\,\mathcal{E}_{o\delta} + T^{(1)}_{\beta\gamma}\,\beta^{(2)}_{\gamma\delta\varepsilon}F^{(2)}_{\varepsilon}\,\mathcal{E}_{o\delta} + \tfrac{1}{2}\,T_{\beta\gamma}\gamma^{(2)}_{\gamma\delta\varepsilon\phi}F^{(2)}_{\varepsilon}F^{(2)}_{\phi}\,\mathcal{E}_{o\delta} \\ &+ T^{(1)}_{\beta\gamma}\,\alpha^{(2)}_{\gamma\delta}\,T^{(2)}_{\delta\varepsilon}\,\alpha^{(1)}_{\varepsilon\phi}\,\mathcal{E}_{o\phi} + \cdots \quad .\end{aligned} \tag{6.33}$$

A similar approach may be used to show that

$$\mathcal{F}^{(1)}_{\beta\gamma} = T^{(1)}_{\beta\gamma\delta}\alpha^{(2)}_{\delta\varepsilon}\,\mathcal{E}_{o\varepsilon} \quad . \tag{6.34}$$

Substitution of (6.33) and (6.34) into (6.25) yields

$$\begin{aligned}\mu^{(1)}_{\alpha}(\mathcal{E}_o) &= \alpha^{(1)}_{\alpha\beta}\,\mathcal{E}_{o\beta} + \alpha^{(1)}_{\alpha\beta}\,T^{(1)}_{\beta\gamma}\,\alpha^{(2)}_{\gamma\delta}\,\mathcal{E}_{o\delta} + \beta^{(1)}_{\alpha\beta\gamma}F^{(1)}_{\gamma}\,\mathcal{E}_{o\beta} \\ &+ \alpha^{(1)}_{\alpha\beta}\,T^{(1)}_{\beta\gamma}\,\beta^{(2)}_{\gamma\delta\varepsilon}F^{(2)}_{\varepsilon}\,\mathcal{E}_{o\delta} + \tfrac{1}{2}\,\alpha^{(1)}_{\alpha\beta}T^{(1)}_{\beta\gamma}\,\gamma^{(2)}_{\gamma\delta\varepsilon\phi}F^{(2)}_{\varepsilon}F^{(2)}_{\phi}\,\mathcal{E}_{o\delta} \\ &+ \alpha^{(1)}_{\alpha\beta}\,T^{(1)}_{\beta\gamma}\,\alpha^{(2)}_{\gamma\delta}\,T^{(2)}_{\delta\varepsilon}\,\alpha^{(1)}_{\varepsilon\phi}\,\mathcal{E}_{o\phi} + \beta^{(1)}_{\alpha\beta\gamma}F^{(1)}_{\gamma}\,T^{(1)}_{\beta\varepsilon}\,\alpha^{(2)}_{\varepsilon\delta}\,\mathcal{E}_{o\delta} \\ &+ \tfrac{1}{2}\,\gamma^{(1)}_{\alpha\beta\gamma\delta}F^{(1)}_{\gamma}F^{(1)}_{\delta}\,\mathcal{E}_{o\beta} + \phi^{(1)}_{\alpha\beta,\gamma\delta}F^{(1)}_{\gamma\delta}\,\mathcal{E}_{o\beta} \\ &+ \tfrac{1}{3}\,A^{(1)}_{\alpha,\beta\gamma}T^{(1)}_{\beta\gamma\delta}\alpha^{(2)}_{\delta\varepsilon}\,\mathcal{E}_{o\varepsilon} + \cdots \quad .\end{aligned} \tag{6.35}$$

If the mathematical operation $\frac{\partial(\ )}{\partial \mathcal{E}_o}\,e_{\alpha}$ is performed on the above expression for $\mu^{(1)}_{\alpha}$ each term will contain the product $e_{\alpha}e_{\beta}$ of unit vectors in the direction of the applied field. Since all orientations in the light wave field are equally probable the product $e_{\alpha}e_{\beta}$ may be replaced by the average isotropic quantity $\frac{1}{3}\,\delta_{\alpha\beta}$. This leads to the result

$$\left(\frac{\partial \mu_\alpha}{\partial \mathscr{E}_o} e_\alpha - \alpha_o\right) = \alpha^{(1)} - \alpha_o + \frac{1}{3}\alpha^{(1)}_{\alpha\beta} T^{(1)}_{\beta\gamma} \alpha^{(2)}_{\gamma\alpha}$$

$$+ \frac{1}{3}\beta^{(1)}_{\alpha\alpha\gamma} F^{(1)}_\gamma + \frac{1}{3}\alpha^{(1)}_{\alpha\beta} T^{(1)}_{\beta\gamma} \beta^{(2)}_{\gamma\alpha\varepsilon} F^{(2)}_\varepsilon$$

$$+ \frac{1}{6}\alpha^{(1)}_{\alpha\beta} T^{(1)}_{\beta\gamma} \gamma^{(2)}_{\gamma\alpha\varepsilon\phi} F^{(2)}_\varepsilon F^{(2)}_\phi$$

$$+ \frac{1}{3}\alpha^{(1)}_{\alpha\beta} T^{(1)}_{\beta\gamma} \alpha^{(2)}_{\gamma\delta} T^{(2)}_{\delta\varepsilon} \alpha^{(1)}_{\varepsilon\alpha}$$

$$+ \frac{1}{3}\beta^{(1)}_{\alpha\beta\gamma} F^{(1)}_\gamma T^{(1)}_{\beta\varepsilon} \alpha^{(2)}_{\varepsilon\alpha} + \frac{1}{6}\gamma^{(1)}_{\alpha\alpha\gamma\delta} F^{(1)}_\gamma F^{(1)}_\delta$$

$$+ \frac{1}{3}\phi^{(1)}_{\alpha\alpha,\gamma\delta} F^{(1)}_{\gamma\delta} + \frac{1}{9} A^{(1)}_{\alpha,\beta\gamma} T^{(1)}_{\beta\gamma\delta} \alpha^{(2)}_{\delta\alpha} + \cdots . \qquad (6.36)$$

In order to evaluate (6.36) for a molecule it is necessary to introduce the explicit forms of parameters like $T_{\alpha\beta}$, $T_{\alpha\beta\gamma}$, $F^{(1)}_\alpha$ and $F^{(1)}_{\alpha\beta}$ and to use symmetry considerations to establish the non-zero molecular property tensors.

§4. $\left(\frac{\partial \mu_\alpha}{\partial \mathscr{E}_o} e_\alpha - \alpha_o\right)$ for the inert gases

The spherical symmetry of the inert-gas molecules in their ground state greatly simplifies the form of (6.36). These molecules possess no zero field multipole moments of any order (Buckingham 1967) so that $F^{(i)}_\alpha$ and $F^{(i)}_{\alpha\beta}$ in (6.36) are identically zero. Also the molecular property tensor $A_{\alpha\beta\gamma}$ has no non-zero components (Buckingham 1967); the molecular polarizability tensor $\alpha^{(i)}_{\alpha\beta}$ is isotropic so that

$$\alpha^{(i)}_{\alpha\beta} = \alpha^{(i)} \delta_{\alpha\beta} \qquad (6.37)$$

where $\alpha^{(i)} = \frac{1}{3}\alpha^{(i)}_{\alpha\alpha}$.

On substitution of $\alpha^{(i)}_{\alpha\beta}$ from (6.37) and $T^{(1)}_{\alpha\beta}$ from (6.27) in the remaining terms of (6.36) it is easy to show that

$$\left(\frac{\partial \mu_\alpha}{\partial \mathscr{E}_o} e_\alpha - \alpha_o\right) = (\alpha^{(1)} - \alpha_o) + \frac{2(\alpha^{(1)})^3}{(4\pi\varepsilon_o)^2 R^6} . \qquad (6.38)$$

It should be noted that $\alpha^{(1)}_{\alpha\beta}$ may be a function of R, the intermolecular separation, in which case $(\alpha^{(1)} - \alpha_o)$ would represent the change in the

effective polarizability of molecule 1 due to the presence of a neighbouring molecule. Although a classical molecular theory of B_R fails to take this into account quantum mechanical calculations, using *ab initio* methods, for helium pairs (O'Brien, Gutschick, McKoy & McTague 1973; Buckingham & Watts 1973) indicate that the polarizability of a molecule is diminished at short range and increased at long range. The second term in (6.38) is the Kirkwood 'fluctuation' contribution to B_R introduced in chapter 1 and arises from the extra field at a molecule due to the induced dipole in a neighbour.

It then follows from (6.38) and (6.19) that for spherically symmetric molecules

$$B_R = \frac{N_A^2}{3\varepsilon_o \Omega} \int \left[(\alpha^{(1)} - \alpha_o) + \frac{2(\alpha^{(1)})^3}{(4\pi\varepsilon_o)^2 R^6} \right] \exp(-U_{12}(\tau)/kT)\, d\tau \,. \qquad (6.39)$$

Also the second dielectric virial coefficient B_ε given by (6.22) may be shown to have an identical form. This arises since $(\underset{\sim}{\mu}^{(1)} + \underset{\sim}{\mu}^{(2)})$ is zero for spherically symmetric molecules. However, it should be noted that for B_ε, α_o and $\alpha^{(1)}$ are the static polarizabilities, whilst α_o and $\alpha^{(1)}$ in B_R are the polarizabilities at the frequency of the light wave.

§5. $\left(\frac{d\mu_\alpha}{\partial \mathscr{E}_o} e_\alpha - \alpha_o\right)$ for axially symmetric polar molecules

The relative configuration τ of two axially symmetric molecules may be specified by the four parameters θ_1, θ_2, ϕ and R (Buckingham 1967) shown in figure 1.

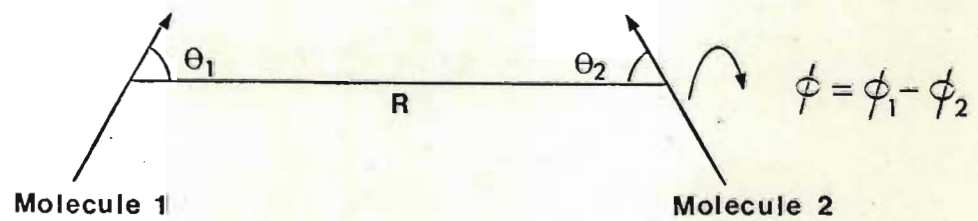

Figure 1. The coordinates R, θ_1, θ_2 and ϕ describing the configuration of two axially symmetric molecules.

Here R is the distance between centres, θ_1 and θ_2 are the angles between the line of centres and the dipole axes of molecules 1 and 2, and ϕ is the angle between the planes formed by the molecular axes and the line of centres. A similar set of coordinates has been used by Kielich (1962) and Copeland & Cole (1976) but their symbol θ_2 denotes the complement of θ_2 in figure 1.

Molecular property tensors are normally specified with respect to mutually perpendicular axes fixed in the molecule in a way that one of the axes will coincide with a symmetry axis. For example in figure 2 the properties of molecules 1 and 2 would be specified relative to axes O(123) and O'(1'2'3') in which the 3 and 3' axes correspond to the direction of the symmetry axes.

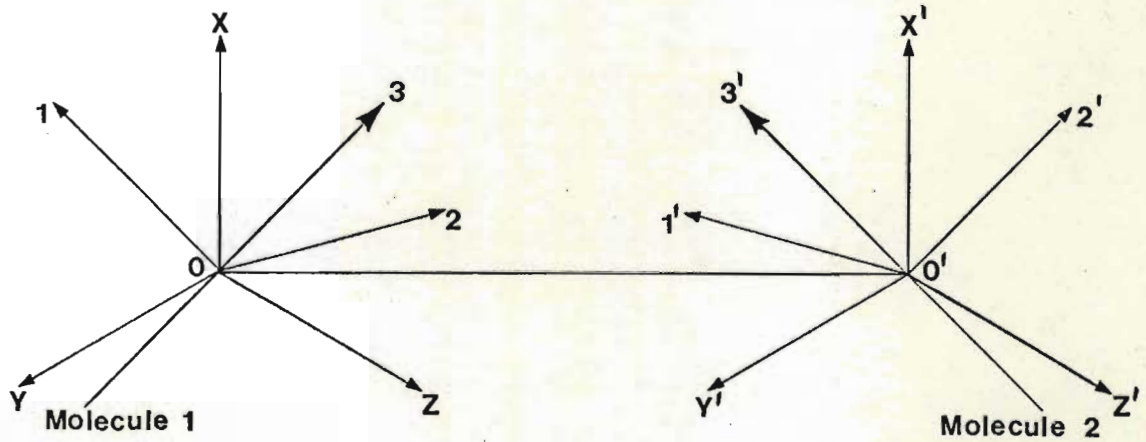

Figure 2.

If $P^{(1)}_{ijk...n}$ is a polar property tensor of molecule 1 in O(123), then $P^{(1)}_{\alpha\beta\gamma...\phi}$ relative to a new set of axes O(XYZ) is given by the transformation equation (Jeffreys 1931)

$$P^{(1)}_{\alpha\beta\gamma...\phi} = \ell_{\alpha i}\,\ell_{\beta j}\,\ell_{\gamma k} \cdots \ell_{\phi n}\,P^{(1)}_{ijk...n} \quad , \qquad (6.40)$$

where $\ell_{\alpha i}$ is the direction cosine between the α-axis in the new system and an i-axis in the old system of axes. Similarly a polar property tensor $P^{(2)}_{ijk...n}$ of molecule 2 in O'(1'2'3') relative to a new set of axes O'(X'Y'Z') is described by an analogous equation.

If O(XYZ) and O'(X'Y'Z') are related by a linear translation only then OX is parallel to O'X' etc. Also if $\ell^{(1)}_{\alpha}$ is a unit vector along the dipole

axis of molecule 1 referred to O(XYZ), with an analogous definition for $\ell^{(2)}_{\alpha'}$, then

$$\ell_{\alpha z} = \ell^{(1)}_{\alpha} \quad \text{and} \quad \ell_{\alpha' z'} = \ell^{(2)}_{\alpha'} = \ell^{(2)}_{\alpha} \tag{6.41}$$

and if λ_α is a unit vector along the line of centres directed from 1 to molecule 2

$$\begin{aligned} \ell^{(1)}_{\alpha} \lambda_\alpha &= \cos\theta_1 \quad , \\ \ell^{(2)}_{\alpha} \lambda_\alpha &= -\cos\theta_2 \quad , \end{aligned} \tag{6.42}$$

$$\text{and} \quad \ell^{(1)}_{\alpha} \ell^{(2)}_{\alpha} = \cos\theta_{12} = -\cos\theta_1\cos\theta_2 + \sin\theta_1\sin\theta_2\cos\phi \quad . \tag{6.43}$$

For example, the third rank tensor $A^{(1)}_{\alpha,\beta\gamma}$ which is symmetric in β and γ has only two independent components for molecules belonging to the $C_{\infty v}$ symmetry group (Buckingham 1967), namely

$$A^{(1)}_{113} = A^{(1)}_{223} = A^{(1)}_{131} = A^{(1)}_{232} = A^{(1)}_{\perp} \quad \text{and} \quad A^{(1)}_{333} = -2A^{(1)}_{322} = -2A^{(1)}_{311} = A^{(1)}_{\parallel} \quad , \tag{6.44}$$

where the subscripts $\parallel$ and $\perp$ denote components along and at right angles to the symmetry axis (the 3-axis). The use of (6.44) together with (6.41) in the transformation equation (6.40) gives,

$$A^{(1)}_{\alpha,\beta\gamma} = \tfrac{1}{2} A^{(1)}_{\parallel} \ell^{(1)}_{\alpha} (3\ell^{(1)}_{\beta}\ell^{(1)}_{\gamma} - \delta_{\beta\gamma}) + A^{(1)}_{\perp} (\ell^{(1)}_{\beta} \delta_{\alpha\gamma} + \ell^{(1)}_{\gamma} \delta_{\alpha\beta} - 2\ell^{(1)}_{\alpha} \ell^{(1)}_{\beta} \ell^{(1)}_{\gamma}) \quad . \tag{6.45}$$

For molecules with $C_{\infty v}$ symmetry similar manipulations may be used to show that :-

$$\mu^{(1)}_{\alpha} = \mu^{(1)} \ell^{(1)}_{\alpha} \quad , \tag{6.46}$$

where $\mu^{(1)} = \mu^{(1)}_3$;

$$\alpha^{(1)}_{\alpha\beta} = \alpha^{(1)} \delta_{\alpha\beta} + K\alpha^{(1)} (3\ell^{(1)}_{\alpha} \ell^{(1)}_{\beta} - \delta_{\alpha\beta}) \quad , \tag{6.47}$$

where $\alpha^{(1)} = \frac{1}{3} \alpha^{(1)}_{\alpha\alpha}$ and $K = \dfrac{\alpha^{(1)}_{33} - \alpha^{(1)}_{11}}{3\alpha^{(1)}}$;

$$\gamma^{(1)}_{\alpha\alpha\gamma\delta} = \frac{5}{2}\gamma^{(1)}\delta_{\gamma\delta} - (\frac{1}{2}\gamma^{(1)}_{3333} + \gamma^{(1)}_{3311})\delta_{\gamma\delta} + (\gamma^{(1)}_{3333} + \gamma^{(1)}_{3311} - \frac{4}{3}\gamma^{(1)}_{1111})\ell^{(1)}_{\gamma}\ell^{(1)}_{\delta} \quad , \tag{6.48}$$

where

$$\gamma^{(1)} = \frac{1}{5}(\gamma^{(1)}_{1111} + \gamma^{(1)}_{2222} + \gamma^{(1)}_{3333} + 2\gamma^{(1)}_{1122} + 2\gamma^{(1)}_{2233} + 2\gamma^{(1)}_{3311}) \; ;$$

$$\beta^{(1)}_{\alpha\beta\gamma} = \beta^{(1)}_{\perp}(\ell^{(1)}_{\alpha}\delta_{\beta\gamma} + \ell^{(1)}_{\beta}\delta_{\alpha\gamma} + \ell^{(1)}_{\gamma}\delta_{\alpha\beta}) + (\beta^{(1)}_{\parallel} - 3\beta^{(1)}_{\perp})\ell^{(1)}_{\alpha}\ell^{(1)}_{\beta}\ell^{(1)}_{\gamma} \quad , \tag{6.49}$$

where $\beta^{(1)}_{113} = \beta^{(1)}_{131} = \beta^{(1)}_{311} = \beta^{(1)}_{\perp}$ and $\beta^{(1)}_{333} = \beta^{(1)}_{\parallel}$,

and

$$\phi^{(1)}_{\alpha\alpha\gamma\delta} = (\phi^{(1)}_{1111} + \phi^{(1)}_{2211} + \phi^{(1)}_{3311})\delta_{\gamma\delta} + (\phi^{(1)}_{3333} + 2\phi^{(1)}_{1133} - \phi^{(1)}_{1111} - \phi^{(1)}_{2211} - \phi^{(1)}_{3311})\ell^{(1)}_{\gamma}\ell^{(1)}_{\delta} \quad . \tag{6.50}$$

The molecular quadrupole moment $\theta^{(1)}_{\alpha\beta}$ may similarly be written in the form

$$\theta^{(1)}_{\alpha\beta} = \tfrac{1}{2}\theta^{(1)}(3\ell_{\alpha}\ell_{\beta} - \delta_{\alpha\beta}) \quad , \tag{6.51}$$

where $\theta^{(1)} = \theta^{(1)}_{33} = -2\theta^{(1)}_{11} = -2\theta^{(1)}_{22}$.

It is also necessary to write explicit forms for $F^{(i)}_{\alpha}$ and $F^{(i)}_{\alpha\beta}$. For uncharged molecules (Buckingham 1967),

$$F^{(1)}_{\alpha} = T^{(1)}_{\alpha\beta}\mu^{(2)}_{\beta} - \frac{1}{3}T^{(1)}_{\alpha\beta\gamma}\theta^{(2)}_{\beta\gamma} \tag{6.52}$$

and

$$F^{(1)}_{\alpha\beta} = T^{(1)}_{\alpha\beta\gamma}\mu^{(2)}_{\gamma} - \frac{1}{3}T^{(1)}_{\alpha\beta\gamma\delta}\theta^{(2)}_{\gamma\delta} \quad , \tag{6.53}$$

where $T^{(1)}_{\alpha\beta}$ and $T^{(1)}_{\alpha\beta\gamma}$ are tensors defined in (6.27) and (6.28), and where

$$T^{(1)}_{\alpha\beta\gamma\delta} = \frac{1}{4\pi\varepsilon_o}\nabla_{\alpha}\nabla_{\beta}\nabla_{\gamma}\nabla_{\delta}R^{-1} \quad .$$

Now if (6.27), (6.28), (6.46) and (6.51) are substituted into (6.52) and (6.53), it can be shown that

$$F_\alpha^{(1)} = \frac{1}{4\pi\varepsilon_o}\mu^{(2)}R^{-3}(3\lambda_\alpha\lambda_\beta - \delta_{\alpha\beta})\ell_\beta^{(2)} - \frac{1}{4\pi\varepsilon_o}\tfrac{1}{2}\theta^{(2)}R^{-4}$$

$$\times [5\lambda_\alpha\lambda_\beta\lambda_\gamma - (\lambda_\alpha\delta_{\beta\gamma} + \lambda_\beta\delta_{\gamma\alpha} + \lambda_\gamma\delta_{\alpha\beta})][3\ell_\beta^{(2)}\ell_\gamma^{(2)} - \delta_{\beta\gamma}] + \cdots\cdot \quad , \qquad (6.54)$$

and

$$F_{\alpha\beta}^{(1)} = 3\mu^{(2)}R^{-4}[5\lambda_\alpha\lambda_\beta\lambda_\gamma - (\lambda_\alpha\delta_{\beta\gamma} + \lambda_\beta\delta_{\gamma\alpha} + \lambda_\gamma\delta_{\alpha\beta})]\ell_\gamma^{(2)} + \cdots\cdot \quad . \qquad (6.55)$$

Finally, a general expression for $\left(\frac{\partial\mu_\alpha}{\partial\mathscr{E}_o}\ e_\alpha - \alpha_o\right)$ may be obtained by substituting into (6.36) the equations (6.45); (6.47) to (6.50); (6.54) and (6.55). The general expression will contain products of the form $\ell_\alpha^{(1)}\ell_\alpha^{(2)}\ell_\beta^{(1)}\lambda_\beta^{(1)}\ell_\gamma^{(2)}\lambda_\gamma^{(2)}$ which may be written in terms of cosines and sines of the angular coordinates θ_1, θ_2 and ϕ through (6.42) and (6.43). Lengthy but simple manipulation leads to the following expressions for the terms in (6.36) :

$$\Delta_1 = \alpha^{(1)} - \alpha_o \quad ; \qquad (6.56)$$

$$\Delta_2 = \tfrac{1}{3}\alpha_{\alpha\beta}^{(1)}T_{\beta\gamma}^{(1)}\alpha_{\gamma\alpha}^{(2)} = \frac{\alpha^2}{4\pi\varepsilon_o}R^{-3}\{K(1-K)(3\cos^2\theta_1 + 3\cos^2\theta_2 - 2)$$

$$+ 3K^2(2\cos^2\theta_1\cos^2\theta_2 - \sin\theta_1\cos\theta_1\sin\theta_2\cos\theta_2\cos\phi$$

$$- \sin^2\theta_1\sin^2\theta_2\cos^2\phi)\} \quad ; \qquad (6.57)$$

$$\Delta_3 = \tfrac{1}{3}\alpha_{\alpha\beta}^{(1)}T_{\beta\gamma}^{(1)}\alpha_{\gamma\delta}^{(2)}T_{\delta\varepsilon}^{(2)}\alpha_{\varepsilon\alpha}^{(1)} = \frac{\alpha^3}{(4\pi\varepsilon_o)^2}R^{-6}\{2(1-K)^3 + K(2+K)(1-K)$$

$$\times (3\cos^2\theta_1 + 1) + K(1-K)^2(3\cos^2\theta_2 + 1) + 3K^2(2+K)$$

$$\times (2\cos\theta_1\cos\theta_2 + \sin\theta_1\sin\theta_2\cos\phi)^2\} \quad ; \qquad (6.58)$$

$$\Delta_4 = \tfrac{1}{3}\beta_{\alpha\alpha\gamma}^{(1)}F_\gamma^{(1)} = -\frac{5}{9}\frac{\mu\beta}{4\pi\varepsilon_o}R^{-3}\{2\cos\theta_1\cos\theta_2 + \sin\theta_1\sin\theta_2\cos\phi\}$$

$$- \frac{5}{6}\frac{\theta\beta}{4\pi\varepsilon_o}R^{-4}\{3\cos^2\theta_2\cos\theta_1 + 2\cos\theta_2\sin\theta_1\sin\theta_2\cos\phi - \cos\theta_1\} \quad ; \qquad (6.59)$$

$$\Delta_5 = \tfrac{1}{3}\alpha^{(1)}_{\alpha\beta} T^{(1)}_{\beta\gamma}{}^{\beta}{}^{(2)}_{\gamma\alpha\varepsilon} F^{(2)}_{\varepsilon} = -\tfrac{1}{3}\frac{\mu\alpha}{(4\pi\varepsilon_o)^2} R^{-6}\{\beta_\perp[2(1-K)(3\cos\theta_1\cos\theta_2 - \cos\theta_{12})$$
$$+ 9K(6\cos^3\theta_1\cos\theta_2 + \cos^2\theta_1\cos\theta_{12} - 2\cos\theta_1\cos\theta_2 - \cos\theta_{12})]$$
$$+ (\beta_{\parallel} - 3\beta_\perp)[(1-K)(3\cos^2\theta_2 - 1)(3\cos\theta_1\cos\theta_2 + \cos\theta_{12})$$
$$+ 3K(-9\cos^2\theta_1\cos^2\theta_2\cos\theta_{12} - 6\cos\theta_1\cos\theta_2\cos^2\theta_{12} - \cos^3\theta_{12})]\} \quad ; \qquad (6.60)$$

$$\Delta_6 = \tfrac{1}{3}\beta^{(1)}_{\alpha\beta\gamma} F^{(1)}_{\gamma} T^{(1)}_{\beta\varepsilon}{}^{\alpha}{}^{(2)}_{\varepsilon\alpha} = -\tfrac{1}{3}\frac{\mu\alpha}{(4\pi\varepsilon_o)^2} R^{-6}\{\beta_\perp[2(1-K)(3\cos\theta_1\cos\theta_2 - \cos\theta_{12})$$
$$+ 9K(6\cos^3\theta_2\cos\theta_1 + \cos^2\theta_2\cos\theta_{12} - 2\cos\theta_1\cos\theta_2 - \cos\theta_{12})]$$
$$+ (\beta_{\parallel} - 3\beta_\perp)[(1-K)(3\cos^2\theta_1 - 1)(3\cos\theta_1\cos\theta_2 + \cos\theta_{12})$$
$$+ 3K(-9\cos^2\theta_1\cos^2\theta_2\cos\theta_{12} - 6\cos\theta_1\cos\theta_2\cos^2\theta_{12} - \cos^3\theta_{12})]\} \quad ; \qquad (6.61)$$

$$\Delta_7 = \tfrac{1}{6}\gamma^{(1)}_{\alpha\alpha\gamma\delta} F^{(1)}_{\gamma} F^{(1)}_{\delta} = \frac{5}{12}\frac{\mu^2}{(4\pi\varepsilon_o)^2} R^{-6}\{\gamma - \tfrac{1}{5}(\gamma_{3333} + 2\gamma_{3311})\}$$
$$\times \{1 + 3\cos^2\theta_2\} + \frac{8}{5}\frac{\mu^2}{(4\pi\varepsilon_o)^2} R^{-6}\{\gamma_{3333} + \gamma_{3311} - \tfrac{4}{3}\gamma_{1111}\}$$
$$\times \{(\cos\theta_1\cos\theta_2 + \tfrac{1}{2}\sin\theta_1\sin\theta_2\cos\phi)^2\} \quad ; \qquad (6.62)$$

$$\Delta_8 = \tfrac{1}{9}A^{(1)}_{\alpha\beta\gamma} T^{(1)}_{\beta\gamma\delta}{}^{\alpha}{}^{(2)}_{\delta\alpha} = \tfrac{1}{2}\frac{\alpha}{(4\pi\varepsilon_o)} R^{-4}\{(A_{\parallel} - \tfrac{4}{3}A_\perp)[(1-K)(5\cos^3\theta_1 - 3\cos\theta_1)$$
$$- K(15\cos\theta_{12}\cos^2\theta_1\cos\theta_2 + 6\cos^2\theta_{12}\cos\theta_1)]$$
$$+ (A_{\parallel} + \tfrac{4}{3}A_\perp)[K(15\cos\theta_1\cos^2\theta_2 + \cos\theta_{12}\cos\theta_2)]$$
$$- K(15A_{\parallel}\cos\theta_1\cos^2\theta_2 + 4A_\perp\cos\theta_1)\} \quad ; \qquad (6.63)$$

and

$$\Delta_9 = \tfrac{1}{3}\phi^{(1)}_{\alpha\alpha\gamma\delta} F^{(1)}_{\gamma\delta} = -\frac{\mu}{4\pi\varepsilon_o} R^{-4}(\phi_{3333} + 2\phi_{1133} - \phi_{1111} - \phi_{2211} - \phi_{3311})$$
$$\times (3\cos^2\theta_1\cos\theta_2 + 2\cos\theta_1\sin\theta_1\sin\theta_2\cos\phi - \cos\theta_2) \quad , \qquad (6.64)$$

and we may write

$$\left(\frac{\partial \mu_\alpha}{\partial \mathscr{E}_o} - \alpha_o\right) = \sum_{n=1}^{9} \Delta_n + \cdots . \qquad (6.65)$$

In the derivation of the above equations only terms of sixth and lower orders in the electric dipole moment operator have been retained. For the purposes of assessing the order of a term, μ_α, $\alpha_{\alpha\beta}$, $\beta_{\alpha\beta\gamma}$.... are regarded as first, second, third .... order in the electric dipole moment operator (Graham 1971). $F_\alpha^{(i)}$ and $F_{\alpha\beta}^{(i)}$ are in principle infinite series but to the above approximation $F_\alpha^{(i)}$ and $F_{\alpha\beta}^{(i)}$ are due to a zero-field dipole moment in a neighbouring molecule only, while in (6.59), $F_\alpha^{(i)}$ is truncated after the quadrupole term. In Δ_9 only the leading fifth-order term has been retained and a complicated sixth-order term involving $T^{(1)}_{\alpha\beta\gamma\delta}$ has been omitted.

It is important to realize that the molecular property tensors in (6.65) (except α_o) may depend on the intermolecular separation R, especially in the overlap region. However, as in the case of the inert gases (§4.), these would require a general quantum mechanical description which has only been achieved for simple molecules.

In the present work (as in the molecular theories of Buckingham (1956) and Kielich (1962)) we neglect any changes in the intrinsic molecular properties at short range and use the isolated-molecule physical property tensors in our molecular model, both at long and short range. With this assumption it follows from (6.19) and (6.65) that B_R may be written in the form

$$B_R = \frac{N_A^2}{3\varepsilon_o \Omega} \int \left[\sum_{n=1}^{9} \Delta_n\right] \exp(-U_{12}(\tau)/kT)\, d\tau \quad , \qquad (6.66)$$

where τ now represents the set of coordinates R, θ_1, θ_2 and ϕ which describe the relative configuration of molecules 1 and 2. $d\tau$ is the volume element.

Classical expressions for the intermolecular potential energy $U_{12}(\tau)$ required for the evaluation of (6.66) are discussed in the next section.

§6. Classical expressions for the intermolecular potential energy $U_{12}(\tau)$

For intermolecular separations R which are large when compared with a molecular diameter, the pair interaction energy $U_{12}(\tau)$ may be considered to consist of three components (Buckingham & Utting 1970) namely,

(i) the electrostatic energy, U_{elec}, which arises from the interaction of zero-field electric moments (dipole, quadrupole, etc.) of the molecule;

(ii) the induction energy, U_{ind}, which arises from the distortion of the electronic structure of a molecule due to zero-field electric moments in a neighbouring molecule; and

(iii) the London dispersion energy, U_{disp}, which arises from interactions of the electric moments due to fluctuations in the charge distributions of the molecules.

The above interaction energies are the result of long range forces which are well understood (Buckingham 1967; Mason & Spurling 1969; Buckingham & Utting 1970) and are evaluated with the assumption that the overlap of the molecular wavefunctions is small. The long range interaction energy for two dipolar molecules (given by Buckingham 1967) is

$$U_{12}^{LR}(\tau) = U_{elec} + U_{ind} + U_{disp} \quad ,$$

where

$$\begin{aligned} U_{elec} = \frac{1}{4\pi\varepsilon_o} \{ & \mu^2 R^{-3}(2\cos\theta_1\cos\theta_2 + \sin\theta_1\sin\theta_2\cos\phi) \\ & + \tfrac{3}{2}\mu\theta R^{-4}[\cos\theta_1(3\cos^2\theta_2 - 1) + \cos\theta_2(3\cos^2\theta_1 - 1) \\ & + 2\sin\theta_1\sin\theta_2\cos\theta_2\cos\phi + 2\sin\theta_1\cos\theta_1\sin\theta_2\cos\phi] \\ & + \tfrac{3}{4}\theta^2 R^{-5}(1 - 5\cos^2\theta_1 - 5\cos^2\theta_2 + 17\cos^2\theta_1\cos^2\theta_2 \\ & + 2\sin^2\theta_1\sin^2\theta_2\cos^2\phi + 16\sin\theta_1\cos\theta_1\sin\theta_2\cos\theta_2\cos\phi) \\ & + \cdots \} \quad ; \end{aligned} \tag{6.67}$$

$$\begin{aligned} U_{ind} &= U_{ind}^{(1)} + U_{ind}^{(2)} \\ &= \frac{1}{(4\pi\varepsilon_o)^2} \{ -\tfrac{1}{2}\alpha\mu^2 R^{-6}[(3\cos^2\theta_1 + 1) + (3\cos^2\theta_2 + 1)] \\ & - 6\alpha\mu\theta R^{-7}[\cos^3\theta_1 + \cos^3\theta_2] \\ & - \tfrac{1}{6}(\alpha_{\parallel} - \alpha_{\perp})\mu^2 R^{-6}[24\cos^2\theta_1\cos^2\theta_2 + 6\sin^2\theta_1\sin^2\theta_2\cos^2\phi \\ & - 3\cos^2\theta_1 - 3\cos^2\theta_2 - 2 \\ & + 24\sin\theta_1\cos\theta_1\sin\theta_2\cos\theta_2\cos\phi] \\ & - \tfrac{3}{2}A_{\parallel}\mu^2 R^{-7}[6\cos^2\theta_1\cos^3\theta_2 + 6\cos^2\theta_2\cos^3\theta_1 \end{aligned}$$

continued

$$
\begin{aligned}
&- 2\cos^2\theta_1\cos\theta_2 - 2\cos^2\theta_2\cos\theta_1 \\
&+ 7\sin\theta_1\cos\theta_1\sin\theta_2\cos^2\theta_2\cos\phi + 7\sin\theta_2\cos\theta_2\sin\theta_1 \\
&\times \cos^2\theta_1\cos\phi - \sin\theta_1\cos\theta_1\sin\theta_2\cos\phi \\
&- \sin\theta_2\cos\theta_2\sin\theta_1\cos\phi + 2\sin^2\theta_1\sin^2\theta_2 \\
&\times \cos\theta_2\cos^2\phi + 2\sin^2\theta_2\sin^2\theta_1\cos\theta_1\cos^2\phi] \\
&+ 2A_\perp\mu^2R^{-7}[6\cos^2\theta_1\cos^3\theta_2 + 6\cos^2\theta_2\cos^3\theta_1 \\
&- 5\cos^2\theta_1\cos\theta_2 - 5\cos^2\theta_2\cos\theta_1 \\
&+ 7\sin\theta_1\cos\theta_1\sin\theta_2\cos^2\theta_2\cos\phi + 7\sin\theta_2\cos\theta_2\sin\theta_1 \\
&\times \cos^2\theta_1\cos\phi - 2\sin\theta_1\cos\theta_1\sin\theta_2\cos\phi \\
&- 2\sin\theta_2\cos\theta_2\sin\theta_1\cos\phi + 2\sin^2\theta_1\sin^2\theta_2\cos\theta_2\cos^2\phi \\
&+ 2\sin^2\theta_2\sin^2\theta_1\cos\theta_1\cos^2\phi - \cos\theta_1 - \cos\theta_2] \\
&+ \cdots\cdots \} \qquad ; \qquad (6.68)
\end{aligned}
$$

and

$$
\begin{aligned}
U_{disp} = &- \frac{1}{(4\pi\varepsilon_o)^2}\cdot\frac{3}{4}UR^{-6}[\alpha^2 + \tfrac{1}{3}\alpha(\alpha_{\parallel} - \alpha_\perp)\{(\tfrac{3}{2}\cos^2\theta_1 - \tfrac{1}{2}) + (\tfrac{3}{2}\cos^2\theta_2 - \tfrac{1}{2})\} \\
&+ 2\alpha A_{\parallel}R^{-1}\{\cos^3\theta_1 + \cos^3\theta_2\} \\
&+ \tfrac{4}{3}\alpha A_\perp R^{-1}\{(3\cos\theta_1 - 2\cos^3\theta_1) + (3\cos\theta_2 - 2\cos^3\theta_2)\} \\
&+ \cdots\cdots] \quad . \qquad (6.69)
\end{aligned}
$$

U in (6.69) is the first ionization potential energy of an isolated molecule (Buckingham & Utting 1970).

At small ranges of interaction the electron clouds of the molecules overlap significantly and it is unrealistic to derive the interaction energy $U_{12}(\tau)$ using non-overlapping wave functions and perturbation theory, in which the interaction Hamiltonian is expanded as a multipole series (Buckingham & Utting 1970). However, the theory of short-range interaction is not well understood and no general equations for all molecules can be stated. It has therefore been customary in calculations of B_R, B_ε and the pressure virial coefficient B_P (Buckingham & Pople 1955a; Buckingham 1956;

Copeland & Cole 1976) to assume that (6.67) to (6.69) or their equivalents are applicable to long range and short range interactions, and to add an additional energy term $U_{overlap}$ to account for repulsive short range interactions. We then write

$$U_{12}(\tau) = U_{elec} + U_{ind} + U_{disp} + U_{overlap} \quad , \tag{6.70}$$

where U_{elec}, U_{ind}, and U_{disp} are given by (6.67) to (6.69) for all R. In most work on the equilibrium properties of gases (Buckingham & Pople 1955a; Buckingham 1956; Sutter & Cole 1970; Brookmeyer 1973; Buckingham & Graham 1974; Copeland & Cole 1976) the Lennard-Jones 6 : 12 potential U_{LJ},

$$U_{LJ} = 4e\left[\left(\frac{R_o}{R}\right)^{12} - \left(\frac{R_o}{R}\right)^{6}\right] \tag{6.71}$$

is used to represent $(U_{disp} + U_{overlap})$, where $4e\left(\frac{R_o}{R}\right)^{6}$ describes the attractive part of the potential and where $4e\left(\frac{R_o}{R}\right)^{12}$ describes the short range repulsive part. The symbols e and R_o are the well-known Lennard-Jones parameters. Since U_{LJ} is spherically symmetric, Buckingham & Pople (1955a) proposed that a further term be added to $U_{overlap}$ to account for the angular dependence of short range overlap repulsive forces for non-spherical molecules. In their theory of B_ε they used

$$U_{disp} + U_{overlap} = 4e\left[\left(\frac{R_o}{R}\right)^{12} - \left(\frac{R_o}{R}\right)^{6}\right] + 4De\left(\frac{R_o}{R}\right)^{12} \times (3\cos^2\theta_1 + 3\cos^2\theta_2 - 2) \quad , \tag{6.72}$$

where D is a shape factor which may vary between -0.25 and 0.5 so that the shape potential is always repulsive.

In the next chapter the explicit forms of the intermolecular potentials discussed in this section are substituted into the expression

$$B_R = \frac{N_A^2}{3\varepsilon_o \Omega}\int\left[\sum_{n=1}^{9}\Delta_n\right]\exp\{-(U_{elec} + U_{ind} + U_{disp} + U_{overlap})/kT\}\,d\tau \quad , \tag{6.73}$$

which is integrated numerically using Simpson's rule for a range of molecules.

REFERENCES

Brookmeyer, B. 1973 M.S. thesis, Brown University.

Buckingham, A.D. 1956 *Trans. Faraday Soc.* 52, 747.

Buckingham, A.D. 1967 *Adv. Chem. Phys.* 12, 107.

Buckingham, A.D. & Graham, C. 1974 *Proc. R. Soc. Lond. A* 336, 275.

Buckingham, A.D. & Orr, B.J. 1967 *Q. Rev. Chem. Soc. Lond.* 21, 195.

Buckingham, A.D. & Pople, J.A. 1955a *Trans. Faraday Soc.* 51, 1029, 1173.

Buckingham, A.D. & Pople, J.A. 1955b *Proc. Phys. Soc. A* 68, 905.

Buckingham, A.D. & Utting, B.D. 1970 *Annu. Rev. Phys. Chem.* 21, 287.

Buckingham, A.D. & Watts, R.S. 1973 *Molec. Phys.* 26, 7.

Copeland, T.G. & Cole, R.H. 1976 *J. Chem. Phys.* 64, 1741.

Graham, C. 1971 Ph.D. thesis, University of Cambridge.

Jeffreys, H. 1931 *Cartesian Tensors.* Cambridge : Univ. Press.

Kielich, S. 1962 *Acta Phys. Polon.* 22, 477.

Mason, E.A. & Spurling, T.H. 1969 *The Virial Equation of State.* Oxford : Pergamon Press.

O'Brien, E.F., Gutschick, V.P., McKoy, C. & McTague, J.P. 1973 *Phys. Rev. A* 8, 690.

Sutter, H. & Cole, R.H. 1970 *J. Chem. Phys.* 52, 132.

CHAPTER 7

EVALUATION OF B_R BY NUMERICAL INTEGRATION

§1. Previous evaluations of B_R

Buckingham (1956) and Kielich (1962) have evaluated some of the terms in the expression for B_R,

$$B_R = \frac{N_A^2}{3\varepsilon_o \Omega} \int \left[\sum \Delta_n \right] \exp\{-(U_{elec} + U_{ind} + U_{disp} + U_{overlap})/kT\} d\tau \ , \qquad (7.1)$$

given in (6.73) of chapter 6. In their analytical procedure they represented $(U_{disp} + U_{overlap})$ by the Lennard-Jones 6:12 potential U_{LJ}; and on the assumption that

$$U_{elec} + U_{ind} << kT \ , \qquad (7.2)$$

performed a series expansion of the orientational part of the Boltzmann factor in powers of $1/kT$, so that

$$\exp\{-(U_{elec} + U_{ind} + U_{disp} + U_{overlap})/kT\} \approx$$

$$\exp(-U_{LJ}/kT)\left[1 - (U_{elec} + U_{ind})/kT + \frac{1}{2!}\{(U_{elec} + U_{ind})/kT\}^2 - \cdots\right]. \qquad (7.3)$$

Substitution of (7.3) into (7.1) yields an expression for B_R in which the integrals over angular coordinates are readily evaluated analytically; and in which the radial integrals may be expressed in terms of $H_k(y)$ functions given by the expression (Buckingham & Pople 1955a)

$$\int_o^\infty R^{-k} \exp(-U_{LJ}/kT) R^2 dR = \frac{1}{12} R_o^{3-k} y^{-4} H_k(y) \qquad (7.4)$$

where

$$y = 2\left(\frac{e}{kT}\right)^{\frac{1}{2}} \ ,$$

and

$$H_k(y) = y^{\frac{27-k}{6}} \sum_{p=0}^{\infty} \Gamma\left(\frac{6p + k - 3}{12}\right) \frac{y^p}{p!} \qquad (7.5)$$

The symbols e/k and R_o are the Lennard-Jones parameters. Values of $H_k(y)$ have been tabulated by Buckingham & Pople (1955a) for k ranging from 6 to 17 in integral steps, and for y ranging from 0.6 to 3.2 in steps of 0.1.

The condition that, $U_{elec} + U_{ind} << kT$, ensures that the series of (7.3) will converge rapidly (Pople 1954). However, this condition is not always satisfied for all ranges of interaction and all molecular orientations, since at short range ($R \approx R_o$) , U_{elec} and U_{ind} are large, resulting in a series which converges slowly (Sutter 1969).

In this chapter we assume an intermolecular potential energy and evaluate some of the terms in B_R by numerical integration using a computer. The development of the computer program is discussed; and calculated B_R values for our range of molecules (with the exception of CH_2F_2) are compared with our experimental values.

§2. A model for pair interactions

§§2.1 Introduction

In our classical model we have neglected any changes in the intrinsic molecular properties at short range and have used the isolated-molecule physical property tensors in our expressions for B_R , which are then applied at both long and short range. Although this is a weakness of a classical model for pair interactions, a quantum mechanical description is extremely complicated for many electron molecules, and so far has only been applied to the evaluation of B_ε , the second dielectric virial coefficient, for helium (Buckingham & Watts 1973; O'Brien, Gutschick, McKoy & McTague 1973).

§§2.2 The intermolecular potential energy

The intermolecular potential energy used in our calculations is the sum of a number of contributions. As presented in chapter 6 they are : a central force potential U_{LJ} described by the Lennard-Jones 6:12 potential; the electrostatic energy U_{elec} , described by permanent dipole moment μ and quadrupole moment θ (as defined in (6.51)); the induction energy U_{ind} ; and the anisotropy of repulsive forces represented by U_{shape} .

The Lennard-Jones 6:12 potential U_{LJ} has the form

$$U_{LJ} = 4e\left[\left(\frac{R_o}{R}\right)^{12} - \left(\frac{R_o}{R}\right)^{6}\right] , \qquad (7.6)$$

while the electrostatic energy and the induction energy are the sum of five terms,

$$U_{elec} + U_{ind} = U_{\mu,\mu} + U_{\mu,\theta} + U_{\theta,\theta} + U_{\mu,ind\,\mu} + U_{\theta,ind\,\mu} , \qquad (7.7)$$

where (for systems with threefold or higher rotation-symmetry) in the

coordinate system of figure 1 in chapter 6 ,

$$U_{\mu,\mu} = \frac{1}{4\pi\varepsilon_o}\{\mu^2 R^{-3}(2\cos\theta_1\cos\theta_2 + \sin\theta_1\sin\theta_2\cos\phi)\} \quad ; \tag{7.8}$$

$$U_{\mu,\theta} = \frac{1}{4\pi\varepsilon_o}\{\tfrac{3}{2}\mu\theta R^{-4}[\cos\theta_1(3\cos^2\theta_2 - 1) + \cos\theta_2(3\cos^2\theta_1 - 1) + 2\sin\theta_1\sin\theta_2\cos\theta_2\cos\phi + 2\sin\theta_1\cos\theta_1\sin\theta_2\cos\phi]\} \quad ; \tag{7.9}$$

$$U_{\theta,\theta} = \frac{1}{4\pi\varepsilon_o}\{\tfrac{3}{4}\theta^2 R^{-5}(1 - 5\cos^2\theta_1 - 5\cos^2\theta_2 + 17\cos^2\theta_1\cos^2\theta_2 + 2\sin^2\theta_1\sin^2\theta_2\cos^2\phi + 16\sin\theta_1\cos\theta_1\sin\theta_2\cos\theta_2\cos\phi)\} \quad ; \tag{7.10}$$

$$U_{\mu,\text{ind }\mu} = \frac{1}{(4\pi\varepsilon_o)^2}\{-\tfrac{1}{2}\alpha\mu^2 R^{-6}[(3\cos^2\theta_1 - 1) + (3\cos^2\theta_2 - 1)]\} \quad ; \tag{7.11}$$

and

$$U_{\theta,\text{ind }\mu} = \frac{1}{(4\pi\varepsilon_o)^2}\{-\tfrac{9}{8}\alpha\theta^2 R^{-8}(4\cos^4\theta_1 + 4\cos^4\theta_2 + \sin^4\theta_1 + \sin^4\theta_2)\} \; . \tag{7.12}$$

It should be noted that $U_{\mu,\text{ind }\mu}$ has been written so that its unweighted average over angles is zero and is thus purely orientational. The orientational independent part is assumed to be incorporated in the R^{-6} term of the central force potential U_{LJ} (Buckingham & Pople 1955a; Copeland & Cole 1976).

The shape potential is

$$U_{\text{shape}} = 4De\left(\frac{R_o}{R}\right)^{12}(3\cos^2\theta_1 + 3\cos^2\theta_2 - 2) \tag{7.13}$$

where D is a shape factor which can vary between -0.25 and +0.5 in order to ensure that the R^{-12} term is always repulsive at short range. A positive D corresponds to a rod-like molecule and U_{shape} will be most negative for an antiparallel dipole arrangement. A negative D corresponds to a plate-like molecule and U_{shape} will be most negative for a parallel dipole arrangement. For spherically symmetric molecules D = 0 .

The intermolecular potential energy expressions given by (7.6) to (7.12) are directly applicable to pair interactions of linear dipolar molecules, but may also be used for non-polar linear molecules and spherical molecules by setting the relevant multipole moments to zero. In our model

(as in those of Sutter & Cole (1970); Brookmeyer (1973); Copeland & Cole (1976)) the molecules CH_3F and CHF_3 are assumed to be linear with the dipole lying along the threefold rotation axis.

§§2.3 Expressions for B_R for our range of molecules

Expressions for B_R may be obtained if the explicit expressions for the Δ_n terms given in (6.56) to (6.64) of chapter 6 and the intermolecular potential energy $U_{12}(\tau)$ given in (7.6) to (7.13) are substituted into the general expression

$$B_R = \frac{N_A^2}{3\varepsilon_o \Omega} \int \left[\sum_{n=1}^{9} \Delta_n \right] \exp\left(-U_{12}(\tau)/kT\right) d\tau \ . \qquad (7.14)$$

The symbol Ω is given by

$$\Omega V_m = \int d\tau \ ,$$

and for the coordinate system of figure 1 in chapter 6, $\Omega = 4\pi$. Since the explicit form of B_R depends on the symmetry of a molecule it is helpful to summarize expressions for B_R for our range of molecules.

Spherically symmetric molecules have no multipole moments of any order in their ground state so that we may write

$$B_R = \frac{N_A^2}{3\varepsilon_o 4\pi} \int \left[\frac{2\alpha_o^3}{(4\pi\varepsilon_o)^2 R^6} \right] \exp\left(-U_{LJ}/kT\right) d\tau \ . \qquad (7.15)$$

This expression has also been used to evaluate B_R for the tetrahedral molecules CH_4 and CF_4 ; and for SF_6 of the O_h point group.

The *linear* molecules CO_2 and N_2 belong to the $D_{\infty h}$ point group and have no polar property tensors of odd rank. The form of B_R for these molecules is

$$B_R = \frac{N_A^2}{3\varepsilon_o 4\pi} \int \left[\Delta_2 + \Delta_3\right] \exp\left\{-(U_{LJ} + U_{\theta,\theta} + U_{\theta,\mathrm{ind}\,\mu} + U_{\mathrm{shape}})/kT\right\} d\tau \ , \qquad (7.16)$$

where the leading multipole moment is the quadrupole moment θ .

The '*linear*' *polar* molecules CH_3F and CHF_3 belong to the C_{3v} point group and have first and second rank property tensors of the same form. The Δ_n terms given in (6.56) to (6.64) of chapter 6 may be used to evaluate B_R for these if only first and second rank tensors, or higher rank tensors

contracted to first rank are retained in the calculation. The forms of Δ_2, Δ_3, Δ_4, Δ_7 and Δ_9 are rigorously appropriate to polar molecules with C_{3v} symmetry; however, the physical property tensors of Δ_7 and Δ_9 are unavailable and are omitted from our calculations of B_R. The terms Δ_5, Δ_6 and Δ_8 contain third and fourth rank property tensors and are not applicable to these molecules and are omitted. The form of B_R for these molecules is then

$$B_R = \frac{N_A^2}{3\varepsilon_o 4\pi} \int [\Delta_2 + \Delta_3 + \Delta_4] \exp\{-(U_{LJ} + U_{\mu,\mu} + U_{\mu,\theta} + U_{\theta,\theta} + U_{\mu,\text{ind}\,\mu} + U_{\theta,\text{ind}\,\mu} + U_{\text{shape}})/kT\}\, d\tau \,. \quad (7.17)$$

In all our expressions for B_R, $\Delta_1 = \alpha^{(1)} - \alpha_o$ is zero since $\alpha^{(1)}$ is assumed to be independent of R and $\alpha^{(1)} = \alpha_o$.

§3. Computer program

§§3.1 Introduction

Experience in the computer evaluation of B_R using Simpson's rule (Gerald 1970) was obtained by first treating two much simpler expressions :

(i) $$\int_o^R R^2 dR \int_o^\pi \sin\theta\, d\theta \int_o^{2\pi} d\phi \quad ,$$

and

(ii) the second pressure virial coefficient (Buckingham & Pople 1955a)

$$B_p = \frac{N_A}{8\pi} \int [1 - \exp(-U_{12}(\tau)/kT)]\, d\tau \quad .$$

§§3.2 Computer evaluation of $\int_o^R R^2 dR \int_o^\pi \sin\theta\, d\theta \int_o^{2\pi} d\phi$

A numerical integration program using a three-variable Simpson's rule was used to evaluate the above expression. Fortran language was used and all calculations were carried out on a Hewlett Packard 2100B computer. In this program the R-integral had a range of 0 to 3.0 and the R, θ and ϕ axes were divided into 6, 4 and 8 divisions respectively. For this grid size numerical integration gave 111.3 , while exact integration gave $[4/3\pi R^3]_o^{3.0}$, which has a value of 113.1. Since the expression could be evaluated by an independent method the validity of the program could be tested. A finer grid would produce results in better agreement.

As an illustration of the application of Simpson's rule in numerical

integration we show in detail in an appendix how the above expression may be evaluated.

§§3.3 Computer evaluation of B_p

Unlike the three-variable problem discussed above the evaluation of the second pressure virial coefficient B_p, like B_R, involves an integration over five variables (R, θ_1, θ_2, ϕ_1, ϕ_2) of the form,

$$\int_0^\infty R^2 dR \int_0^\pi \sin\theta_1 d\theta_1 \int_0^{2\pi} d\phi_1 \int_0^\pi \sin\theta_2 d\theta_2 \int_0^{2\pi} d\phi_2 F(R,\theta_1,\theta_2,\phi_1-\phi_2) \quad . \qquad (7.18)$$

However, since ϕ_1 and ϕ_2 never appear separately (pair interactions depend on the relative planes of the two molecules) but only as $(\phi_1 - \phi_2)$, (7.18) may be written as a four-variable integral (Sutter 1969),

$$2\pi \int_0^\infty R^2 dR \int_0^\pi \sin\theta_1 d\theta_1 \int_0^{2\pi} d\phi \int_0^\pi \sin\theta_2 d\theta_2 \, F(R,\theta_1,\theta_2,\phi) \quad , \qquad (7.19)$$

where

$$\phi = \phi_1 - \phi_2 \quad .$$

Since the expressions for B_p and B_R depend only on $\cos\phi$, an even function of ϕ, the integration limits on ϕ may be changed from 0 to 2π radians, to 0 to π radians and the results multiplied by 2 (Brookmeyer 1973). These simplifications significantly reduce the computing time.

Since similar programming techniques are required in the evaluation of B_p and B_R, and accurate experimental data for B_p is readily accessible, numerical evaluations of B_p were first undertaken to acquire experience and confidence in these techniques.

For CHF_3,

$$\begin{aligned} \alpha &= 3.97 \times 10^{-40} \text{ C}^2 \text{ m}^2 \text{ J}^{-1} \text{ (static polarizability)} \\ \mu &= 5.50 \times 10^{-30} \text{ C m} \\ \theta &= 15.0 \times 10^{-40} \text{ C m}^2 \\ D &= -0.10 \\ e/k &= 184.0 \text{ K} \\ R_o &= 0.380 \text{ nm} \end{aligned}$$

(Copeland & Cole 1976), and numerical evaluation of the expression for B_p with R ranging from 0.2 to 2.0 nm in 60 steps, and with each angle axis divided into 10 divisions gives $B_p = -162 \times 10^{-6}$ m^3 mol^{-1}, which compares favourably with the experimental value of -157×10^{-6} m^3 mol^{-1} at 323.2 K.

§4. Computer evaluation of B_R using a 4-variable Simpson's rule integration procedure

§§4.1 Introduction

Modification of the above program to evaluate B_R using a 4-variable Simpson's rule was easily achieved. A Fortran listing of our program together with a flow chart illustrating the sequence of operations is given in the appendix.

The ranges of θ_1, θ_2 and ϕ from 0 to π radians were divided into 10 subdivisions and the range of R from 0.2 to 2.0 nm into 60 divisions. Doubling the number of divisions along each of the angle axes changed the calculated B_R values by 0.01% whereas doubling the number of divisions along the R axis only, produced a change of about 3% . Integrating over a wider radial range of 0.05 to 3.8 nm resulted in a change in B_R of less than 1%. Single precision was used for all calculations. The computing time of B_R for CH_3F and CHF_3 was about 6 hours each for a full run while the other molecules each required 3 hours.

§§4.2 Numerical values of B_R

In table 1 below we list the contributions to B_R from each of the terms Δ_2, Δ_3 and Δ_4, together with the total calculated B_R values for the range of gases investigated. Also shown are the experimentally observed B_R values. The calculated and observed B_R values given below are all for λ = 632.8 nm and room temperature (298.2K).

molecule	$10^{12} B_R^{\Delta_2}$ / $m^6\ mol^{-2}$	$10^{12} B_R^{\Delta_3}$ / $m^6\ mol^{-2}$	$10^{12} B_R^{\Delta_4}$ / $m^6\ mol^{-2}$	$10^{12} B_R$ / $m^6\ mol^{-2}$	
				calc.	obs.
CH_4	0	7.29	0	7.29	7.76 ± 1.32
CH_3F	-0.61	10.58	-7.13	2.84	4.32 ± 1.87
CHF_3	0.78	6.29	5.13	12.20	2.54 ± 1.35
CF_4	0	4.15	0	4.15	4.27 ± 1.38
Ne	0	0.051	0	0.051	-0.14 ± 0.14
Ar	0	2.10	0	2.10	1.57 ± 0.58
Kr	0	6.74	0	6.74	6.23 ± 1.55
Xe	0	22.12	0	22.12	25.50 ± 2.85
CO_2	-2.82	6.65	0	3.83	4.75 ± 1.30
N_2	-0.58	2.05	0	1.47	0.74 ± 0.65
SF_6	0	15.87	0	15.87	27.28 ± 5.18

Table 1. A comparison of the calculated and the observed B_R values for λ = 632.8 nm at room temperature (298.2K).

molecules	$10^{40}\ \alpha_o$ †	$10^{30}\ \mu$	$10^{40}\ \theta$	$10^{50}\ \beta$	K	D	e/k	R_o	$10^{12}\ B_R$	
	$C^2\ m^2\ J^{-1}$	Cm	$C\ m^2$	$C^3\ m^3\ J^{-2}$			K	nm	$m^6\ mol^{-2}$	
									calc.	obs.
CH_4	2.897	0	0	0	0	0	184.5 [7]	0.362 [7]	7.29	7.76 ± 1.32
CH_3F	2.916	6.17 [6]	7.7 [6]	-0.19 [5]	0.026 [3]	0.254 [6]	199.0 [6]	0.380 [6]	2.84	4.32 ± 1.87
CHF_3	3.097	5.50 [6]	15.0 [6]	0.27 [5]	0.029 [3]	-0.10 [6]	184.0 [6]	0.440 [6]	12.20	2.54 ± 1.35
CF_4	3.164	0	0	0	0	0	153.0 [2]	0.470 [2]	4.15	4.27 ± 1.38
Ne	0.4401	0	0	0	0	0	35.7 [9]	0.2789 [9]	0.051	-0.14 ± 0.14
Ar	1.850	0	0	0	0	0	124.0 [9]	0.3418 [9]	2.10	1.57 ± 0.58
Kr	2.806	0	0	0	0	0	190.0 [9]	0.3610 [9]	6.74	6.23 ± 1.55
Xe	4.569	0	0	0	0	0	229.0 [9]	0.4055 [9]	22.12	25.50 ± 2.85
CO_2	2.907	0	-14.3 [4]	0	0.266 [3]	0.2 [7]	190.0 [10]	0.400 [10]	3.83	4.75 ± 1.30
N_2	1.961	0	- 5.0 [4]	0	0.131 [3]	0.2 *	91.5 [9]	0.3681 [9]	1.47	0.736± 0.65
SF_6	4.983	0	0	0	0	0	200.9 [9]	0.551 [9]	15.87	27.28 ± 5.18

† Calculated from the A_R values of this work.

* Arbitrarily chosen value.

Table 2. Molecular parameters used to calculate B_R; the superscripts refer to references at the end of the chapter.

The molecular parameters used in our calculations are given in table 2.

We note from table 1 that the agreement between the calculated and observed B_R values is good for the molecules CH_4, CF_4, Ar, Kr and Xe whose B_R values are determined by $B_R^{\Delta 3}$, the Kirkwood 'fluctuation' term. The molecular parameters used in the evaluation of this term are the Lennard-Jones parameters and the polarizability α_o. We believe the values of α_o to be reliable, being obtained as they were from our own precise refractive index measurements. There is, in practice, a wide disparity in the experimental values of e/k and R_o reported by various workers, and the calculated values of B_R in table 1 are based on what are believed to be the most reliable data (usually extracted from viscosity measurements). However, table 3 lists B_R values calculated with the use of other pairs of *reported* Lennard-Jones parameters to show, in part, how sensitive the calculated B_R values are to the Lennard-Jones parameters used.

molecule	e/k / K	R_o / nm	$10^{12}\ B_R$ / $m^6\ mol^{-2}$ calc.	obs.
CH_4	184.5 [7]	0.362 [7]	7.29	7.76 ± 1.32
	137.0 [9]	0.388 [9]	5.51	
	144.0 [10]	0.380 [10]	5.90	
Ne	35.7 [9]	0.2789 [9]	0.051	-0.14 ± 0.14
	60.9 [1]	0.2648 [1]	0.057	
Ar	124.0 [9]	0.3418 [9]	2.10	1.57 ± 0.58
	152.8 [1]	0.3292 [1]	2.42	
Kr	190.0 [9]	0.3610 [9]	6.74	6.23 ± 1.55
	206.4 [1]	0.3522 [1]	7.53	
SF_6	259.0 [8]	0.5005 [8]	15.87	27.28 ± 5.18
	200.9 [9]	0.551 [9]	10.72	

Table 3. Sensitivity to the Lennard-Jones parameters of the calculated B_R values; the superscripts refer to the references at the end of the chapter.

A comparison between the calculated and observed B_R values in table 3 reveals that the model is sensitive to uncertainties in the Lennard-Jones parameters. The most significant discrepancies occur with CH_4 and SF_6. Monchick & Mason (1961) have shown that measurements of viscosity as a function of temperature provide a better procedure for determining Lennard-Jones parameters than fitting second virial coefficients (B_p and B_ε). The viscosity is primarily determined by central forces with orientational forces having a

much less effect. Consequently, viscosity based Lennard-Jones parameters are thought to be more accurate than those determined by other procedures.

Of the remaining molecules in table 1, CH_3F and CHF_3 are polar while CO_2 and N_2 are non-polar. However, all four are quadrupolar. The calculated B_R values of CH_3F, CO_2 and N_2 are in reasonable agreement with the observed values but the agreement for CHF_3 is poor.

It is important to note that reliable experimental molecular parameters are essential in the assessment of any model for pair interactions. Of the parameters required for the evaluation of B_R for these molecules, experimental quadrupole moments have only been determined for CO_2 and N_2. The quadrupoles of CH_3F and CHF_3, given in table 2, are the calculated values of Copeland & Cole (1976). Their quadrupole moments θ are fitting parameters in a numerical integration procedure which attributes differences of observed B_p values from values calculated using viscosity based U_{LJ} and dipole energies to dipole-quadrupole and quadrupole-quadrupole interaction energies. A small adjustment is later made to account for the minor effect of shape as expressed by D on B_p after values of the shape factor D were obtained from B_ε. The shape factor interaction was then included in B_p calculations and the calculations were iterated until self-consistent quadrupole moments and shape factors resulted. These values of θ and D have been used in our calculations of B_R for CH_3F and CHF_3. Copeland & Cole (1976) comment that the calculated θ for CH_3F (7.7×10^{-40} C m^2) is reasonable although θ for CHF_3 (15.0×10^{-40} C m^2) may be a bit large. The D factors, namely 0.254 for CH_3F and -0.1 for CHF_3 are in agreement with the original requirement of Buckingham & Pople (1955b) that D should be within the range -0.25 to 0.5 and be positive for rod-like molecules (CH_3F) and negative for plate-like molecules (CHF_3).

In the case of CO_2 and N_2 experimental quadrupole moments have been used in our calculations of B_R. The shape factor for CO_2, namely D = 0.2, was determined by Datta & Singh (1971) in their calculation of multipole moments from viscosity and second pressure virial coefficients. The D factor for N_2 has not been reported in the literature and was arbitrarily given a value of 0.2 so as to be in the range 0 to 0.5 for rod-like molecules.

In table 4 below the sensitivity of our calculated B_R values for N_2 and CHF_3 to different values of D is illustrated. The other molecular parameters used in the calculations are given in table 2.

molecule	D	$10^{12}\ B_R^{\Delta 2}$ / $m^6\ mol^{-2}$	$10^{12}\ B_R^{\Delta 3}$ / $m^6\ mol^{-2}$	$10^{12}\ B_R^{\Delta 4}$ / $m^6\ mol^{-2}$	$10^{12}\ B_R$ / $m^6\ mol^{-2}$ calc.	obs.
N_2	0	0.045	2.01	0	2.06	0.74 ± 0.65
	0.1	-0.26	2.01	0	1.75	
	0.2	-0.58	2.05	0	1.47	
	0.4	-1.75	2.39	0	0.64	
CHF_3	0	0.35	6.03	4.78	11.16	2.54 ± 1.35
	-0.05	0.55	6.12	4.92	11.59	
	-0.1	0.78	6.29	5.13	12.20	
	-0.2	1.57	7.06	6.05	14.68	

Table 4. Sensitivity of the calculated B_R values for N_2 and CHF_3 to the D factor, for $\theta_{N_2} = -5.0 \times 10^{-40}\ C\,m^2$ and $\theta_{CHF_3} = 15.0 \times 10^{-40}\ C\,m^2$.

We note for N_2 that the calculated and the observed B_R values are in closer agreement for D = 0.4 than for our earlier assumed value of 0.2. However, for CHF_3 no significant improvement is evident for the range of D factors chosen. Since the calculated B_R values tend to decrease as the D factor becomes more positive, better agreement may result for a positive D. However, a positive D factor would be at variance with the suggested plate-like configuration of CHF_3 and may indicate that θ is in error.

In order to discover the sensitivity of our calculated B_R values to θ a similar analysis was performed for N_2 and CHF_3. In these calculations D = 0.2 for N_2 and -0.1 for CHF_3. The other molecular parameters used in the calculations are given in table 2.

molecule	$10^{40}\theta$ / $C\,m^2$	$10^{12}\ B_R^{\Delta 2}$ / $m^6\ mol^{-2}$	$10^{12}\ B_R^{\Delta 3}$ / $m^6\ mol^{-2}$	$10^{12}\ B_R^{\Delta 4}$ / $m^6\ mol^{-2}$	$10^{12}\ B_R$ / $m^6\ mol^{-2}$ calc.	obs.
N_2	0	-0.64	2.05	0	1.41	0.74 ± 0.65
	-2.5	-0.62	2.05	0	1.42	
	-5.0	-0.58	2.05	0	1.47	
	-10.0	-0.34	2.14	0	1.80	
	+ 5.0	-0.58	2.05	0	1.47	
CHF_3	0	0.81	5.67	4.08	10.56	2.54 ± 1.35
	7.5	0.76	5.73	4.20	10.69	
	15.0	0.78	6.29	5.13	12.20	
	30.0	5.45	26.02	36.20	67.67	
	-15.0	0.78	6.27	5.11	12.16	

Table 5. Sensitivity of the calculated B_R values for N_2 and CHF_3 to the quadrupole moment θ, for $D_{N_2} = 0.2$ and $D_{CHF_3} = -0.1$.

We note from table 5 that the calculated B_R values are insensitive to the sign of θ and increase with increasing $|\theta|$. The agreement between the calculated and observed B_R values for CHF_3 is still poor. It is difficult to say whether the model is inappropriate for CHF_3 since no observed values of θ are available.

Although reasonable agreement between the calculated and observed B_R values may in part indicate that our long-range classical expressions for B_R and the chosen intermolecular potential energy are an adequate description of pair interactions, it should be realized, that in cases where the agreement is poor it is difficult to say whether the model is inadequate at short range or the intermolecular potential energy is inappropriate. A definitive resolution of this ambiguity must await the accumulation of a large body of independently measured molecular parameters and the determination of reliable intermolecular potential functions with which the isolated-molecule assumption may be tested. Consistency between theory and experiment for a range of pair interaction effects such as viscosity, pressure virial coefficients, dielectric virial coefficients and Kerr virial coefficients would be the acid test for the success of a potential function and the validity of the isolated-molecule assumption.

REFERENCES

[1] *American Institute of Physics Handbook.* (McGraw-Hill Book Co., N.Y., 1972), 3rd edition, Section 2, p. 238.

[2] Bose, T.K., Sochanski, J.S. & Cole, R.H. 1972 *J. Chem. Phys.* 57, 3592.

[3] Bridge, N.J. & Buckingham, A.D. 1966 *Proc. R. Soc. Lond. A* 295, 334.

Brookmeyer, B. 1973 M.Sc. thesis, Brown University.

Buckingham, A.D. 1956 *Trans. Faraday Soc.* 52, 747.

[4] Buckingham, A.D. 1967 *Adv. Chem. Phys.* 12, 107.

[5] Buckingham, A.D. & Orr, B.J. 1969 *Trans. Faraday Soc.* 65, 673.

Buckingham, A.D. & Pople, J.A. 1955a *Trans. Faraday Soc.* 51, 1173.

Buckingham, A.D. & Pople, J.A. 1955b *Trans. Faraday Soc.* 51, 1179.

Buckingham, A.D. & Watts, R.S. 1973 *Molec. Phys.* 26, 7.

[6] Copeland, T.G. & Cole, R.H. 1976 *J. Chem. Phys.* 64, 1741.

[7] Datta, K.K. & Singh, Y. 1971 *J. Chem. Phys.* 55, 3541.

[8] Ellis, C.P. 1958 Ph.D. thesis, University of Natal.

Gerald, C.F. 1970 *Applied Numerical Analysis.* Addison-Wesley Publishing Company : California.

[9] Hirschfelder, J.O., Curtiss, C.F. & Bird, R.B. 1954 *Molecular Theory of gases and liquids.* New York : Wiley.

Kielich, S. 1962 *Acta Phys. Polon.* 22, 477.

[10] Mason, E.A. & Spurling, T.H. 1969 *The Virial Equation of State.* Oxford : Pergamon Press.

Monchick, L. & Mason, E.A. 1961 *J. Chem. Phys.* 35, 1676.

O'Brien, E.F., Gutschick, V.P., McKoy, C. & McTague, J.P. 1973 *Phys. Rev. A* 8, 690.

Pople, J.A. 1954 *Proc. R. Soc. Lond. A* 221, 498.

Sutter, H.G. 1969 Ph.D. thesis, Brown University.

Sutter, H.G. & Cole, R.H. 1970 *J. Chem. Phys.* 52, 132.

APPENDIX

USE OF SIMPSON'S RULE TO EVALUATE B_R

A§1. Introduction

Polynomial approximation serves as the basis for a wide variety of integration formulas, the main idea being that if p(x) is an approximation to y(x) then (Scheid 1968),

$$\int_a^b p(x)\,dx \approx \int_a^b y(x)dx \ . \qquad \text{(A1.1)}$$

In Simpson's rule the area under the curve y(x) is divided into several divisions of equal width h ,

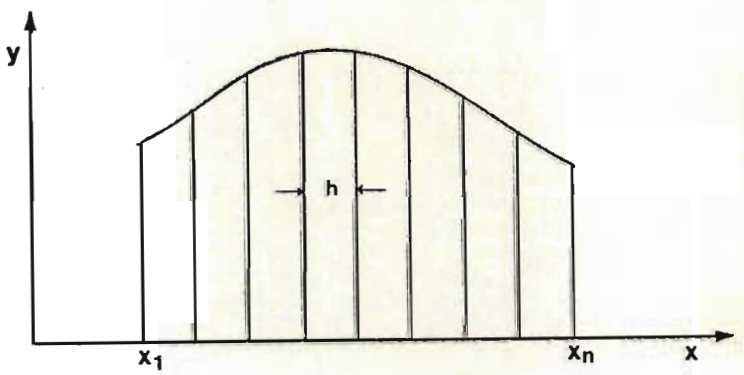

and the actual area is approximated by segments of parabolas. The rule states that the integral is given approximately by the expression (Scheid 1968)

$$\int_{x_1}^{x_n} y(x)\,dx \simeq \frac{h}{3}\,[y_1 + 4y_2 + 2y_3 + 4y_4 \ldots\ + 2y_{n-2} + 4y_{n-1} + y_n] \ , \qquad \text{(A1.2)}$$

where x_i is x at the beginning of interval i, and y_i is $y(x_i)$. The number of divisions must be even so that n must be odd.

The adaptation of Simpson's rule for the numerical integration of a function involving *more* than one variable may be carried out as follows : We note from (A1.2) that the integration formula is a linear combination of weighted functional values with varying values of the independent variable. In the case of a function of two variables f(x,y) we may write (Gerald 1970),

$$\int\int f(x,y)dA = \int_a^b\left(\int_c^d f(x,y)dy\right)dx = \int_c^d\left(\int_a^b f(x,y)dx\right)dy \ , \qquad \text{(A1.3)}$$

where the region A is bounded by the lines $x = a$, $x = b$, $y = c$ and $y = d$. The inner integral is now written as a weighted sum of function values using Simpson's rule with one variable held constant. For a two variable function the evaluation is completed by taking a weighted sum of these sums. The procedure is illustrated by evaluating the expression,

$$\int_0^{3\cdot0} R^2 dR \int_0^{2\pi} d\phi \int_0^{\pi} \sin\theta \, d\theta = \int_0^{2\pi} f(\phi)d\phi \int_0^{3\cdot0} \left(\int_0^{\pi} f(R,\theta)d\theta \right) dR$$

$$= \int_0^{2\pi} f(\phi)d\phi \int_0^{\pi} \left(\int_0^{3\cdot0} f(R,\theta)dR \right) d\theta \quad . \qquad \text{(A1.4)}$$

We have chosen to divide the range of the R integral into 6 divisions, each 0.5 wide; the range of the ϕ integral into 8 divisions; and the range of the θ integral into 4 divisions. The width of the ϕ and θ divisions is $\frac{\pi}{4}$. The evaluation of (A1.4) comprises two separate applications of Simpson's rule : a one-variable function $f(\phi)$; and a two variable function $f(R,\theta)$. Applying (A1.2) to $f(\phi)$ gives,

$$\int_0^{2\pi} f(\phi)d\phi = \left(\frac{\pi}{4}\right)\left(\frac{1}{3}\right)[1 + 4 + 2 + 4 + 2 + 4 + 2 + 4 + 1]$$

$$= 2\pi \quad . \qquad \text{(A1.5)}$$

We now tabulate $f(R,\theta) = R^2 \sin\theta$ for all values of R and θ in table A1 .

θ \ R	0	0.5	1.0	1.5	2.0	2.5	3.0
0	0	0	0	0	0	0	0
$\frac{\pi}{4}$	0	0.177	0.707	1.59	2.83	4.42	6.36
$\frac{\pi}{2}$	0	0.250	3.00	2.25	4.00	6.25	9.00
$\frac{3\pi}{4}$	0	0.177	0.707	1.59	2.83	4.42	6.36
π	0	0	0	0	0	0	0

Table A1. Tabulation of $f(R,\theta)$.

Applying Simpson's rule to $f(R,\theta)$ keeping R constant :

$$\theta = 0 , \quad \int_0^{3.0} f(R,\theta)dR = \int_0^{3.0} f(R,0)dR$$

$$= \frac{h}{3}\,[f_1 + 4f_2 + 2f_3 + 4f_4 + 2f_5 + 4f_6 + f_7]$$

$$= \frac{0.5}{3}\,[0 + 4(0) + 2(0) + 4(0) + 2(0) + 4(0) + 0]$$

$$= 0 ,$$

$$\theta = \frac{\pi}{4} , \quad \int_0^{3.0} f(R,\tfrac{\pi}{4})dR = \frac{0.5}{3}\,[0 + 4(0.177) + 2(0.707) + 4(1.59)$$

$$+ 2(2.83) + 4(4.42) + 6.36]$$

$$= 6.36 .$$

Similarly, at $\theta = \frac{\pi}{2}$, $I = 9.00$,

$\theta = \frac{3\pi}{4}$, $I = 6.36$,

$\theta = \pi$, $I = 0$.

The above partial sums, I, are now summed with Simpson's rule in the θ-direction:

$$\int_0^{\pi}\left(\int_0^{3.0} f(R,\theta)dR\right)d\theta = \left(\frac{\pi}{4}\right)\left(\frac{1}{3}\right)[0 + 4(6.36) + 2(9.00) + 4(6.36) + 0]$$

$$= 18.03 . \qquad \text{(A1.6)}$$

From (A1.4), and using the results of (A1.5) and (A1.6) gives,

$$\int_0^{3.0} R^2dR \int_0^{2\pi} d\phi \int_0^{\pi} \sin\theta\, d\theta = (2\pi)(18.03) = 113.3 .$$

The above expression may be integrated exactly to give, $\left[\frac{4}{3}\pi R^3\right]_0^{3.0}$, which has a value of 113.1 .

A§2. A computer program for the numerical integration of B_R : a four-variable function

A manual evaluation of a four-variable function using Simpson's rule is a laborious task. However, with the use of a high-speed computer, a task of this nature is readily accomplished. In the previous section a detailed analysis was given of Simpson's rule for the integration of a two-variable function; and the extension of this analysis for the integration of a four-variable function is straightforward.

Our computer program 'Insim' to evaluate the integrals for B_R is given in A§§2.2 . In this program all possible function values are generated, for a particular grid size, by four consecutive 'do loops'. These function values are then summed in the R-direction according to Simpson's rule by a subprogram called 'Simp', which can be called repeatedly. The resulting partial sums, which correspond to the I values obtained in the previous analysis, are then summed by 'Simp' in the θ_1-direction. This gives rise to further partial sums which are summed in the θ_2-direction. A final summation in the ϕ-direction completes the integration. The sequence of operations is illustrated with a simplified flow chart of the program overleaf.

A§§2.1 A simplified flow chart of our computer program for the evaluation of B_R using Simpson's rule

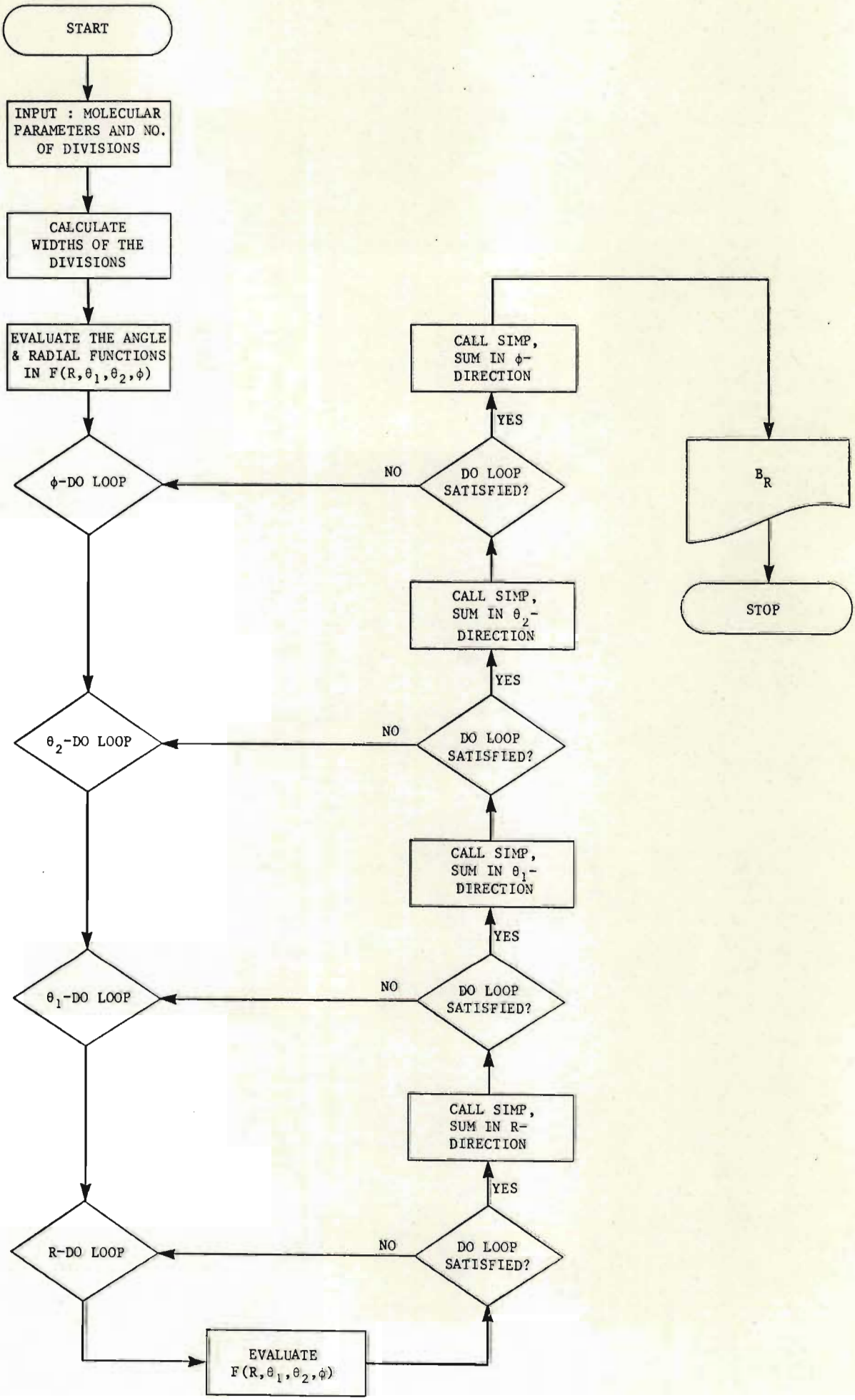

A§§2.2 A Fortran program to evaluate the integrals in B_R using Simpson's rule

```
      PROGRAM INSIM
      DIMENSION D(50),O(50),C(50),F(50),G(50),X(80)
      DIMENSION V(80),T(80),Q(80),Y(80),Z(1),Y1(80),S(80),R(80)
      READ(1,*)A,B,C1,D2,E,F2,UN,U,N1,N2,N3,N4,E1,R1,D3,D1,F1,BTA
     1,QD,F5,T1
      WRITE(6,3)
    3 FORMAT("1")
      S4=(U-UN)/FLOAT(N4)
      S1=(B-A)/FLOAT(N1)
      S2=(D2-C1)/FLOAT(N2)
      S3=(F2-E)/FLOAT(N3)
      N1=N1+1
      N2=N2+1
      N3=N3+1
      N4=N4+1
      WRITE(6,4)
    4 FORMAT("2")
      P1=0.0
      DO 10 J3=1,N2
      W=S2*P1
      D(J3)=SIN(W)
      O(J3)=COS(W)
      P1=P1+1.0
   10 CONTINUE
      WRITE(6,11)
   11 FORMAT("HR")
      P1=0.0
      DO 15 J4=1,N4
      Y2=S4*P1
      C(J4)=COS(Y2)
      P1=P1+1.0
   15 CONTINUE
      P1=0.0
      DO 20 J5=1,N3
      Q1=S3*P1
      F(J5)=SIN(Q1)
      G(J5)=COS(Q1)
      P1=P1+1.0
   20 CONTINUE
      P1=0.0
      DO 25 J6=1,N1
      X(J6)=A+S1*P1
      P1=P1+1.0
   25 CONTINUE
      BA=0.0
      I8=1
   26 I2=1
      J2=1
      K2=1
      L2=1
      I1=0
      J1=0
      K1=0
      L1=0
      M1=-3
```

```
      M2=-6
      M3=-9
      DO 60 I=1,N4
      WRITE(6,27)N1,N2,N3,N4
   27 FORMAT(4I2)
      DO 50 J=1,N3
      DO 40 K=1,N2
      DO 30 L=1,N1
      U1=4.0*E1*((R1/X(L))**12-(R1/X(L))**6)
      U2=6.50979E+02*(D1**2)*(X(L)**M1)
     1*(2.0*O(K)*G(J)+D(K)*F(J)*C(I))
      U4=-2.92535E+02*F1*D1**2*X(L)**M2
     1*(3.0*(O(K)**2)+3.0*(G(J)**2)-2.0)
      U6=9.76468E+02*D1*QD*(X(L)**(-4))*(O(K)*(3.0*(G(J)**2)-1.0
     1)+G(J)*(3.0*(O(K)**2)-1.0)+2.0*D(K)*F(J)*G(J)*C(I)+2.0*D(K)
     1*O(K)*F(J)*C(I))
      U7=4.88234E+02*(QD**2)*(X(L)**(-5))*(1.0-5.0*(O(K)**2)-5.0*
     1(G(J)**2)+17.0*(O(K)**2)*(G(J)**2)+2.0*(D(K)**2)*(F(J)**2)*(
     1C(I)**2)+16.0*D(K)*O(K)*F(J)*C(I)*G(J))
      U10=-6.58204E+02*QD*F1*(X(L)**(-8))*(4.0*(O(K)**4)
     1+4.0*(G(J)**4)+(D(K)**4)+(F(J)**4))
      U8=(4.0*E1*D3*(R1/X(L))**12)*(3.0*O(K)**2+3.0*G(J)**2-2.0)
      U9=(U1+U2+U4+U6+U7+U8+U10)/T1
      IF(U9-85.90)23,29
   23 H=EXP(-U9)
   24 GO TO 31
   29 H=0.0
   31 I1=I1+K2
      GO TO (101,102,103,104),I8
  101 V(I1)=6.13546E-13*(F1**2)*H*X(L)**(-1)*D(K)*F(J)
      Y1(I1)=V(I1)*(F5*(1.0-F5)*(3.0*(O(K)**2)+3.0*G(J)**2-2.0))
      R(I1)=V(I1)*(3.0*(F5**2)*(2.0*O(K)**2*G(J)**2-D(K)*O(K)
     Y*F(J)*G(J)*C(I)))
      S(I1)=-V(I1)*((3.0*(F5**2))*(D(K)**2)*(F(J)**2)*C(I)**2)
      V(I1)=Y1(I1)+R(I1)+S(I1)
      GO TO 30
  102 V(I1)=5.51428E-13*(F1**3)*H*X(L)**(-4)*D(K)*F(J)
      Y1(I1)=V(I1)*(2.0*((1.0-F5)**3)+F5*(2.0+F5)*(1.0-F5)*(3.0*
     1O(K)**2+1.0))
      R(I1)=V(I1)*(F5*((1.0-F5)**2)*(3.0*(G(J)**2)+1.0))
      S(I1)=V(I1)*(3.0*(F5**2)*(2.0+F5)*((2.0*O(K)*G(J)+D(K)*F(J)
     1*C(I))**2))
      V(I1)=Y1(I1)+R(I1)+S(I1)
      GO TO 30
  103 V(I1)=-3.40859E-13*D1*BTA*H*X(L)**(-1)*D(K)*F(J)
      Y1(I1)=V(I1)*(2.0*O(K)*G(J)+D(K)*F(J)*C(I))
      V(I1)=Y1(I1)
      GO TO 30
  104 V(I1)=-5.11289E-13*BTA*QD*H*(X(L)**(-2))*D(K)*F(J)
      Y1(I1)=V(I1)*(3.0*O(K)*G(J)**2+2.0*G(J)*D(K)*F(J)*C(I)-O(K))
      V(I1)=Y1(I1)
   30 CONTINUE
      CALL SIMP (I1,N1,T,V,S1,J1,I2)
      I1=0
   40 CONTINUE
      CALL SIMP (J1,N2,Q,T,S2,K1,J2)
      J1=0
   50 CONTINUE
```

```
      WRITE(6,52)
   52 FORMAT("6")
      CALL SIMP (K1,N3,Y,Q,S3,L1,L2)
      K1=0
   60 CONTINUE
      WRITE(6,62)
   62 FORMAT("7")
      I4=0
      I5=1
      CALL SIMP (L1,N4,Z,Y,S4,I4,I5)
      Z(1)=2.0*Z(1)
      WRITE(6,82)
      WRITE(6,70)Z(1)
   70 FORMAT(E14.6)
   82 FORMAT("THE ANS IS ----------------")
      BA=BA+Z(1)
      WRITE(6,95)BA
   95 FORMAT(E14.6)
      I8=I8+1
      IF(I8-5)26,83
   83 STOP
      END
      SUBROUTINE SIMP (L,N6,S,R,ST,K,N)
      DIMENSION S(80),R(80)
      I=L-1
      K=K+N
      S(K)=R(1)+R(N6)
      I3=1
      DO 80 J=2,I
      IF(I3)75,45
   45 P=4.0
      GO TO 77
   75 P=2.0
   77 S(K)=S(K)+P*R(J)
      I3=I3*(-1)
   80 CONTINUE
      S(K)=S(K)*ST/3.0
      RETURN
      STOP
      END
      ENDS
```

REFERENCES

Gerald, C.F. 1970 *Applied Numerical Analysis.* California : Addison-Wesley Publishing Company, Inc.

Scheid, F. 1968 *Numerical Analysis.* New York : McGraw-Hill Book Company.